JOURNAL OF THE AERONAUTICAL SCIENCES

VOLUME 22 MAY, 1955 NUMBER 5

MAY 17 1955

CONTENTS

The Correction of Flexible Plate Supersonic Nozzle Contours by Influence Methods.. WILLIAM N. MACDERMOTT 289

Unsteady Aerodynamic Reactions on Airfoils in Cascade.... F. SISTO 297

On the Motion of a Flat Plate at High Speed in a Viscous Compressible Fluid—II. Steady Motion.... K. STEWARTSON 303

Methods for Computing Supersonic Aerodynamic Flutter Coefficients for Two-Dimensional Flow.... ERNEST C. KENNEDY 310

Effect of Rotatory Inertia and Shear on Maximum Strain in Cantilever Impact Excitation.... MARCEL K. NEWMAN 313

The Buckling of Isosceles Triangular Plates.... HUGH L. COX AND BERTRAM KLEIN 321

A Fraction Series Solution for Characteristic Values Useful in Some Problems of Airplane Dynamics.... E. L. LEPPERT, JR. 326

Stability of Compressible Laminar Boundary Layer with Internal Heat Sources or Sinks.... GEORGE M. LOW 329

Readers' Forum: "Note on the Unsteady Heat Regenerator," by R. E. Meyer and T. A. d'Ews Thomson; "A Procedure for the Approximate Analysis of Buckled Plates," by Sara R. Boley; "On Distributed Roughness as a Means of Fixing Transition at High Supersonic Speeds," by William B. Fallis; "Stagnation Temperature Control for a Blow-Down Supersonic Wind Tunnel," by T. A. d'Ews Thomson; "Aerodynamic Coefficients for Cambering and Aileron Motions," by E. F. Tyler; "The Lift of a Blowing Wing in a Parallel Stream," by Heinrich B. Helmbold; "Transonic Lift over the Front Surface of a Two-Dimensional Diamond Airfoil," by Robert Wesley Truitt; "On Determining Turbulent Boundary-Layer Separation in Incompressible and Compressible Flow," by H. Schuh; "On the Effect of Reynolds Number upon the Peak Pressure-Rise Coefficient Associated with the Separation of a Turbulent Boundary Layer in Supersonic Flow," by E. S. Love; "Transient Temperatures and Stresses in Plates Attained in High-Speed Flight," by J. S. Przemieniecki.. 337–348

Published by

INSTITUTE OF THE AERONAUTICAL SCIENCES, INC.

JOURNAL OF THE AERONAUTICAL SCIENCES

Editor: HUGH L. DRYDEN, *Director, NACA*

Associate Editor: ROBERT R. DEXTER *Managing Editor:* BERNEICE H. JARCK

Editorial Committee

Aerodynamics

Dean R. Chapman
Francis H. Clauser
Antonio Ferri
Alexander Flax
R. Paul Harrington
R. T. Jones
Carl Kaplan
H. W. Liepmann
C. C. Lin
H. F. Ludloff
Harold Luskin
John R. Markham
Clark B. Millikan
Shatswell Ober
W. Bailey Oswald
C. D. Perkins
Elliott G. Reid
H. J. E. Reid
Russell Robinson
George S. Schairer
G. B. Schubauer
W. R. Sears
John Stack
Theodore Theodorsen
Th. von Kármán

Air Transport

Charles Froesch
J. A. Herlihy
R. D. Kelly
Otto E. Kirchner
Jerome Lederer
John C. Leslie
R. Dixon Speas

Flight Testing

R. R. Gilruth
Melvin N. Gough
W. L. Howland
W. F. Milliken, Jr.
E. G. Stout

Structures and Materials

W. B. Bleakney
E. W. Conlon
John E. Duberg
E. C. Hartmann
N. J. Hoff
Samuel Levy
J. F. McBrearty
Alfred S. Niles
W. Ramberg
F. R. Shanley
C. R. Strang
S. Timoshenko
H. S. Tsien

Rotating Wing Aircraft

F. B. Gustafson
K. H. Hohenemser
Bartram Kelley
R. B. Maloy
Ralph McClarren
R. H. Miller
R. H. Prewitt
Igor I. Sikorsky

Vibration and Flutter

Lee Arnold
M. A. Biot
R. L. Bisplinghoff
William Bollay
Chieh-Chien Chang
J. P. Den Hartog
I. E. Garrick
Martin Goland
Theodore Theodorsen

Aircraft Design

W. E. Beall
E. H. Heinemann
Hall L. Hibbard
Richard Hutton
C. L. Johnson
A. A. Kartveli
E. G. Stout
F. K. Teichmann
Robert J. Woods

Electronics in Aviation

Welcome W. Bender
K. C. Black
M. V. Kiebert, Jr.
David S. Little
S. B. Rogers
Paul Rosenberg
L. M. Sherer

Physiologic Problems

H. G. Armstrong
Louis H. Bauer
Robert J. Benford
W. Randolph Lovelace, II
Ross A. MacFarland

Fuels and Oils

D. P. Barnard
J. H. Doolittle
Graham Edgar
R. T. Goodwin
A. M. Rothrock

Flight Propulsion

George W. Brady
Frank W. Caldwell
L. S. Hobbs
E. E. Johnson
Joseph Keenan
R. P. Kroon
Hans Reissner
Abe Silverstein
C. Fayette Taylor
E. S. Taylor
P. B. Taylor
E. S. Thompson
H. S. Tsien

Instruments

Allan G. Binnie
Charles H. Colvin
Frank R. Cook
C. S. Draper
S. G. Eskin
O. E. Esval
C. F. Savage
R. C. Sylvander

Meteorology

C. F. Brooks
D. M. Little
F. W. Reichelderfer
K. C. Spengler

SUBSCRIPTION RATES

JOURNAL OF THE AERONAUTICAL SCIENCES, Published Monthly.—United States and Possessions: 1 Year, $12.00; Single Copies, $1.50. Foreign Countries Including Canada (American Currency Rates): 1 Year, $13.00; Single Copies, $1.50.

AERONAUTICAL ENGINEERING REVIEW, Published Monthly.—United States and Possessions: 1 Year, $3.00; Single Copies, $0.50. Foreign Countries Including Canada (American Currency Rates): 1 Year, $3.50; Single Copies, $0.50.

Notices of change of address should be sent to the Institute at least 30 days prior to actual change of address.

Manuscripts for publication, proofs, and all correspondence should be addressed to the Editorial Office of the JOURNAL.

Correspondence regarding subscriptions may be addressed to Publication Office, 20th and Northampton Sts., Easton, Pa., or to the Editorial Office of the JOURNAL OF THE AERONAUTICAL SCIENCES, 2 East 64th Street, New York 21, N.Y.

Copyright, 1955, by the Institute of the Aeronautical Sciences, Inc.

Entered as Second Class Matter at the Post Office, Easton, Pa., May 1, 1937. Acceptance for mailing at a special rate of Postage provided for in the Act of August 24, 1912. Authorized April 29, 1937.

JOURNAL OF THE AERONAUTICAL SCIENCES

VOLUME 22 MAY, 1955 NUMBER 5

The Correction of Flexible Plate Supersonic Nozzle Contours by Influence Methods*

WILLIAM N. MacDERMOTT†

ARO, Inc.‡

SUMMARY

Methods of obtaining the contour corrections necessary for the production of a satisfactory flow uniformity at the exit of a flexible plate supersonic nozzle are reviewed. Basic requirements of the methods are considered, and in particular it is found that contour corrections, small in comparison with the boundary-layer thickness, produce flow changes which cannot be adequately described by the simple theory of characteristics. A procedure involving use of experimentally determined jack influences was successfully applied to correction of nozzle profiles in a 12-in. supersonic wind tunnel. Considerations of further application of this method are discussed.

SYMBOLS

x	=	longitudinal coordinate along nozzle centerline, measured upstream from end of nozzle
x_w	=	coordinate along surface of nozzle, measured upstream from end of nozzle
x_i	=	any finite set of points on the nozzle centerline at which an ideal correction is desired
M	=	Mach Number
θ	=	flow angle with respect to centerline
$C(x)$	=	the ideal correction to the centerline airflow which would yield perfectly uniform flow
$I_i(x)$	=	effect of unit deflection of jack (pair) i on Mach Number or angle of the airflow of point x
Δ_i	=	symmetric or antisymmetric deflection of jack (pair) i, positive for deflection of top plate away from axis of nozzle
n	=	number of jacks used in the correction
P_0	=	total pressure of airstream
P_0'	=	stagnation pressure behind a normal shock wave as measured by a total head tube

Received July 12, 1954.

* This investigation was performed as part of USAF Contract AF 18(600)-854. The helpful suggestions of Ronald Smelt and Raymond Schneyer and the valuable assistance of Wilbur C. Armstrong, Charles E. Bond, Gene H. Hull, and Gerald Staton are hereby acknowledged.

† Engineer, Gas Dynamics Facility.

‡ ARO, Inc., is the operating contractor for the USAF of the Arnold Engineering Development Center.

INTRODUCTION

A NOZZLE DESIGNED TO PRODUCE a uniform supersonic flow field never produces a flow of perfect uniformity because of combined effects of viscosity, defects in fabrication, and possible distortions of the nozzle caused by air loads. The question of whether or not the contour of such a nozzle must be altered to improve the flow will depend upon the magnitude of the initial nonuniformity, the use to which the nozzle is to be put, and the amount of effort required to modify the contour. For nozzles used in wind-tunnel testing the flow uniformity is usually extremely important, particularly if stability and control testing is involved.

Many wind-tunnel nozzles utilize the solid-block type of construction. Modification of the contours of such nozzles is accomplished by the addition and removal of nozzle material. Various methods of calculating the exact distribution of the required corrections along the nozzle surface have been given.[1-3] In each the same basic procedure is followed—i.e., determining the required flow corrections by measurement of the flow in the uncorrected nozzle and relating these to the necessary changes in the wall shape by assuming disturbances to be propagated along characteristic lines of the flow. The ideal correction, in general arbitrary, which would produce perfectly uniform flow, could theoretically be made by a single application of this process, since the addition and removal of nozzle material could also be made arbitrary. It has been found, however, that corrections so determined are often less than ideal in practice and that the process must be applied repeatedly to obtain a particular degree of flow uniformity.[2, 3]

A considerable number of supersonic wind tunnels have been constructed in which the nozzle contours are formed by bending thin flexible plates between parallel sidewalls by means of jack screws hinged to the

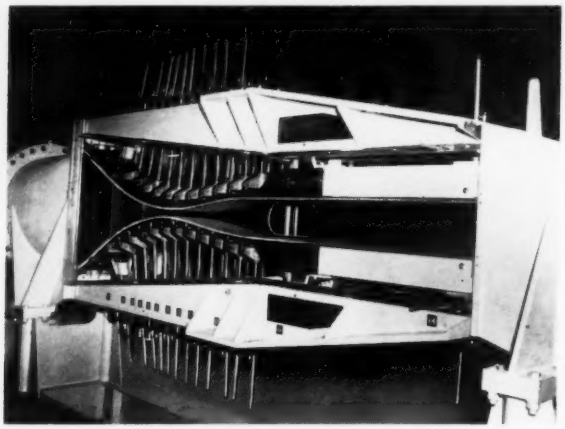

FIG. 1. The flexible plate nozzle of tunnel E-1.

plates at intervals. An example of such construction is shown in Fig. 1, which is a view of the nozzle of Tunnel E-1 of the Gas Dynamics Facility at the Arnold Engineering Development Center. Corrections to the contours of such a flexible wall nozzle are easily effected by small movements of the various jack screws. The plate behavior is governed by various laws of bending and arbitrary corrections to the nozzle profiles cannot be made without using an infinite number of jacks. The usual procedure is to correct flexible plate nozzles until a point of diminishing return is reached. This point is considered to be determined by limitations on the contours imposed by the laws of bending and by deflection of the plate between jacks caused by air loads.

A procedure for determining the best possible correction of a flexible plate nozzle based on the influences of individual jacks on the airflow has been given by Puckett.[4] Because of certain simplifying assumptions made in the development of this method, it has not met with complete success, and most flexible plate nozzles have been corrected by various methods of successive approximation which are partly empirical and partly trial and error. Although satisfactory profiles have been obtained by such methods, the procedure is lengthy and time-consuming, especially when applied to nozzles utilizing a relatively large number of jacks. An investigation of the method of reference 4 has indicated the major shortcoming to be the neglect of the effect of the boundary layer on the process of transmission of disturbances from the wall into the main flow. A modification of the method of reference 4, based on the use of experimentally determined jack influences, has been found capable of producing optimum corrections of a given uncorrected contour with a minimum expenditure of time and effort.

Tunnel E-1, on which the experimental work connected with this investigation was carried out, is a 12-in. intermittent blowdown wind tunnel with a Mach Number range of 1.3 to 5.0. It incorporates a flexible plate (0.20 in. thick) nozzle that is shaped by a series of twelve jacks spaced at 6-in. intervals. The tunnel is supplied with air from a 5,200-cu.ft. high-pressure tank and exhausts into a 200,000-cu.ft. vacuum sphere. Stagnation pressures of 1 to 4 atm. are available, but operation so far has been limited to atmospheric inlet pressure. The nozzle itself is a modified version of the

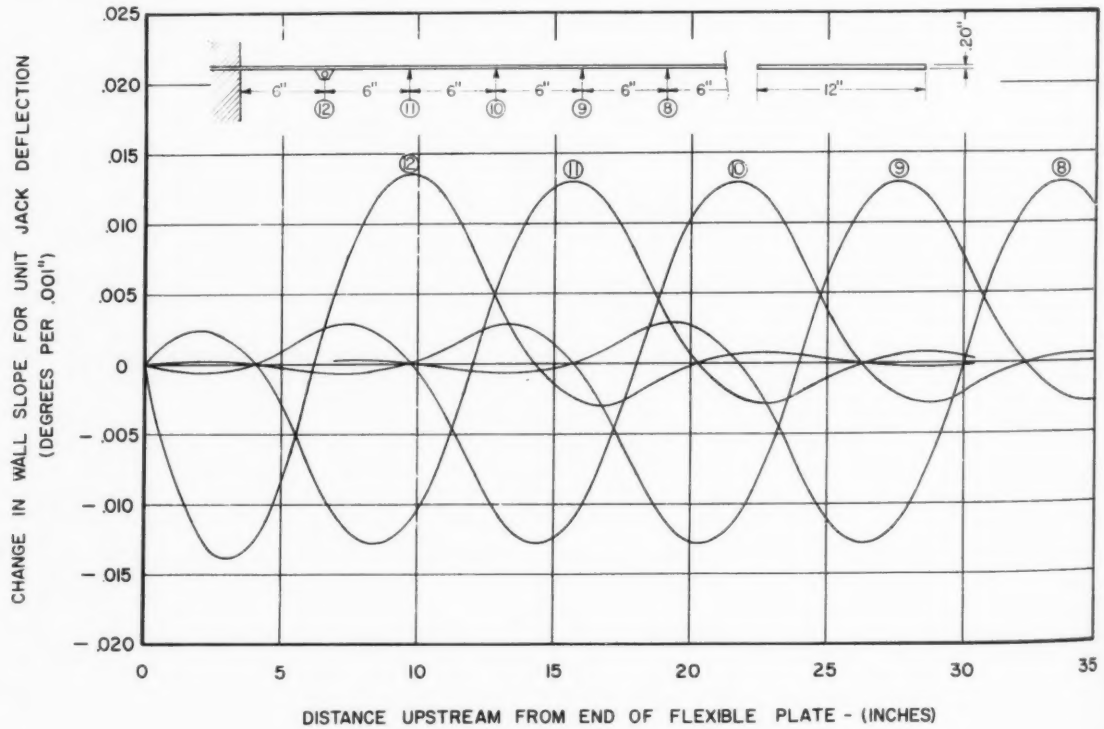

FIG. 2. Theoretical influence of jacks on wall slope.

flexible plate nozzle used in the 12-in. supersonic wind tunnel at the Jet Propulsion Laboratory of the California Institute of Technology.

Analysis of Influence Methods of Flexible Plate Nozzle Correction

Method Proposed by Puckett

The method proposed by Puckett[4] is based upon the establishment of curves of influence of each jack on the airflow in the test region of a nozzle and the performance of certain mathematical operations on these curves which theoretically will yield an optimum correction to that nozzle. The change in slope of the surface of the flexible plates caused by unit deflections of each jack can be calculated by the theory of bending of a simply supported continuous beam, assuming that slope changes for small deflections are independent of the initial curvature of the plates. Curves of jack influence on wall slope calculated for the plates of Tunnel E-1 are shown in Fig. 2. By assuming propagation of disturbances along characteristic lines of the flow, these wall slope changes can be converted to changes in test section airflow:

(a) The correspondence of centerline points x_1 influenced by wall disturbances at points x_{w_1}, Fig. 3, can be determined from a characteristics network.

(b) A change in slope at a point x_{w_1} will produce the same change in flow angle at x_1,

$$\Delta\theta(x_1) = \Delta\theta(x_{w_1}) \tag{1}$$

(c) Mach Number changes at x_1 will be produced by the slope change at x_{w_1} according to

$$\Delta M(x_1) = -\frac{\{1 + [(\gamma - 1)/2]M^2(x_1)\}M(x_1)}{\sqrt{M^2(x_1) - 1}}\,\Delta\theta(x_{w_1}) \tag{2}$$

(d) Proper account must also be made for any waves reflected at x_{w_1}, as well as for the waves that originate at those points.

Since both the bending theory and characteristics theory for small changes in the flow predict that the influences will be linear and obey the superposition principle, the net effect on centerline airflow of any combination of jack deflections is expressed as a linear combination of all the individual jack influences,

$$\sum_{i=1}^{n} \Delta_i I_i(x) \tag{3}$$

For simplicity, attention is focused on corrections of the flow on the nozzle centerline, under the assumption that a betterment of flow there will result in corresponding improvement elsewhere. To simplify the problem further, the deflections Δ_i are restricted to symmetric and antisymmetric deflections of each pair of jacks (top and bottom plate) at the same longitudinal position on the nozzle. A symmetric deflection of a given jack (pair) will introduce identical families of characteristics from each plate. At the intersection of

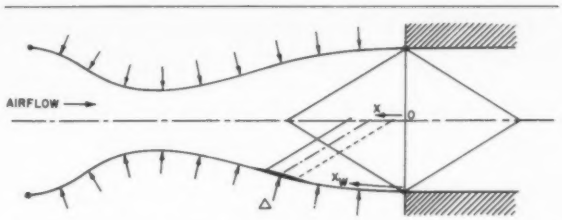

Fig. 3. Propagation of wall corrections to centerline of nozzle.

these characteristics of the nozzle centerline Mach Number changes exactly twice those of either family will be produced, while the airflow deflections will exactly cancel; conversely for antisymmetric deflections. In the above summation (3), if Δ_i is a symmetric deflection, the influence $I_i(x)$ is the effect on Mach Number only; if Δ_i is antisymmetric, $I_i(x)$ is the effect on flow angle. Thus, centerline corrections of Mach Number distribution and flow angularity can be made independently.

All the possible corrections that can be imposed on the flow in a flexible nozzle by symmetric or antisymmetric adjustment of the n jacks is represented by the series (3). If measurement of the airflow in the uncorrected nozzle indicates that an arbitrary distribution of Mach Number or flow angle corrections, $C(x)$, would produce a perfectly uniform flow, the best correction that can be made in practice will be some approximation to $C(x)$, since series (3) cannot represent any arbitrary function. Assuming that this optimum correction will be that which minimizes, in the sense of least squares, the differences between the actual and ideal corrections over some interval in the test region of the nozzle, this condition can be represented as

$$\int_a^b \left[C(x) - \sum_{i=1}^{n} \Delta_i I_i(x)\right]^2 dx = \text{a minimum} \tag{4}$$

Since this minimum must be with respect to any of the n possible jack deflections,

$$\frac{d}{d\Delta_k}\left[\int_a^b [C(x) - \sum_{i=1}^{n} \Delta_i I_i(x)]^2\, dx\right] = 0 \qquad (k = 1, 2, \ldots, n) \tag{5}$$

When the indicated operations are performed, Eqs. (5) reduce to the following system of n linear simultaneous equations in the jack deflections, Δ_i:

$$\sum_{i=1}^{n}\left[\int_a^b I_k(x)I_i(x)\,dx\right]\Delta_i = \int_a^b C(x)I_k(x)\,dx \qquad (k = 1, 2, \ldots, n) \tag{6}$$

Puckett noted that the integrals forming the coefficients of the Δ_i would be fairly tedious to obtain and proposed a variation in which not the best least squares correction is sought but one that merely matches the ideal correction at a finite number of points. By adjustment of n jacks, the ideal correction $C(x)$ could be imposed on the flow at any n points x_j, which condition is represented mathematically by another system of

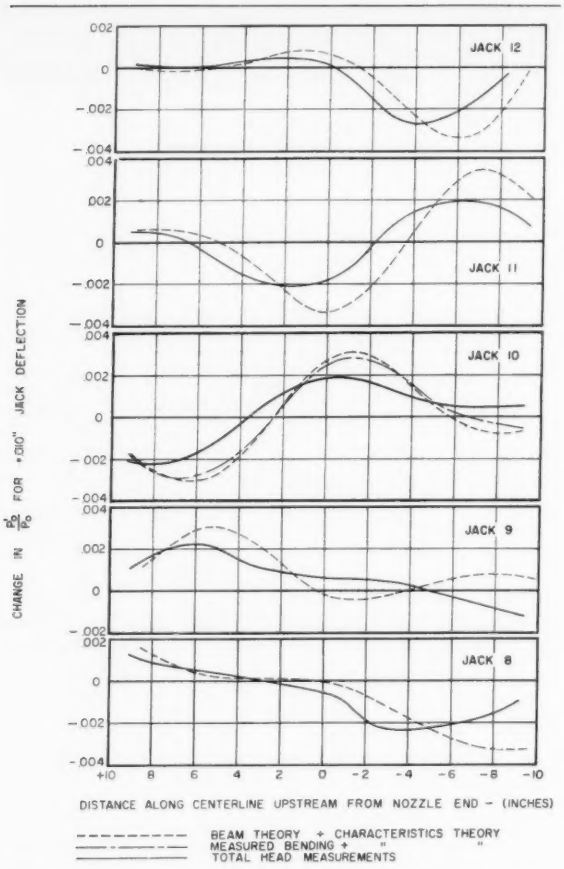

FIG. 4. Comparison of theoretical and experimental jack influence.

simultaneous equations

$$\sum_{i=1}^{n} \Delta_i I_i(x_j) = C(x_j) \qquad (j = 1, 2, \ldots, n) \qquad (7)$$

Here the coefficients of Δ_i are simply the ordinates of the influence curves at the points x_j. By selection of the x_j near peaks of both the influence curves and the ideal correction curve, theoretically the maximum corrections would occur where most needed, and the corrections at points intermediate to the x_j should be small.

Accuracy of the Influence Curves

Initial attempts to correct the Mach Number distribution of the nozzle profiles of Tunnel E-1 by the finite point influence method [Eq. (7)] were unsuccessful, and an extended investigation indicated the failure was mainly the result of inaccuracies in the calculated influence curves. A comparison of these influence curves and similar curves obtained by total head measurements in the tunnel at a nominal $M = 3.5$ is given in Fig. 4. The change in Mach Number is represented by the change in the easily measured pressure ratio, P_0'/P_0, which is a function of local Mach Number alone. Since the calculated influence curves would introduce errors in the nozzle correction at any point equal to the sum of the errors of the individual influence curves at that point, discrepancies shown in Fig. 4 constitute ample reason for the initial failure of the method.

The discrepancies were initially thought to result from simplifying assumptions made in applying the beam theory. However, measurements of the actual plate bending characteristics demonstrated that the beam theory was quite accurate. This can be seen in Fig. 5, which presents a comparison of a calculated slope change curve and a corresponding curve given by numerical differentiation of measured plate deflection data. On the influence curves for jack 10 (Fig. 4), the discrepancies caused by errors in the beam theory can be observed. These are small compared with the total discrepancies, indicating that the discrepancies are largely due to deficiencies of the aerodynamic theory. Such deficiencies obviously result from neglect of the boundary layer. The expected boundary-layer effect would be a general upstream shift of the characteristics network due to both the curvature of the characteristics within the boundary layer and the larger Mach angles accompanying the decrease in Mach Number. Experimental influence curves for jacks 10, 11, and 12 (Fig. 4) clearly exhibit such a shift. Curves for jacks farther upstream are apparently further complicated by disturbance waves originating so far upstream that they negotiate the boundary layer more than once in their transit to the test section.

A further discrepancy was noted in the reduction of the peaks of the influence curves. The changes in the flow produced at the flexible plate were not transmitted in full strength to the main flow because of some damping effect of the boundary layer entirely distinct from the shifting effect just discussed. In most practical applications such damping is of relatively minor importance and, consequently, it has been given little consideration in currently available treatments of the interaction of boundary layers and disturbance waves in supersonic flow. Various investigators have demonstrated theoretically that a weak wave incident on a supersonic shear layer does not reflect as a single wave but as a series of waves constituting a diffusion of the wave in the downstream direction. These reflected waves, nevertheless, have a net strength equal to the strength of the single wave that would be reflected in the absence of the shear layer—i.e., the inviscid reflection.[5–7] Similar results have been found for theoretical models of a subsonic layer adjacent to a supersonic layer except that the diffusion of the disturbance wave extends upstream as well as downstream.[8, 9]

Experimental studies of boundary-layer shock-wave interactions have indicated that at points removed from the immediate vicinity of the interaction the flow is similar to that which would be expected in the absence of the boundary layer. The extent of the interaction region, in which severe nonlinearities such as separation and reattachment occur, decreases as the wave strength decreases. It has been observed, for example, that the nonlinear region is completely ab-

sent, and the flow is close to the theoretical models for a 7° wave incident on a turbulent boundary layer at $M = 3.0$.[10] Thus, theoretical and experimental indications are that extremely weak disturbance waves are merely diffused and not altered in overall strength by a supersonic shear layer. Reflections that occur entirely within the supersonic portion of the boundary layer will be free of damping, but waves resulting from disturbances at the physical flow boundary will definitely be subject to damping between the wall and the sonic streamline because of the basic nature of an elliptic (subsonic) flow field. This damping would be expected to be significant only when the wall deflections are so small as to be of the same order of magnitude as the subsonic portion of the boundary layer, and this provides a possible explanation of the damping of the peaks of the experimental influence curves. Boundary-layer measurements have not yet been made in Tunnel E-1, but at a nominal $M = 3.50$ and atmospheric supply pressure, the boundary layer is known to be turbulent and about 1 in. thick at the end of the nozzle. The subsonic thickness of a turbulent boundary layer at $M = 3.50$ is of the order of 1 per cent of the total thickness, and this is of the same order of magnitude as the deflections of the flexible plate used in establishing the influence curves of Fig. 4. The damping effect at $M = 2.50$ was observed to be less than at 3.50.

The inaccuracies of the calculated influence curves could be reduced somewhat by modifying the calculations to allow for the boundary-layer effects. Computed displacement thicknesses would enable an estimate of the Mach Number reduction and, in turn, the increase in Mach angles. An allowance for curvature of the characteristics could be made by use of the "reflection thickness" concept suggested by Tucker.[6] The theory of interaction between boundary layers and weak waves is not yet sufficiently developed to predict accurately the damping effect that was observed to occur when the boundary layer is much thicker than disturbances causing the waves. In view of the rather large amount of work which would be required to produce only partial reductions of the inaccuracies of the calculated influence curves, the readily obtainable experimental influence curves are much to be preferred for use in making nozzle corrections.

Superposition and Linearity of Influence Curves

The series of Eq. (3) can be justified only if the jack influences obey the superposition principle and are linear functions of the jack deflections. Linearity is required from the standpoint of obtaining solutions of the correction Eqs. (6) and (7). Simple beam theory and characteristics theory for small changes in a nonviscous supersonic flow both predict that linearity and superposition will prevail, but since the boundary layer and any interaction with disturbance waves may behave in nonlinear fashion for changes of the order of magnitude for which the main flow will be linear, the extent to which these two requirements are met in any particular case must be determined by experiment.

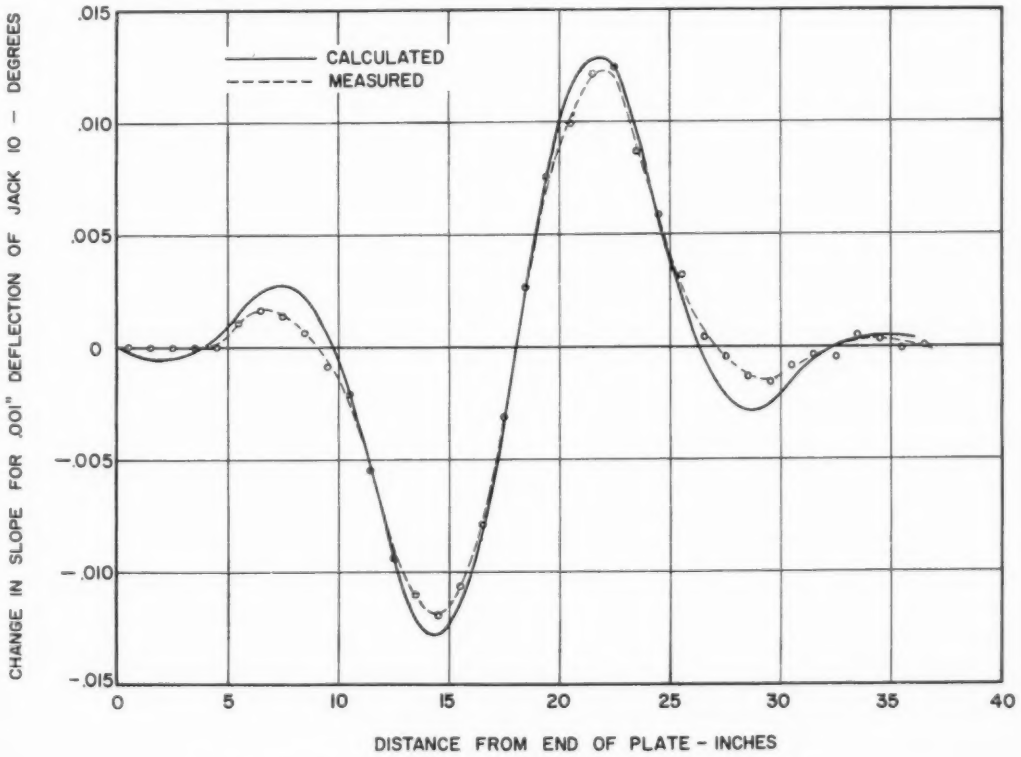

FIG. 5. Comparison of calculated and measured change in slope of plate.

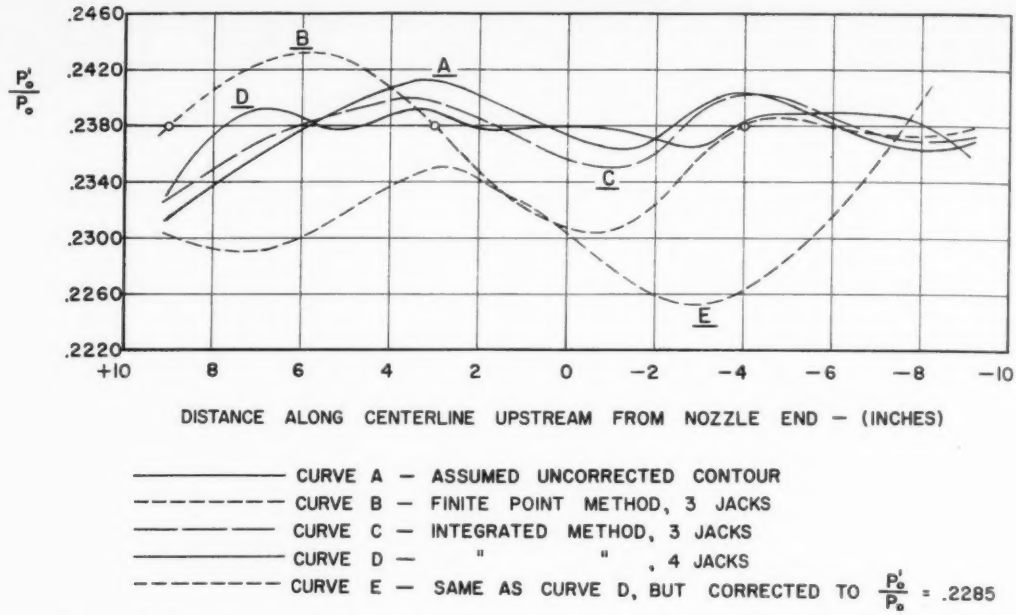

FIG. 6. Centerline pressure distribution for several hypothetical nozzle corrections, nominal $M = 3.50$.

A large number of P_0'/P_0 measurements for a given nozzle profile were compared with P_0'/P_0 values predicted from some other profile by various combinations of the experimental influence curves. Since the discrepancies between these two sets of data were found to represent solely the statistical scatter of the small experimental errors of the individual influence curves, it was concluded that superposition was obtained.

By direct measurement, linearity of influences was found to occur in Tunnel E-1 over an average range of ± 0.035 in. jack deflection at a nominal Mach Number of 3.5. Departure from linearity was gradual, so that for some distance beyond this range the correction equations could be solved as though linear and the resulting jack corrections modified by small increments to allow for the nonlinearity. The simultaneous existence of both linearity and damping of the influences is a confusing phenomenon that could be clarified only by a more detailed investigation.

Considerations of Form of Influence Method Most Suitable for Tunnel E-1 Nozzle Corrections

Since it was suspected that the appropriate form of influence method for any nozzle correction would depend upon factors peculiar to a particular installation, such as boundary layer and relative jack spacing, a number of hypothetical corrections were made to assumed uncorrected pressure distributions utilizing the experimental influence curves of Fig. 4. In Fig. 6 are shown several of the indicated corrected pressure distributions, differing from those that would be produced in the tunnel by only the accumulated random uncertainties of the individual influence curves. Curve (A) is the pressure distribution of an assumed uncorrected profile. Curve (B) demonstrates that the finite point method, Eq. (7), will produce desired corrections at selected points, x_j, but overcorrections at intermediate points may give a poor overall correction. Curves (C) and (D) show the integrated method is a decided improvement which increases with the number of jacks used.

The solution for curve (D), however, would have no practical value because the correction to the last jack was so large that a decided bump would have been produced at the end of the nozzle and at the same time excessive curvature would have been imposed on the plate. Jack corrections that were physically reasonable could be obtained by correcting to some pressure level other than the mean of the uncorrected distribution, but such corrections invariably produced pressure distributions that were poor, curve (E). It was thought that the physical restriction of small corrections to the last jack before the end of the plate could not be recognized by the correction equations, and hence it was arbitrarily decided to omit the last jack from the corrections. It was later found in practice that this omission was unnecessary at low Mach Numbers.

It was also determined that the overcorrections of the finite point method depend upon the location of the x_j, being largely eliminated if the x_j are chosen to coincide with points at which an integrated solution (for the same number of jacks) produces the ideal correction, $C(x)$, exactly. Since these latter points were not observed to be correlated in any particular fashion, successful x_j can be found by trial-and-error process only. Thus the integrated method is preferable for corrections involving a small number of jacks (3 to 6). When a large number of jacks (10 to 20) is used this preference may be reversed for two reasons: First,

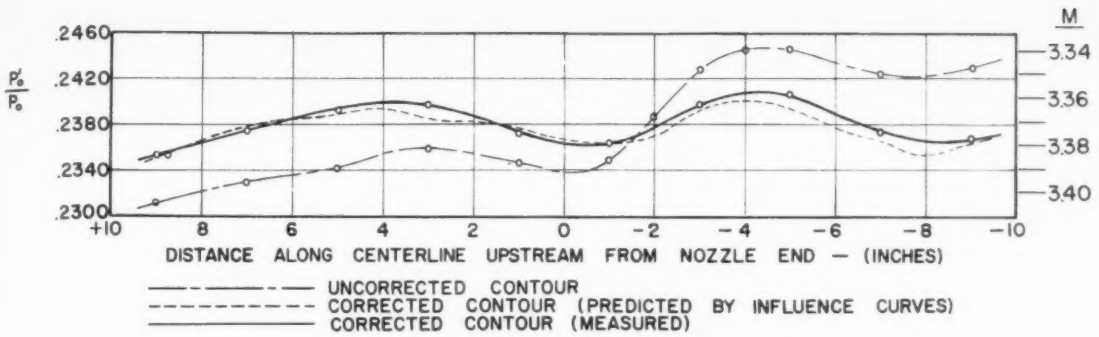

FIG. 7. Correction of pressure distribution at $M = 3.50$.

the number of integrations for the coefficients of (6) becomes inconveniently large $(n^2 + 3n)/2$. Second, sensitivity of the overcorrections to the location of the x_j will probably decrease because of the decreased relative spacing of the points x_j at which desired corrections can be imposed.

EXPERIMENTAL VERIFICATION OF NOZZLE CORRECTIONS USING INFLUENCE METHOD

Procedure

Attempts were made to correct the Mach Number distributions of the nozzle contours of Tunnel E-1 using the influence method of reference 4 modified in accordance with the considerations discussed in the preceding paragraphs. Experimental influence curves were formed by obtaining the influences for the largest jack deflections possible within the linearity limits. The percentage error of the influence curves can be reduced by this procedure since the probable error in total head measurements is the same regardless of the size of the jack deflection. For reasons concerned with the ease of solution of the correction equations, the number of jacks used was restricted to four, and this restriction required that the integrated method of Eq. (6) be used. Jacks 8, 9, 10, and 11 were those used, because jacks upstream of a nozzle inflection point were found to have less influence on the detailed flow distribution in the test rhombus than jacks downstream and because of the omission of jack 12 for the reason discussed previously.

Example of the Formation and Solution of the Correction Equations

In accordance with Eq. (6), the elements of the following matrix equation were formed by numerical integration of all the possible products of two experimental influence curves for $M = 3.5$, Fig. 4, and $C(x)$ was taken to represent correction to $P_0'/P_0 = 0.2380$:

$$\begin{bmatrix} 34.50 & 5.72 & -22.40 & -16.07 \\ 5.72 & 24.52 & -10.47 & -14.04 \\ -22.40 & -10.47 & 33.82 & -6.66 \\ -16.07 & -14.04 & -6.66 & 37.68 \end{bmatrix} = \begin{bmatrix} 78.87 \\ 64.08 \\ -46.70 \\ -82.20 \end{bmatrix} \quad (8)$$

All the elements have been multiplied by an appropriate constant to give numbers of convenient magnitude. The solving of Eq. (8) by the method of minors is simplified by the fact that the left-hand matrix is always symmetric. The solution yielded the following symmetric jack corrections for the top and bottom plates, rounded off to the nearest 0.001 in. corresponding to the least count of the jack indicators:

$$\Delta_8 = +0.047 \text{ in.}$$
$$\Delta_9 = +0.041 \text{ in.}$$
$$\Delta_{10} = +0.034 \text{ in.}$$
$$\Delta_{11} = +0.020 \text{ in.}$$

Pressure and Mach Number Distribution of the Corrected Contours

The above jack corrections were applied to the uncorrected contour for $M = 3.5$, and the total head survey then taken in the tunnel exhibited marked improve-

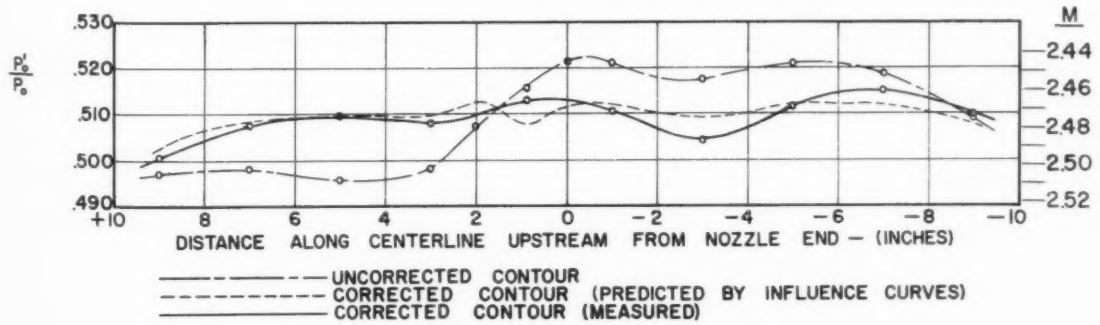

FIG. 8. Correction of pressure distribution at $M = 2.50$.

ment over that of the uncorrected profile, Fig. 7. The overall degree of correction was good, but small discrepancies remained between measured and predicted values of the corrected distribution, indicating that small errors in the experimental influence curves were not completely eliminated. A similar correction procedure was carried out at a nominal $M = 2.5$, and the resulting pressure distribution curves are given in Fig. 8. The influence curves at this Mach Number were not obtained as precisely as at $M = 3.5$, and this is reflected in a slightly lesser degree of correction of the Mach Number distribution. Each of these corrections required the taking of only six total head surveys—i.e., one for the uncorrected contour, four for the influence curves, and one for the corrected contour.

An evaluation of the merit of the influence method should be based on the following considerations:

(1) At $M = 3.5$, the influence method corrected the Mach Number distribution from an original variation of ± 0.032 in M to a variation of ± 0.013 in M (± 0.4 per cent) utilizing only six total head surveys. A previous correction of this contour by a trial-and-error process required over 60 surveys to produce a variation of ± 0.014 in M. This was an extreme case, but the average number of surveys required for nozzle correction by the trial-and-error process was 20 to 30 for each Mach Number.

(2) At $M = 2.5$ the influence method corrected the Mach Number distribution from a variation of ± 0.033 in M to a variation of ± 0.018 in M (± 0.7 per cent) using six surveys. No direct comparison with the trial-and-error method is possible because no attempt had been made to correct the uncorrected contour for this Mach Number by trial-and-error means.

Conclusions

(1) An influence method has been verified in which empirical influence curves can be used to determine the corrections to the calculated contours of a flexible wall nozzle which will produce a more uniform flow. Calculated influence curves based on beam theory and simple characteristics theory will not be sufficiently accurate if a relatively thick boundary layer is present. Experimental influence curves are so easily obtained that they are to be preferred even in cases where the boundary layer is thin enough to allow an approximate correction for boundary-layer effects.

(2) Since the superposition and linearity characteristics will vary from nozzle to nozzle and with Reynolds Number and Mach Number for a given nozzle, they should be determined experimentally in any given case. Jack corrections given by solutions of the correction equations should fall within the limits of superposition and linearity. To achieve physically reasonable jack corrections it was found necessary in some instances to omit the last downstream jack from the correction.

(3) Two methods of correcting flexible nozzles by influence methods are available: an integral method that yields an optimum correction, and a finite-point method that yields exact corrections at a finite number of points. The integral method is generally preferable. It is, in fact, required for corrections involving a small number of jacks if reversion to a lengthy trial-and-error process of selecting the locations of the finite points is to be avoided, because the exact location of these points is a critical factor in determining the size of overcorrections at intermediate points.

(4) The finite-point method will give an approximation to the optimum correction of the integral method. The degree of approximation will increase with the number of jacks involved, since the sensitivity of the overcorrections to the location of the chosen correction points will decrease as the relative jack spacing decreases. For nozzle corrections involving a large number of jacks, the finite method then may become more practical, since the number of integrations required for the integral method increases rapidly with the number of jacks.

(5) The above conclusions have been confined to corrections of centerline Mach Number distribution by symmetric deflections of the jacks. It is probable that the same conclusions will hold for independent corrections of flow angularity by antisymmetric jack deflections.

References

[1] Harrop, R., Bright, P. I., Salmon, J., and Caiger, M. T., *Design and Testing of Supersonic Nozzles*, British ARC R.-M. 2712, 1953.

[2] Meyer, R. E., and Holt, M., *The Correction of Wind Tunnel Nozzles for Two-dimensional Supersonic Flow*, The Aeronautical Quarterly, Vol. II, Part III, p. 195, November, 1950.

[3] LaBerge, J. G., *Design, Calibration and Correction of a 1.6 Mach Number Nozzle*, National Aeronautical Establishment of Canada, Laboratory Report LR-41, November 5, 1952. (ASTIA No. AD-2068.)

[4] Puckett, Allen E., *Design and Operation of a 12" Supersonic Wind Tunnel*, Institute of Aeronautical Sciences, Preprint No. 160, July 16, 1948.

[5] Marble, F., *The Reflection of a Weak Wave from a Supersonic Shear Layer*, Part III of "Problems in Shock Reflection," GALCIT Transonic Research Group, Final Report on Contract No. W-33-039-ac-1717(11592), USAF, July 1948. (ASTIA No. ATI 41302.)

[6] Tucker, Maurice, *Approximate Turbulent Boundary Layer Development in Plane Compressible Flow along Thermally Insulated Surfaces with Application to Supersonic-Tunnel Contour Correction*, NACA TN No. 2045, March, 1950.

[7] Chang, C. C., and Chu, B. T., *Propagation of Disturbances Through Shear Layers of Compressible Flow*, Part I of Final Report on Supplemental Agreement No. 4(52-141), Contract AF 33(038)-12919, OSR, ARDC, USAF, September 25, 1952, Department of Aeronautics, Johns Hopkins University. (ASTIA No. ATI 170700.)

[8] Tsien, H. S., and Finston, M., *Interaction Between Parallel Streams of Subsonic and Supersonic Velocities*, *Journal of the Aeronautical Sciences*, Vol. 16, No. 9, pp. 515–528, Sept., 1949.

[9] Ritter, A., and Kuo, Y. H., *Reflection of a Weak Shock Wave from a Boundary Layer along a Flat Plate, I—Interaction of Weak Shock Waves with Laminar and Turbulent Boundary Layer Analyzed by Momentum-Integral Method*, NACA TN No. 2868, January, 1953.

[10] Bogdonoff, S. M., Kepler, C. E., and Sanlorenzo, E., *A Study of Shock Wave Turbulent Boundary Layer Interaction at $M = 3.0$*, Princeton University Report No. 222, July, 1953.

Unsteady Aerodynamic Reactions on Airfoils in Cascade*

F. SISTO†

Wright Aeronautical Division, Curtiss-Wright Corporation

SUMMARY

For one blade in a cascade of fluttering blades, under conditions of small incidence and small camber, the aerodynamic reactions are calculated and are found to depend strongly on the phase between the motions of adjacent blades. As compared to one isolated blade the lift due to bending and the moment due to pitching are both changed mainly in the out-of-phase component, whereas the lift due to pitching and the moment due to bending are changed predominantly in the in-phase component. These effects increase with decreased blade spacing. It is concluded that only for exceedingly small gap/chord ratios can the effect of cascading account for any large decrease in critical flutter speeds.

NOTATION

a = fraction of semichord from midchord to rotation point (elastic axis), positive aft
b = blade semichord
C_L = lift coefficient, $C_L = \bar{L}/4qb$
C_M = moment coefficient, $C_M = \bar{M}/4qb^2$
L = lift, positive down
M = aerodynamic moment, positive stalling, taken about the rotation point
p = pressure
Δp = pressure difference
q = dynamic pressure, $q = \rho V^2/2$
t = time
V = stream velocity
ρ = density
ϕ = velocity potential

Subscripts

a = airfoil (blade)
h = due to pure bending
n = nth blade from central (or reference) blade
w = wake
α = due to pure pitch

Superscripts

$\bar{(\ )}$, bar = complex amplitude of a harmonically varying quantity

INTRODUCTION

THE POSSIBILITY OF serious aerodynamic excitation in the blading of axial-flow compressors first received consideration around 1945. At that time it was noted[1] that certain critical speeds (stresswise) of compressor test rigs could not be correlated satisfactorily on a conventional Campbell diagram: the resonances occurring away from the integral engine-order lines.

Received July 9, 1954.

* Portions of this paper are from an investigation conducted at the Gas Turbine Laboratory, Massachusetts Institute of Technology. Permission to include these portions is gratefully acknowledged.

† Head, Flutter Unit.

Inquiries into a possible mechanism have yielded the following possibilities:

(1) Stall flutter, or single-degree-of-freedom excitation due to periodic separation and reattachment of the flow about the blades.[2–6]

(2) Propagating stall, or the periodic entrance of the blades into stalled regions that rotate at a fraction of compressor speed around the blade annulus.[6–10]

(3) Cascade flutter due to alteration of aerodynamic reactions by interference of neighboring blades.[4, 11, 12]

(4) Shock flutter, akin to compressibility flutter of aircraft components, but complicated by multiplane effects and by involved flow passage geometry.[4]

(5) Buffeting between adjacent blade rows, or due to fixed obstructions in the flow passage.[4, 13, 14]

(6) Mixed effects.

Calculations of classical flutter for airfoils with compressor blade properties invariably yielded critical air speeds several times larger[2] than the critical speed observed experimentally. Consequently greater credence was given to items (1) and (2). However, the possibility of strong cascading effects that suitably modify the classical flutter expressions so as to account, in part at least, for the lowered critical air speeds was not overlooked. Mendelson[3] admitted this possibility, and an approximate correction was developed by Bellenot and d'Epinay[11] for steady cascading effects. Reports due to Reissner,[15] Timman,[16] Gordon,[17] and Lilley[12] may be interpreted as giving the modification of classical theory which is dependent on time-varying interference effects for the special case of adjacent blades oscillating in antiphase. (Actually this particular phasing corresponds to the wind tunnel wall correction problem.) In the present investigation the scope is limited to a generalization of these cascade interference effects.

CASCADING EFFECTS

With the introduction of cascaded airfoils the flutter problem assumes a new complexity characterized by an additional length ratio. The dimensionless ratio that fixes the cascades geometry is taken to be

$$P = (\pi b/s)e^{i\beta}$$

where b is blade semichord, s is blade spacing, and β is cascade stagger angle (see Fig. 1). Actually, when β is different from zero, P is complex and contains two new length ratios.

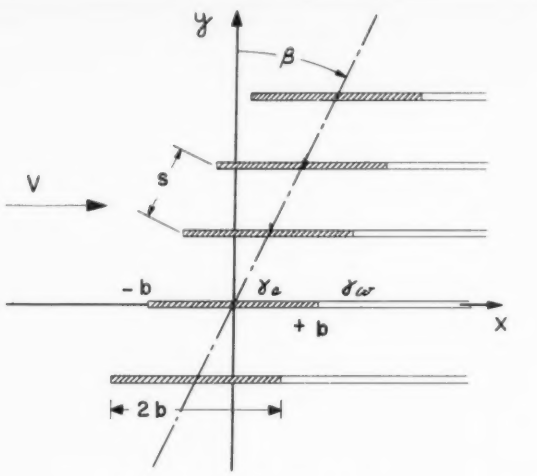

FIG. 1. Cascade nomenclature.

In addition to this formal complication, certain other difficulties of a practical nature appear. In order to obtain simple analytical expressions for the lift and moment on a blade in a fluttering cascade, it is convenient to assume some regularity or ordered nature in the phenomenon. Consequently, the assumption is made that the blades are oscillating in the same mode, at the same frequency, and with some constant phase, $m\pi$, between the motions of adjacent blades.

Restricting the development to a cascade of thin, slightly cambered blades and assuming small displacements, small stream turning and plane wakes, the integral equation for the amplitude of the vorticity distribution, $\bar{\gamma}_a$, may be formulated along lines laid down by Schwarz,[19] Söhngen,[20, 21] and Reissner.[15, 22, 23] The result (assuming harmonic motion of circular frequency ω and a semichord of unity) is

$$(|x| \leq 1), \qquad \bar{v}_a(x) = -\frac{1}{2\pi} \oint_{-1}^{1} \bar{\gamma}_a(\xi)\, K[m, P(x-\xi)]\, d\xi - \frac{1}{2\pi} \int_{1}^{\infty} \bar{\gamma}_w(\xi) K[m, P(x-\xi)]\, d\xi \quad (1)$$

where the kernel, K, is derived in Appendix (A) and reduces, for $\beta = 0$, to

$$(|m| \leq 1), \qquad K = P \times \cosh\,[(1-|m|)P(x-\xi)]\,\operatorname{csch}\,[P(x-\xi)] \quad (2)$$

The vertical velocity distribution at the central blade, $\bar{v}_a$, is assumed to be given.

For infinite blade spacing, $P \to 0$, Eq. (1) reduces to the well-known equation for a single airfoil in which $K = (x-\xi)^{-1}$.

With the auxiliary condition

$$\bar{\gamma}_w(x) = ik\bar{\Gamma}e^{-ik(x-1)} \quad (3)$$

where

$$\bar{\Gamma} = \int_{-1}^{1} \bar{\gamma}_a(x)\, dx \quad (4)$$

$$k = \omega b/V \quad (5)$$

the integral Eq. (1) may be solved for $\bar{\gamma}_a$ given any m, P, and $\bar{v}_a$. Having obtained $\bar{\gamma}_a$ it is then possible to obtain the distribution of pressure difference from the generalized Bernoulli equation for unsteady flow,

$$-p/\rho = (\partial\phi/\partial t) + V(\partial\phi/\partial x)$$

which, under the previous assumption, becomes

$$\Delta\bar{p}_a/\rho V = \bar{\gamma}_a(x) + ik\int_{-1}^{x} \bar{\gamma}_a(\xi)\, d\xi \quad (6)$$

The oscillatory lift and moment may then be obtained by suitable integrations along the chord.

Approximate Solution

In the present calculations, since K is real and odd ($\beta = 0$), the kernel is approximated by an expression of the form

$$K[m, P(x-\xi)] = [1/(x-\xi)] + A(x-\xi) + B(x-\xi)^3 \quad (7)$$

where the fitting constants A and B are determined in

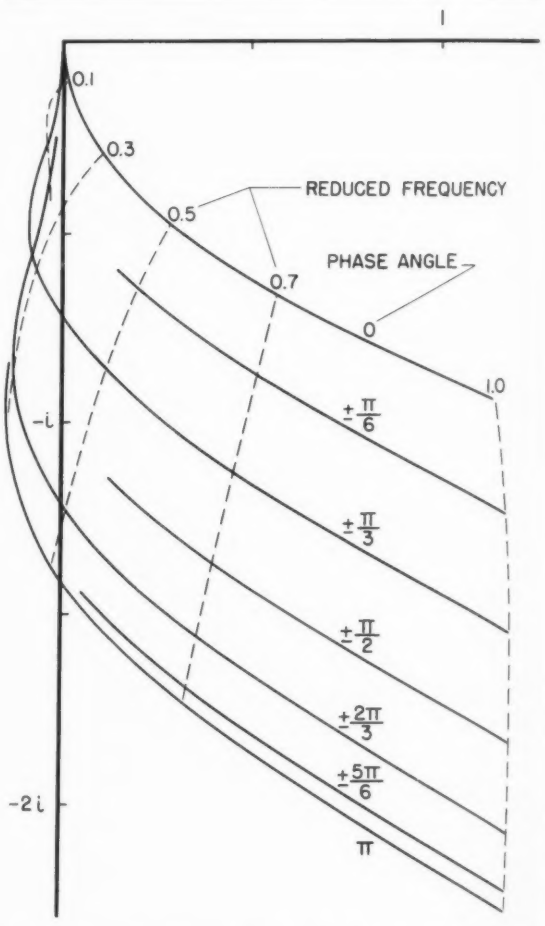

FIG. 2. Lift coefficient due to pure bending, $C_{L\dot{h}}$, for zero stagger and unit gap/chord.

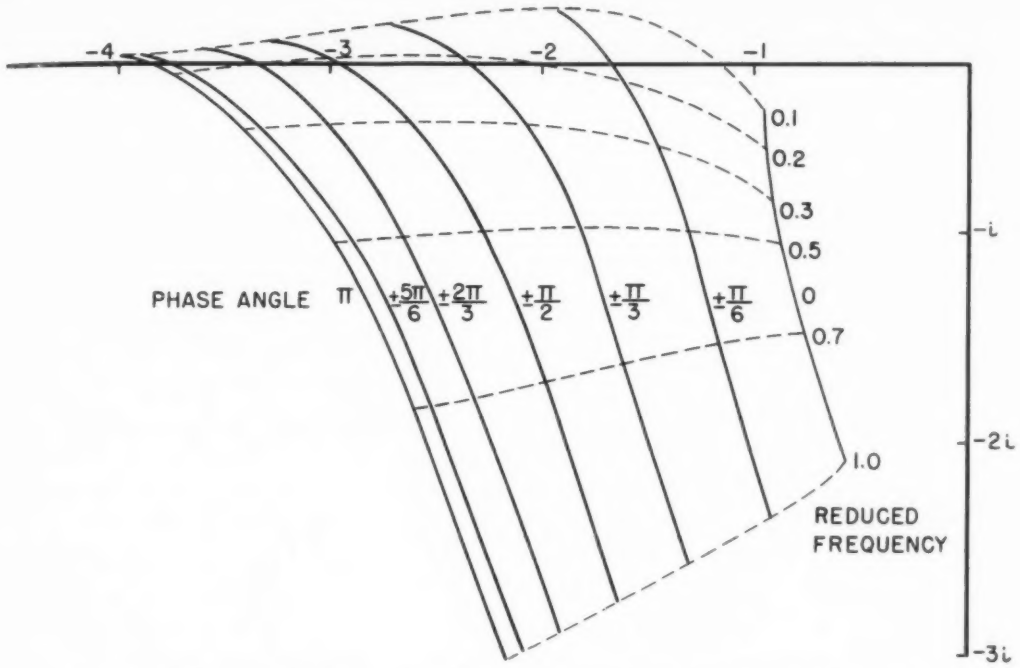

FIG. 3. Lift coefficient due to pure pitch, C_{L_α}, for zero stagger, unit gap/chord, and $a = -0.35$.

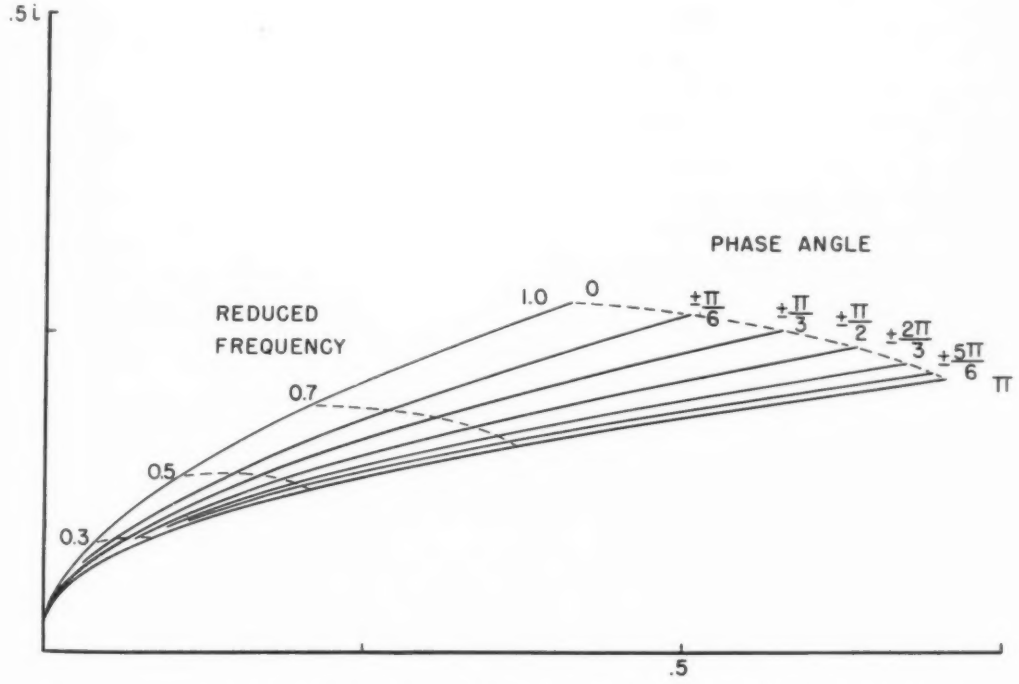

FIG. 4. Moment coefficient due to pure bending, C_{M_h}, for zero stagger, unit gap/chord, and $a = -0.35$.

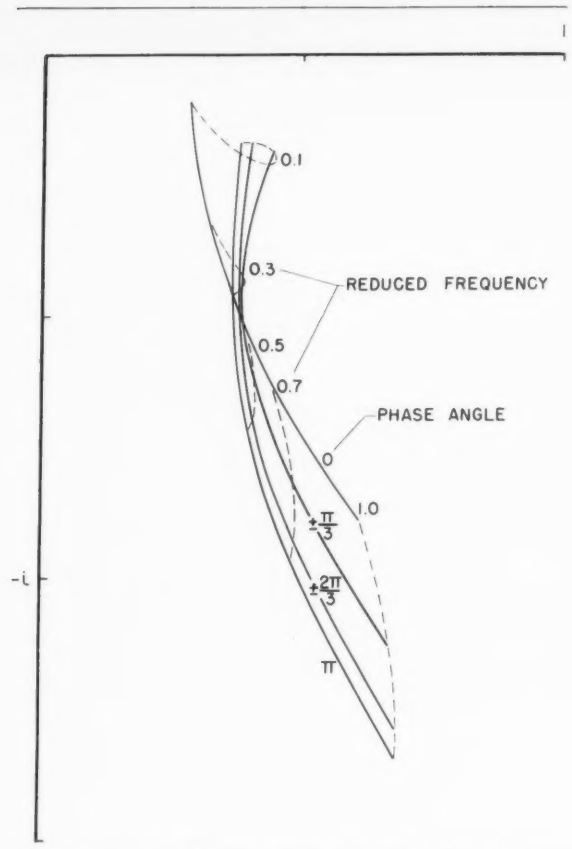

FIG. 5. Moment coefficient due to pure pitch, C_{M_α}, for zero stagger, unit gap/chord, and $a = -0.35$.

the least square sense on the interval $(-2P, 2P)$ for each combination of P and m. This approximation is integrated only over finite intervals. With this simplification the solution proceeds somewhat along the lines of reference 15. Use is made of the Schwarz inversion formulas,[19] and the lift and moment are obtained, finally, in the form of three simultaneous equations in three unknowns. These equations may then be solved by Cramer's rule. (The third unknown is the second moment of the pressure difference.) The development is lengthy[18] and is omitted here. For reference purposes the results may be displayed in the following contracted form:

$$\bar{L} = \pi\rho b V^2 \Delta^{-1}(h_1\bar{\alpha} + h_2 a\bar{\alpha} - h_2\bar{h}/b) \quad (8)$$

$$\bar{M} = \pi\rho b^2 V^2 \Delta^{-1}(j_1\bar{\alpha} + j_2 a\bar{\alpha} - j_2\bar{h}/b) - ab\bar{L} \quad (9)$$

where $\bar{L}$, $\bar{M}$, $\bar{\alpha}$, and $\bar{h}$ are the complex amplitudes of lift, moment, pitching displacement, and bending displacement, respectively. Δ, h_1, h_2, j_1, and j_2 are complicated algebraic functions of A, B, k, and C_c. The "cascade Theodorsen function," C_c, is given by the expression

$$C_c = (Y_1 + f_1 J_1)/[Y_1 + f_1 J_1 + i(Y_0 + f_1 J_0)] \quad (10)$$

where the Y's and J's are Bessel functions with argument k. A listing of the functions Δ, f_1, h_1, h_2, j_1, and j_2 appears in reference 18.

This latter group of functions shows the proper asymptotic behavior as blade spacing increases ($P \to 0$). Furthermore, a comparison with an exact solution (for $m = 1$, $P = 1.82$, reference 17) shows the accuracy of the approximation, Eq. (7), to be fairly good.

Discussion of Results

Expressions (8) and (9) are rather cumbersome when expanded. Consequently, the discussion will be conducted for some numerical examples in which $a = -0.35$.

The first numerical calculations are for a cascade of zero stagger and pitch/chord ratio of unity. The various aerodynamic coefficients are displayed graphically in Figs. 2 through 5 as functions of phase $m\pi$ and reduced frequency, k. In each case the curve for an isolated blade, if it were drawn in, would fall approximately midway between the curves for $m = 0$ and $m = 1$ (with some minor exceptions).

It is interesting to note that in no case is there a radically different type of behavior due to cascading. The lift due to bending and the moment due to pitching (C_{L_h} and C_{M_α}) are both changed mainly in the out-of-phase component, whereas the lift due to pitching and

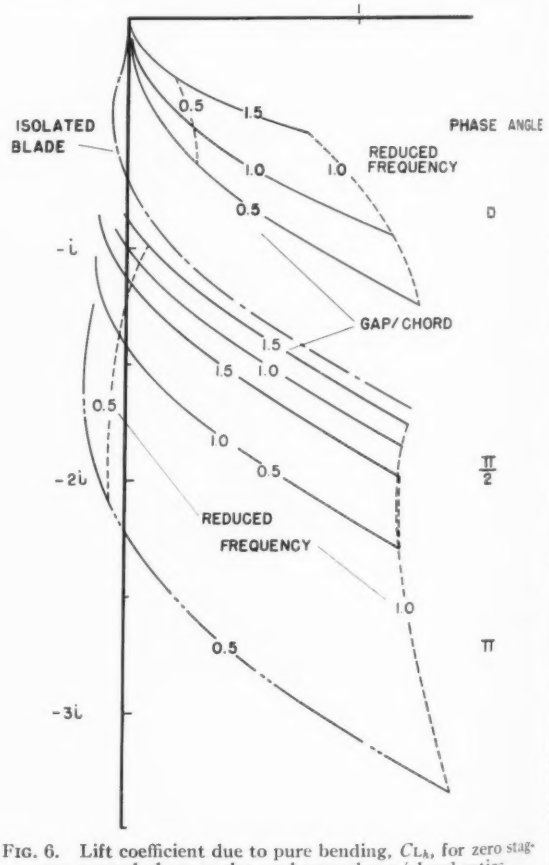

FIG. 6. Lift coefficient due to pure bending, C_{L_h}, for zero stagger, several phase angles, and several gap/chord ratios.

the moment due to bending (C_{L_a} and C_{M_h}) are changed predominantly in the in-phase component.

The effect of solidity, $s/2b$, on the oscillatory aerodynamic reactions is illustrated by one sample plot, Fig. 6, showing lift due to bending. Only for the exceedingly small gap/chord ratios do the aerodynamic reactions seem to be changed sufficiently to account for any several-fold changes in critical flutter speed. This statement is confirmed, essentially, by the experimental work of Lilley.[12]

It seems safe to conclude, therefore, that the radically lowered critical speeds actually encountered in axial-flow compressors are not caused by interference effects in classical flutter aerodynamics.

Appendix (A)

In this appendix an expression is developed for the velocities induced by a cascade of fluttering blades under conditions of two-dimensional potential flow.

Consider a row of equidistant point vortices, of spacing s, and of strength $\gamma_n(\xi, t)\, d\xi$, disposed along a line inclined at an angle β to the y-axis as in Fig. (7). The velocities induced by this array at any point z may be expressed, according to the theorem of Biot and Savart, in complex notation, as

$$dw(z) = du - i\, dv = \frac{i\, d\xi}{2\pi} \sum \frac{\gamma_n(\xi, t)}{z - z_n}$$

where

$$z_n = \xi + ins e^{-i\beta}, \qquad n = 0, \pm 1, \pm 2, \ldots$$

and z is the complex variable, $z = x + iy$. All summations in this appendix are on n, and the range of this index is from $-\infty$ to $+\infty$, unless otherwise noted.

If interest is confined to velocities at the x-axis, there may be written

$$dw(x) = \frac{ie^{i\beta}\, d\xi}{2s} \sum \frac{\gamma_n(\xi, t)}{\pi e^{i\beta}(x - \xi)/s - in\pi}$$

In order to synthesize a cascade of blades it becomes necessary to distribute vorticity along lines representing the chords and wakes of the airfoils. The expression for the total induced velocity at any point on the x-axis becomes

$$w(x) = u - iv = \frac{iP}{2\pi} \oint_{-1}^{\infty} \sum \frac{\gamma_n(\xi, t)\, d\xi}{P(x - \xi) - in\pi}$$

where $P = \pi be^{i\beta}/s$ and the semichord b has been taken equal to unity.

Assuming now that the (distributed) vorticity is an harmonic function of time, say

$$\gamma_n(\xi, t) = \gamma_0(\xi) \cos(\omega t + nm\pi), \qquad (|m| \leqq 1)$$

the following summation appears under the integral sign:

$$\sigma \equiv \sum \{\cos(\omega t + nm\pi)/[P(x - \xi) - in\pi]\}$$

This summation may be expanded, in several steps, to yield

$$\sigma = \cos \omega t \left\{ \frac{1}{P(x - \xi)} + \sum{}' \cos nm\pi \times \left[\frac{1}{P(x - \xi) - in\pi} + \frac{1}{in\pi} \right] \right\} - \sin \omega t \left\{ \sum{}' \sin nm\pi \times \left[\frac{1}{P(x - \xi) - in\pi} + \frac{1}{in\pi} \right] - \sum{}' \frac{\sin nm\pi}{in\pi} \right\}$$

where $\sum'$ indicates that $n = 0$ is to be excluded in the summation, and in the first summation the terms for n and $-n$ are always to be taken in pairs. By an application of the Mittag-Leffler theorem,[24] it may be shown that

$$\sum{}' \cos nm\pi \left[\frac{1}{P(x - \xi) - in\pi} + \frac{1}{in\pi} \right] = \cosh \left[\left(\frac{|m|}{m} - m \right) P(x - \xi) \right] \times \operatorname{csch} [P(x - \xi)] - \frac{1}{P(x - \xi)}$$

$$\sum{}' \sin nm\pi \left[\frac{1}{P(x - \xi) - in\pi} + \frac{1}{in\pi} \right] = i \sinh \left[\left(\frac{|m|}{m} - m \right) P(x - \xi) \right] \times \operatorname{csch} [P(x - \xi)] - i \left(\frac{|m|}{m} - m \right)$$

and consequently

$$\sigma = \cos \omega t \cosh \left[\left(\frac{|m|}{m} - m \right) P(x - \xi) \right] \times \operatorname{csch} [P(x - \xi)] - i \sin \omega t \times \sinh \left[\left(\frac{|m|}{m} - m \right) P(x - \xi) \right] \operatorname{csch} [P(x - \xi)]$$

since it can be verified that

$$\sum{}' \sin nm\pi / in\pi = -i[(|m|/m) - m]$$

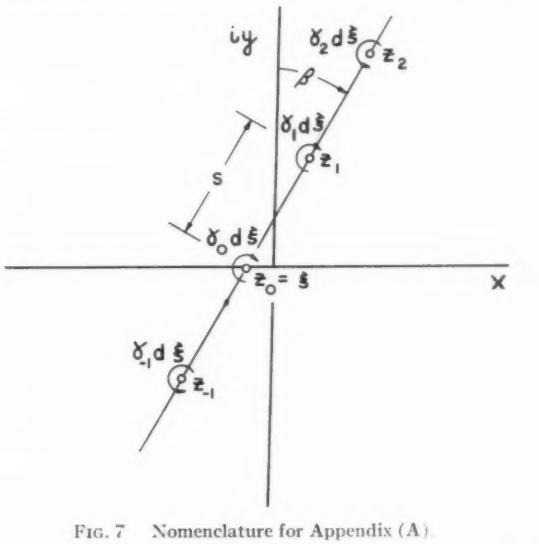

Fig. 7 Nomenclature for Appendix (A)

The final expression for the vertical component of the induced velocity may be written

$$v(x) = -\frac{1}{2\pi} \oint_{-1}^{\infty} \gamma_0(\xi) \times [\text{R.P.}(\sigma') \cos \omega t + \text{I.P.}(\sigma'') \sin \omega t]\, d\xi$$

where

$$\sigma' = P \cosh \left[\left(\frac{|m|}{m} - m \right) P(x - \xi) \right] \operatorname{csch} [P(x - \xi)]$$

$$\sigma'' = P \sinh \left[\left(\frac{|m|}{m} - m \right) P(x - \xi) \right] \operatorname{csch} [P(x - \xi)]$$

For P real and with the replacement of $\gamma_0 \cos \omega t$ by $\bar{\gamma} e^{i\omega t}$, this reduces to Eqs. (1) and (2).

References

[1] Manson, S. S., et al., *Factors Affecting Vibration of Axial-Flow Compressor Blades*, Proceedings of the Society for Experimental Stress Analysis, Vol. 7, No. 2, pp. 1–15, 1948.

[2] Shannon, J. F., *Vibration Problems in Gas Turbines, Centrifugal and Axial-Flow Compressors*, British ARC R. and M. No. 2226, March, 1945.

[3] Mendelson, A., *Aerodynamic Hysteresis as a Factor in Critical Flutter Speed of Compressor Blades at Stalling Conditions*, Journal of the Aeronautical Sciences, Vol. 16, No. 11, pp. 645–652, November, 1949.

[4] Schnittger, J. R., *The Aerodynamic Mechanism of Vibrating Compressor Blades*, Sc.D. Thesis, M.I.T., March, 1953.

[5] Sisto, F., *Stall-Flutter in Cascades*, Journal of the Aeronautical Sciences, Vol. 20, No. 9, pp. 598–604, September, 1953.

[6] Pearson, H., *The Aerodynamics of Compressor Blade Vibration*, Proceedings of the Fourth Anglo-American Aeronautical Conference, 1953.

[7] Iura, T., and Rannie, W. D., *Observations of Propagating Stall in Axial-Flow Compressors*, C.I.T. Mechanical Engineering Laboratory Report No. 4, Pasadena, April, 1953.

[8] Sears, W. R., *On Asymmetric Flow in an Axial-Flow Compressor Stage*, Journal of Applied Mechanics, Vol. 20, No. 1, pp. 57–62, March, 1953.

[9] Emmons, H. W., et al., *Compressor Surge and Stall Propagation*, ASME Paper No. 53-A-65, December, 1953.

[10] Huppert, M. C., and Benser, W. A., *Some Stall and Surge Phenomena in Axial-Flow Compressors*, Journal of the Aeronautical Sciences, Vol. 20, No. 12, pp. 835–845, December, 1953.

[11] Bellenot, Ch. and d'Epinay, J. L., *Self-Induced Vibrations of Turbo-Machine Blades*, Brown Boveri Review, Vol. 37, No. 10, pp. 368–376, October, 1950.

[12] Lilley, G. M., *An Investigation of the Flexure-Torsion Flutter Characteristics of Aerofoils in Cascade*, The College of Aeronautics, Cranfield, Report No. 60, May, 1952.

[13] Kemp, N. H., and Sears, W. R., *Aerodynamic Interference Between Moving Blade Rows*, Journal of the Aeronautical Sciences, Vol. 20, No. 9, pp. 585–597, September, 1953.

[14] Söhngen, H., *Durchgang einer Potentialstörung durch einen Leitschaufelkranz*, Ingenieur-Archiv, Bd. 20, 1952.

[15] Reissner, E., *Wind Tunnel Corrections for the Two-Dimensional Theory of Oscillating Airfoils*, Cornell Aeronautical Laboratory Report No. SB-318-S-3, April, 1947.

[16] Timman, R., *The Aerodynamic Forces on an Oscillating Aerofoil Between Two Parallel Walls*, Applied Scientific Research, Vol. A3, No. 1, pp. 31–57, 1951.

[17] Gordon, C. H., *Tunnel Wall Effects for Non-Uniform Two-Dimensional Motion of Thin Airfoils in Incompressible Flow*, Ph.D. Thesis, M.I.T., 1951.

[18] Sisto, F., *Flutter of Airfoils in Cascade*, Sc.D. Thesis, M.I.T., September, 1952.

[19] Schwarz, L., *Berechnung der Druckverteilung einer harmonisch sich verformenden Tragfläche in ebener Stromung*, Luftfahrtforschung, Bd. 17, Lfg. 11/12, pp. 379–386, 1940.

[20] Söhngen, H., *Bestimmung der Auftriebsverteilung für beliebige instationare Bewegungen (Ebenes Problem)*, Luftfahrtforschung, Bd. 17, Lfg. 11/12, pp. 401–420, 1940.

[21] Söhngen, H., *Die Losungen der Integralgleichung* $g(x) = \frac{1}{2\pi} \oint_{-a}^{a} f(\xi)\, d\xi/(x - \xi)$ *und deren Anwendung in der Tragflugeltheorie*, Math Z., Vol. 45, pp. 245–264, 1939.

[22] Reissner, E., *On The General Theory of Thin Airfoils for Non-Uniform Motion*, NACA TN No. 946, August, 1944.

[23] Reissner, E., *Effect of Finite Span on the Airload Distributions for Oscillating Wings, I-Aerodynamic Theory of Oscillating Wings of Finite Span*, NACA TN No. 1194, March, 1947.

[24] Whittaker, E. T., and Watson, G. N., *A Course of Modern Analysis*, pp. 134–136; The University Press, Cambridge, 1946.

An Authorized Binding for Journal of the Aeronautical Sciences

Arrangements have been made by the Institute of the Aeronautical Sciences for members and subscribers to have their Journals bound into distinctively designed books.

Twelve issues, January through December, bound in best grade blue washable buckram, imprinted with your name on cover, cost but $3.45 per volume.

Ship Journals parcel post insured. Within 30 days after receipt, bound volumes will be shipped prepaid in the U.S.A. Full remittance must accompany order.

Publishers' Authorized Bindery Service
(*Binders of all Journals*)

308 West Randolph St. Chicago 6, Ill.

On the Motion of a Flat Plate at High Speed in a Viscous Compressible Fluid—II. Steady Motion

K. STEWARTSON*

Guggenheim Aeronautical Laboratory, California Institute of Technology

SUMMARY

The theory of the steady flow of a viscous compressible fluid past a flat plate at high Mach Number due to Lees and Probstein[6-8] is extended by a more complete discussion of the flow in the inviscid layer between the shock wave and the boundary layer. It is shown that similar solutions exist in this layer, analogously to those found by Li and Nagamatsu[9] in the boundary layer, and that the two may be joined to give, allowing one minor assumption,† a full account of the flow. It is shown that the boundary-layer equations may be reduced to those for an incompressible fluid and that the von Kármán-Pohlhausen method describes the flow in it with good accuracy. The tangent wedge approximation for the pressure on the plate, used by Lees and his collaborators, is found to be in deficit by 10 per cent for air. Finally, it is shown that the theory for weak interaction[7] cannot be extended further without a complete knowledge of the flow.

NOTATION

(x, y)	= distances along and normal to the plate
(u, v)	= velocity components in the (x, y) directions
p, ρ, T	= pressure, density, and absolute temperature at (x, y)
γ	= ratio of specific heats
σ	= Prandtl Number taken = 1
ν	= kinematic viscosity
U	= velocity of undisturbed fluid
a_0	= velocity of sound in undisturbed fluid
M	= U/a_0
$Y = Y(x)$	= equation of shock wave
ψ	= stream function
$S(\psi)$	= entropy function

Subscripts

0 = conditions in undisturbed fluid
1 = conditions just behind the shock wave
E = conditions at the outer edge of the boundary layer

(1) INTRODUCTION

IN A PREVIOUS PAPER,[10] which we shall refer to as I throughout, the flow induced by the impulsive motion, in its own plane, of an infinite plate immersed in a viscous compressible fluid was considered, assuming that the characteristic Mach Number M was large. It was shown that, provided $[\nu_0/(a_0^2 t)] \log M \ll 1$ where ν_0 is the coefficient of kinematic viscosity, a_0 is the velocity of sound in the undisturbed fluid, $M = U/a_0$, where U is the constant velocity of the plate, and t is the time measured from the instant at which motion began, it is possible to justify, on the grounds of consistency, a division of the flow field into three regions. In region (a) extending from a shock wave outwards, the fluid is undisturbed. In region (c) extending from the plate part of the way to the shock wave, viscous effects are important, but the pressure changes across it are small so that boundary-layer theory may be used to describe the flow within it. In this region the gas is extremely hot in comparison with the fluid in (a) but has negligible density. The outer bound of (c) is clearly defined, and between (a) and (c) there is a third region (b) in which the effect of viscosity is negligible. In this region, however, large entropy gradients occur near the junction with (c).

A similar situation has been shown to hold for the steady motion at high Mach Number past a semi-infinite flatplate.[8] On a typical streamline coming from infinity, the flow field is undisturbed until it meets a shock wave emanating from the leading edge of the plate. Thereafter the streamline is distorted under the laws of inviscid flow, but at no stage do local viscous forces affect the fluid on it. Between nearly all the streamlines and the plate is a boundary layer containing an infinitesimal amount of fluid, but, because of the enormous temperature in it, it is of considerable size and of importance in determining the inviscid flow.

Two parts of the flow are amenable to treatment, and both have been considered by Lees and Probstein.[6-8] First, near the leading edge, but sufficiently far from it for the boundary-layer approximations in the viscous layer to be valid, there is a strong interaction field in which the shock wave exerts a large effect on the flow through it. Second, a long way downstream there is a weak interaction field in which the shock wave exerts only a small effect on the flow through it, so that behind it there is only a small perturbation of the uniform conditions upstream of the shock. The region in which the shock wave is strong was first considered by Li and Nagamatsu,[9] assuming that the shock wave coin-

Received April 23, 1954.

*Research Fellow, on leave from The University, Bristol, England.

† In a paper to be published in this JOURNAL, Mr. Lester Lees considers the effect of this assumption and concludes that the error incurred is indeed $O[(M^2\nu_0/(Ux)]^{1/2-1/2\gamma}$ as we would expect from the unsteady problem, and $\to 0$ as $M \to \infty$, keeping $M^6\nu_0/Ux$ finite. He also estimates the error when $M = 10$ and concludes that, in comparisons with experiments at this Mach Number, it cannot be neglected.

cided with the outer edge of the boundary layer. Their work is of importance because they demonstrated the existence of "similar" solutions in this region, although, as Lees[6] has pointed out, the basic assumption leads to a contradiction, because the edge of the boundary layer must be a streamline; therefore, from the Rankine-Hugoniot relations it cannot also be a shock wave. Lees[6, 8] improved their theory by showing that there must be an inviscid layer between the shock wave and the boundary layer, and, giving a partial justification of the matching procedure, he adopted to join the two layers. He did not discuss the inviscid layer in detail beyond pointing out that conditions at the edge of the boundary layer are determined with good accuracy by means of the tangent wedge approximation; nor did he show that the two layers were contiguous.

The main purpose of this paper is to show that there is a "similar" solution in the inviscid layer which may be joined up to the "similar" solution in the boundary layer without inconsistency so that there is no intermediate layer. In the course of the argument a slight change in the boundary condition at the edge of the boundary layer has to be made. Although it has not been possible to show that such a change has no appreciable effect on the flow field in the steady problem,* this assumption is made more plausible by the fact that in the corresponding unsteady problem (I), a similar change can be completely justified. Using our solution valid from the stock wave to the plate, it may be deduced that when the shock is strong the pressure on the plate is in deficit by 10 per cent if the fluid is air. In addition, we show that the von Kármán-Pohlhausen method may be used to describe the flow throughout the entire boundary layer with an error varying from -1 per cent to $+2^1/_2$ per cent. Finally we show that the solution obtained by Lees and Probstein[7] when the shock wave is weak cannot be further improved without a knowledge of the entropy variation across the inviscid layer—i.e., without a knowledge of the entire inviscid flow.

There is little doubt that the Navier-Stokes equations are inadequate to give a full and correct description of the flow field and that, especially near the leading edge, molecular considerations will be needed. However, it is likely that the assumption that the fluid is a continuum will be justified if $M[\nu_0/(Ux)]^{1/2} \ll 1$,[11] where u is the velocity of the fluid at infinity and x is distance downstream from the leading edge. As we shall see below, this is precisely the condition under which the assumptions of this paper are justified. Further, although the "inert" degrees of freedom would require a longer distance than that to respond to changes in conditions, it is probable that in any practical problem the temperatures would be sufficiently low to assume that either they are not excited at any time, or, if they would then have little influence of the flow. Finally, it is pointed out that the molecular considerations, as typified by the existence of slip flow, may be interpreted as providing some sort of lubrication between the plate and the main stream, reducing the impact of the one on the other, so that the results of the conventional boundary-layer theory would give upper bounds for the disturbances.

* See footnote on page 303.

(2) The Equations of Motion and the Inviscid Layer

We assume that the plate occupies the positive half of the x axis and that the fluid is streaming along it with uniform velocity u at infinity. The Mach Number $M = U/a_0 \ll 1$, where a_0 is the velocity of sound at infinity and the region in which the flow is disturbed is bounded by a shock wave and immediately below the flow is inviscid. We are not concerned here with the thickness of the shock wave nor with the nature of the flow within it, beyond assuming that it is thin and that conditions on either side of it are determined by the Rankine-Hugoniot relations. Under the assumptions of a continuum, these properties of the shock wave may be justified. We denote by p the pressure, ρ the density, T temperature, y distance normal to the plate, u, v the components of the fluid velocity in the x, y directions, respectively, and γ the ratio of the specific heats of the fluid. Let the equation of the shock wave be

$$Y = Y(x) \tag{2.1}$$

where Y is at present unknown; but we shall assume that $(dY/dx)^2 \ll 1$. If subscripts 0, 1 denote the undisturbed values and the values just behind the shock wave of the variables, we have, following Goldsworthy,[3]

$$\left.\begin{aligned} u_1 - U &= UO(dY/dx)^2 \\ v_1 &= [2U/(\gamma+1)]\,(dY/dx) \times \{1 - [1/M^2(dY/dx)^2]\} \\ p_1/p_0 &= [2\gamma/(\gamma+1)]M^2(dY/dx)^2 - [(\gamma-1)/(\gamma+1)] \\ \rho_1/\rho_0 &= [(\gamma+1)M^2(dY/dx)^2]/[(\gamma-1)M^2 \times (dY/dx)^2 + 2] \end{aligned}\right\} \tag{2.2}$$

The flow behind the shock wave is now discussed adopting an heuristic argument. We assume that the flow is either inviscid or of the boundary-layer type in which the pressure is a function of x only. This procedure was used in I with success, and a considerable amount of space was used in showing that the procedure is consistent. Here we shall not devote much space to such a justification, merely pointing out the circumstance in which the argument is valid. For example, the shock conditions given in Eqs. (2.2) are only valid if $dY/dx \ll 1$, which implies that $Y \ll x$.

Consider the following system of equations.

$$[\rho u(\partial u/\partial x)] + [\rho v(\partial u/\partial y)] = -(\partial p/\partial x) + (\partial/\partial y)\,[\mu(\partial u/\partial y)] \tag{2.3}$$

$$\rho u(\partial v/\partial x) + \rho v(\partial v/\partial y) = -\partial p/\partial y \tag{2.4}$$

$$(\partial/\partial x)(\rho u) + (\partial/\partial y)(\rho v) = 0 \tag{2.5}$$

$$\rho c_p u \frac{\partial T}{\partial x} + \rho c_p v \frac{\partial T}{\partial y} - u \frac{\partial p}{\partial x} - v \frac{\partial p}{\partial y} = \mu \left(\frac{\partial u}{\partial y}\right)^2 + \frac{\partial}{\partial y}\left(\frac{\mu c_p}{\sigma} \frac{\partial T}{\partial y}\right) \tag{2.6}$$

$$p = \Re \rho T \tag{2.7}$$

where c_p is the specific heat at constant pressure and σ is the Prandtl Number. Eq. (2.5) is the equation of continuity valid everywhere. Eq. (2.3) is from the x component of the momentum equation valid in the boundary layer regime and in the inviscid regime. Eq. (2.4) is from the y component of the momentum equation valid in the inviscid layer. In the boundary layer its effect on p must be negligible. We shall show this below. Eq. (2.6) is the energy equation valid in both regions, and Eq. (2.7) is the equation of state valid everywhere. There are many terms neglected in these equations, but it may be shown that in both regimes their effect is negligible if $Y \ll x$.

Throughout this paper we shall assume that the fluid possesses the properties

$$\left.\begin{aligned} \sigma &= 1 \\ \mu &= \mu_0(T/T_0) \end{aligned}\right\} \tag{2.8}$$

No fluid has these properties, of course; but if we assume them, the discussion is considerably simplified, and the solution in this idealized case will help us to understand the behavior of more realistic fluids.

The boundary conditions satisfied by the fluid are that just behind the shock wave Eq. (2.2) is satisfied while on the plate $y = 0$, $x > 0$,

$$u = v = 0, \quad \partial T/\partial y = 0 \tag{2.9}$$

taking it to be thermally insulating. The equations of motion then have a simple integral—namely,

$$T/T_0 = 1 + [(\gamma - 1)/(2a_0^2)](U^2 - u^2 - v^2) \tag{2.10}$$

Further, if we define a stream function ψ by the equations

$$\rho_0(\partial\psi/\partial y) = \rho u; \quad \rho_0(\partial\psi/\partial x) = -\rho v \tag{2.11}$$

Eqs. (2.4) and (2.5) reduce to

$$\left.\begin{aligned} \partial v/\partial x &= -(1/\rho_0)(\partial p/\partial \psi) \\ (\partial/\partial\psi)(v/u) &= (\partial/\partial x)(\rho_0/\rho u) \end{aligned}\right\} \tag{2.12}$$

It is noted that ψ is a continuous function of x and y equal to Uy in the undisturbed fluid. Just behind the shock wave, $u - U = UO(dY/dx)^2$, so that $u - U$ may be neglected in comparison with U and in Eq. (2.12) u may be replaced by U. The relevant equations in the inviscid layer behind the shock and also the conditions at the shock are similar in the unsteady problem, and the solution is of the same form. For a fuller discussion of the relation between the unsteady and the steady problems, the reader is referred to a paper by Goldsworthy.[3] It should be pointed out, however, that there is a misstatement in it, for he says that the boundary layer may be neglected in a discussion of the inviscid field. It is now well known, and will be shown here, that such is not the case. The similarity between the unsteady and the steady flows breaks down either when $(u - U)/u$ becomes of order one or when the inviscid assumption is no longer valid. It may be shown that both of these occur simultaneously. From the energy equation in the inviscid regime we find that $p/p_0 = S(x)(\rho/\rho_0)^\gamma$, where S is a function of ψ only, which may be found from its value just behind the shock wave. If we assume that the equation of the shock wave is

$$Y = \vartheta x^{2/3}(1 + \alpha x^{1/3} + \dots) \tag{2.13}$$

leaving the justification until the next section, we find that

$$S = \frac{9\gamma M^2 \zeta^2}{8(\gamma+1)}\left(\frac{\gamma-1}{\gamma+1}\right)^\gamma \left(\frac{\psi}{U\vartheta}\right)^{-2/3}\left[1 + \left(\frac{\psi}{U\vartheta}\right)^{2/3} \times \left(4\alpha + \frac{8(3\gamma-1)(\gamma+1)}{9\gamma(\gamma-1)M^2\vartheta^2} + \dots\right)\right] \tag{2.14}$$

and, if we write

$$\left.\begin{aligned} \eta &= \psi/UY \\ v &= [2U/(\gamma+1)](dY/dx)V(\eta, x) \\ p/p_0 &= [2\gamma M^2/(\gamma+1)](dY/dn)^2 P(\eta, x) \\ V &= V_0(\eta) - x^{1/3}\left[\frac{4}{3}\alpha V_1(\eta) + \frac{16}{9M^2\vartheta^2} V_2(\eta)\right] + \dots \\ P &= P_0(\eta) - x^{1/3}\left[\frac{4}{3}\alpha P_1(\eta) + \frac{16}{9M^2\vartheta^2} P_2(\eta)\right] + \dots \end{aligned}\right\} \tag{2.15}$$

the boundary conditions and equations satisfied by the P's and V's are the same as for the same symbols in I, Section 3. We may conclude therefore that if the inviscid solution is valid anywhere behind the shock it is valid everywhere in $\psi > 0$, because the only singularities develop there. In particular the proportional change in u remains small in $\psi > 0$, but it has a singularity at $\psi = 0$. The boundary layer in terms of ψ can therefore only occupy a narrow layer near $\psi = 0$. Since $\partial p/\partial\psi$ is bounded as $\psi \to 0 +$ and v increases from the plate to the edge of the boundary layer, it follows from Eq. (2.11) that the change in p across the layer is small, and so a conventional boundary-layer theory may be used. It is noted that the end of the inviscid layer is associated with a rapid increase of T and rapid decrease in u and ρ, all of which we must have for a boundary-layer theory. Further, since ψ is a measure of the mass of fluid crossing the shock wave, almost the whole mass of fluid confined between the shock and the plate is in this inviscid layer, and the mass in the boundary layer is negligible. This does not

mean that the boundary layer is of negligible thickness in the physical plane however. In terms of y, the boundary layer is nearly as thick as the inviscid layer when x is small. This is shown below. In the theory of Li and Nagamatsu,[9] it was assumed that the shock wave coincided with the outer edge of the boundary layer, which is equivalent to assuming that the whole of the mass behind the shock wave is confined inside the boundary layer.

(3) The Boundary Layer

It was shown in the previous section that once the flow just behind the shock wave was admitted to be inviscid it followed that the viscous layer was confined to the immediate neighborhood of $\psi = 0$. Further, the variation of p across this layer is small, so that in it p may be assumed to be a function of x only. The relevant equation of motion is then, from Eqs. (2.3) and (2.11),

$$u\left(\frac{\partial u}{\partial x}\right)_{\psi} = -\frac{1}{\rho}\frac{dp}{dx} + \frac{u}{\rho_0}\frac{\partial}{\partial \psi}\left(\frac{\mu \rho u}{\rho_0}\frac{\partial u}{\partial \psi}\right) \tag{3.1}$$

with boundary conditions $u = 0$ at $\psi = 0$ and $u \to U$ outside the boundary layer. It is noted that this boundary condition may be replaced by $u \to U$ as $\psi \to \infty$ because ψ is still small in comparison with Y when u is not sensibly different from U. Further, the boundary condition on u as $\psi \to \infty$ is really $u - U \sim U\psi^{-2/3\gamma}$, from the behavior of T in the inviscid layer; but it is likely, although we have not proved it, that the simpler condition above is justified.* It is certainly justified in the unsteady problem to which the reader is referred. Using the energy integral in which v is neglected in comparison with u and assuming $\mu \propto T$, the equation for u reduces to

$$u\frac{\partial u}{\partial x} = -\frac{1}{\rho_0}\frac{p_0}{p}\left(1 + \frac{\gamma - 1}{2a_0^2}(U^2 - u^2)\right)\frac{dp}{dx} + \nu_0 \frac{p}{p_0} u \frac{\partial}{\partial \psi}\left(u\frac{\partial u}{\partial \psi}\right) \tag{3.2}$$

We now write $u^* = u(p_0/p)^{(\gamma-1)/2\gamma}$, whence u^* satisfies

$$\left(\frac{p}{p_0}\right)^{(\gamma-1)/2\gamma} u^*\frac{\partial u^*}{\partial x} = -\frac{a_0^2}{\gamma p}\left(1 + \frac{\gamma - 1}{2}M^2\right)\frac{dp}{dx} + \nu_0\left(\frac{p}{p_0}\right)^{(5\gamma-3)/2\gamma} u^*\frac{\partial}{\partial \psi}\left(u^*\frac{\partial u^*}{\partial \psi}\right) \tag{3.3}$$

In this equation we may replace $[(\gamma - 1)/2]M^2 + 1$ by $[(\gamma - 1)/2]M^2$. Then if we write

$$\left.\begin{aligned} z &= \int_0^x \left(\frac{p}{p_0}\right)^{(3\gamma-1)/2\gamma} dx \\ W &= U(p_0/p)^{(\gamma-1)/2\gamma} \end{aligned}\right\} \tag{3.4}$$

$$u^*\frac{\partial u^*}{\partial z} = W\frac{dW}{dz} + \nu_0 u^*\frac{\partial}{\partial \psi}\left(u^*\frac{\partial u^*}{\partial \psi}\right) \tag{3.5}$$

which is the same as the boundary-layer equation for an incompressible fluid. The boundary conditions are $u^* = 0$ at $\psi = 0$ and $u^* \to W$ as $\psi \to \infty$.

The normal procedure to determine the v component of the velocity at the edge of the boundary layer is to use the formula

$$\rho v = -\frac{\partial}{\partial x}\int_0^y \rho u\, dy$$

But this method fails here because at the edge of the boundary layer $\rho \sim \psi^{2/3\gamma}$ and is zero on inviscid theory for all values of x. Instead we use Eq. (2.12) from which

$$\left.\begin{aligned} v &= u\frac{\partial}{\partial x}\int_0^{\psi}\frac{\rho_0\, d\psi}{\rho u} \\ &= u\frac{\partial}{\partial x}\int_0^{\psi}\frac{p_0}{pu}\,d\psi \times \left[1 + \frac{\gamma - 1}{2a_0^2}(U^2 - u^2)\right] \end{aligned}\right\} \tag{3.6}$$

Now in the boundary layer $1 \ll [(\gamma - 1)/2a_0^2](U^2 - u^2)$ and may therefore be neglected. Hence

$$v = \frac{\gamma - 1}{2}M^2 u\frac{\partial}{\partial x}\left[\frac{p_0}{p}\int_0^{\psi}\left(\frac{U}{u} - \frac{u}{U}\right)d\psi\right] \tag{3.7}$$

and to find the value of v at the edge of the boundary layer we may replace the upper limit by ∞, since when ψ is large on the scale of the boundary layer $u - U$ is exponentially small. At the edge of the boundary layer therefore

$$v = v_E = \frac{\gamma - 1}{2}M^2 U\frac{\partial}{\partial x} \times \left[\frac{p_0}{p}\int_0^{\infty}\left(\frac{U}{u} - \frac{u}{U}\right)d\psi\right] \tag{3.8}$$

since $u = U$ there. If y^* denotes distance normal to the plate in the corresponding incompressible boundary layer so that

$$\partial\psi/\partial y^* = u^*$$

Eq. (3.8) may be written

$$v_E = \frac{\gamma - 1}{2}M^2 U\frac{d}{dx}\left[\left(\frac{p_0}{p}\right)^{(3\gamma-1)/2\gamma} \times \int_0^{\infty}\left(1 - \frac{u^{*2}}{W^2}\right)dy^*\right] \tag{3.9}$$

Further, in the boundary layer

$$y = \int_0^{\psi}\frac{\rho_0\, d\psi}{\rho u} = \frac{\gamma - 1}{2}M^2\left(\frac{p_0}{p}\right)^{(3\gamma-1)/2\gamma} \times \int_0^{y^*}\left(1 - \frac{U^{*2}}{W^2}\right)dy^*$$

using the same arguments as before. Hence the boundary-layer thickness Y_E is definite and

$$v_E = U(dY_E/dx) \tag{3.10}$$

in marked contrast to the incompressible problem where

* See footnote on page 303.

the outer edge to the boundary layer is vague. It is of interest to note that according to Eq. (3.10) the outer edge of the boundary layer is a streamline of the inviscid flow, and this is in agreement with the conclusion of the previous section that the mass of fluid in the boundary layer is negligible in comparison with that in the inviscid layer.

If the pressure in the boundary layer is

$$p/p_0 = Q_0 x^{-1/2}$$

where Q_0 is a constant, then $z \sim x^{(\gamma+1)/4\gamma}$ and $W \sim z^{(\gamma-1)/(\gamma+1)}$ so that if we write

$$\zeta = \{W\gamma/[\nu_0 z(\gamma + 1)]\}^{1/2} y^*$$

and

$$u^* = W(df/d\zeta)$$

a solution of the boundary-layer equations may be found in which f is a function of ζ only. In fact

$$(d^3f/d\zeta^3) + [f(d^2f/d\zeta^2)] + [(\gamma - 1)/\gamma][1 - (df/d\zeta)^2] = 0 \quad (3.11)$$

$$f = df/d\zeta = 0 \text{ at } \zeta = 0$$

and

$$df/d\zeta \to 1 \text{ as } \zeta \to \infty$$

Eq. (3.11) is one of the family found by Falkner and Skan and integrated by Hartree,[4] from whose paper the value of v at the edge of the boundary layer,

$$\frac{3}{4}(\gamma - 1)\left(\frac{\nu_0}{UQ_0}\right)^{1/2} M^2 U x^{-1/4} \times \int_0^\infty \left[1 - \left(\frac{df}{d\zeta}\right)^2\right] d\zeta \quad (3.12)$$

may be calculated. We note that this value of v_E is of the right form to effect a match with the inviscid solution discussed in the previous section. The significance of the similar solution of the boundary-layer equation was first pointed out by Li and Nagamatsu,[9] and it was obtained in this form by Lees.[6] The similar solution is only valid when $p \propto x^{-1/2}$. In general, p may be represented by a power series in $x^{1/2}$ of which that is the leading term. The appropriate solution of the boundary-layer equations is then found in the form of another series in powers of $x^{1/2}$ of which the leading term is given above. In view of the complicated nature of the transformation such a procedure would rapidly become unwieldy. Since we would expect the pressure on the plate to decrease uniformly as x increases, it follows that W should increase with z, and therefore the von Kármán-Pohlhausen method applied to Eq. (3.5) should be accurate. Following Goldstein[2] we define

$$\Lambda = (\delta^2/\nu_0)(dW/dz) \quad (3.13)$$

where δ is the boundary-layer thickness in the von Kármán-Pohlhausen sense. Then

$$\int_0^\delta \left(1 - \frac{u^{*2}}{W^2}\right) dy^* = \delta(0.4175 - 0.00939\Lambda - 0.000110\,\Lambda^2) = \delta K(\Lambda) \quad (3.14)$$

and

$$\frac{d\Lambda}{dz} = g(\Lambda)\frac{d}{dz}(\log W) + [\Lambda^2 h(\Lambda) + \Lambda] \times \frac{d}{dz}\left(\log \frac{dW}{dz}\right) \quad (3.15)$$

where g and h are tabulated in reference 2. If now we transform back to p/p_0 and x, we find that

$$v_E = \frac{\gamma - 1}{2} M^2 (U\nu_0)^{1/2} \frac{d}{dx} \times \frac{\Lambda^{1/2} K(\Lambda)}{\{[(\gamma - 1)/2\gamma](d/dx)(-p/p_0)\}^{1/2}} \quad (3.16)$$

where

$$\frac{d\Lambda}{dx} = -\left\{\frac{\gamma - 1}{2\gamma} g(\Lambda) + \frac{3\gamma - 1}{\gamma}[\Lambda' L(\Lambda) + \Lambda]\right\} \times \frac{d}{dx}\log p/p_0 + [\Lambda' h(\Lambda) + \Lambda]\frac{d}{dx}\log\frac{d}{dx}\left(\frac{p}{p_0}\right) \quad (3.17)$$

The initial value of Λ, Λ_0 is found by setting $p/p_0 = Q_0 x^{-1/2}$ and requiring that Λ_0 should be finite. It then follows that the right-hand side must vanish whence $\Lambda_0 = 3.256$ if $\gamma = 1.4$, leading to a value of v at the edge of the boundary layer equal to

$$0.391 M^2 U[\nu_0/(Q_0 U)]^{1/2} x^{-1/4} \quad (3.18)$$

If we use the exact boundary-layer solution [Eq. (3.12)], the numerical constant is found to be 0.394 so that there is a deficit of about 1.0 per cent. The form for p, $\propto x^{-1/2}$, assumed above is valid when x is small, and, when x is large, p is nearly equal to p_0. In this case the value of v at the edge of the boundary layer, calculated by the von Kármán-Pohlhausen method is in excess of the correct answer by about $2^1/_2$ per cent. Thus the percentage error involved on assuming v_E as given by Eq. (3.16) varies from -1.0 per cent to $+2^1/_2$ per cent, and it is plausible to assume that in between the error is sufficiently small for us to take Eq. (3.16) as a sufficiently good approximation.

If the pressure is of the form

$$p/p_0 = Q_0 x^{-1/2} + Q_1 + O(x^{1/2}) + \ldots$$

we find that when $\gamma = 1.4$

$$v_E = M^2 U[\nu_0/(Q_0 U)]^{1/2} x^{-1/4}[0.391 - 0.474\,(Q_1/Q_0)x^{1/2} + \ldots] \quad (3.19)$$

We may now effect a match between the inviscid solution at $\psi = 0$ with the boundary-layer solution at $\psi = \infty$. From the previous section and from I, Section 3, we find that if $\gamma = 1.4$ and $\psi = 0$

$$\left.\begin{aligned} p/p_0 &= 0.393 M^2 \vartheta^2 x^{-1/2}(1 + x^{1/2}\{6.984\alpha - [4.748/(M^2\vartheta^2)]\} + \ldots) \\ V_E &= 0.444 U\vartheta x^{-1/4}(1 + x^{1/2}\{5.498\alpha - [6.218/(M^2\vartheta^2)]\} + \ldots) \end{aligned}\right\} \quad (3.20)$$

Hence, comparing Eqs. (3.19) and (3.20) we find that

$$\left.\begin{aligned}\vartheta &= 1.188(M^2\nu_0/u)^{1/4}\\ \alpha &= 0.608\left[\frac{U}{M^6\nu_0}\right]^{1/2}\end{aligned}\right\} \tag{3.21}$$

whence the pressure on the plate is

$$p_w/p_0 = 0.555\ M^3[\nu_0/(Ux)]^{1/2} + 0.489 + \ldots \tag{3.22}$$

and the equation to the outer edge of the boundary layer is

$$y = Y_E = 0.704x[(M^6\nu_0)/(Ux)]^{1/4} - 0.460x[(M^6\nu_0)/(Ux)]^{-1/4} + \ldots \tag{3.23}$$

It is fairly easy to see that the pressure on the plate is a function of $[(M^6\nu_0)/(Ux)]^{1/2}$ only. Lees and Probstein[7] showed that when x is large the pressure on the plate is given by

$$p_w/p_0 = 1 + 0.349\ [(M^6\nu_0)/(Ux)]^{1/2} + 0.052[(M^6\nu_0)/(Ux)] + \ldots \tag{3.24}$$

and the two solutions may be joined in an approximate manner by making use of the tangent wedge approximation in the inviscid region, as suggested by Lees and Probstein,[8] in conjunction with the von Kármán-Pohlhausen method in the boundary layer. The tangent wedge approximation has been used in this way in I where it gives only fair agreement with the exact solution near $x = 0$. It is felt accordingly that there would be little point in using the method here. Perhaps the only suitable method is the method of characteristics, already used by Eggers and Syvertson[1] in related problems.

We can now determine the region of validity of Eqs. (2.3) to (2.7) and of the division of the flow field into a boundary layer and an inviscid layer. We need not discuss it in detail however, because this has already been done for the unsteady problem in I. The equations of motion are set out by Howarth,[5] and we find that we are entitled to reduce them to Eqs. (2.3) to (2.7) if $(Y/x)^2 \ll 1$—i.e., if

$$M^2(\nu_0/Ux) \ll 1 \tag{3.25}$$

Further, we may divide the flow field into inviscid and viscous fields if, in terms of ψ, the thickness of the viscous layer is much thinner than that of the inviscid field. The condition for this is also Eq. (3.25). We conclude therefore that the results of this paper are valid in the range

$$M^2(\nu_0/U) \ll x \ll M^6(\nu_0/U)$$

and note that, according to Tsien,[11] the lower bound is also the lower bound for the validity of the assumption of a continuum.

(4) The Influence of the Entropy

In the previous section we obtained the first two terms of a series for the pressure p_w on the plate in ascending powers of $x^{1/2}$, and it is clear that any further terms may be obtained if desired. Lees and Probstein[7] have bound the first three terms of a series for p_w in *descending* powers of $x^{1/2}$, neglecting entropy variations in the inviscid layer [Eq. (3.24)]. We examine here the effect of the entropy variation at large values of x and show that, notwithstanding the singularity in the entropy at the edge of the viscous layer, its effect on p_w is $O(x^{-3/2})$. But to calculate the fourth term of Eq. (3.24), which will therefore depend on the entropy, we need to know its distribution in the entire inviscid region. It follows that no more terms of the asymptotic series for p_w can be found until the complete solution is known.

To show this we reconsider the equations of motion in the inviscid layer—viz.,

$$\left.\begin{aligned}\partial v/\partial x &= -(1/\rho_0)\,(\partial p/\partial \psi)\\ \partial v/\partial \psi &= -[S^{1/\gamma}/\gamma(p/p_0)^{(\gamma+1)/\gamma}]\,(\partial/\partial x)\,(p/p_0)\end{aligned}\right\} \tag{4.1}$$

The boundary condition at $\psi = 0$ is that $v = v_E(x)$ and at the shock wave Eq. (2.2) must be satisfied. Given v_E we have three conditions to determine—p, v, and y—and then v_E may be found in terms of p_w from the boundary layer, giving us an equation for p_w. The method adopted by Lees and Probstein[7] was to neglect $1 - S$ and use the theory of isentropic flow. They found that the entropy at large values of ψ and x is $\propto \psi^{-3/2}$, because the pressure rise across the shock wave $\propto \psi^{-1/2}$, and concluded that the entropy rise across the shock wave would not affect the first three terms of Eq. (3.24). There is however the entropy variation at small values of ψ to consider, and we can treat the leading terms due to it by replacing the coefficient of $\partial p/\partial x$ in Eq. (4.1) by $-[1/(\gamma p_0)]\ (1 + R)$, where $1 + R = S^{1/\gamma}$, and by neglecting entropy variations across the shock wave. Contributions to the fourth term of Eq. (3.24) arise (1) from the isentropic solution, (2) from the entropy rise across the shock wave, and (3) from the entropy variation near $\psi = 0$. These three contributions are all independent, and the first two may be deduced from the asymptotic solution already known. We now calculate the third using the simplified form of Eq. (4.1). The correction that would have to be applied would not affect the fourth term of Eq. (3.24).

We write

$$\left.\begin{aligned}v &= v_E[x - (\psi/a_0)] + v_1\\ p &= p_0 + a_0\rho_0 v_E[x - (\psi/a_0)] + p_1\end{aligned}\right\} \tag{4.2}$$

where we assume and justify *a posteriori* that $v_1 \ll v_E$ and $p_1 \ll a_0\rho_0 v_E$. The boundary conditions are that $v_1 = 0$ at $\psi = 0$ and $p_1 \to 0$ as $\psi \to \infty$. The leading terms of Eq. (4.2) are simply the leading terms of their asymptotic expansions. Entropy variations near $\psi = 0$ only affect p and v via the interaction between S and these terms.

Substituting for p and v in the modified form of Eq. (4.1) and neglecting $p_1 R$ in comparison with $a_0\rho_0 v_E R$, we obtain

$$\frac{\partial^2 p_1}{\partial \psi^2} - \frac{1}{a_0^2}\frac{\partial^2 p_1}{\partial x^2} = \frac{\rho_0}{a_0} R(\psi) v_E''[x - (\psi/a_0)] \qquad (4.3)$$

with boundary conditions

$$\partial p_1/\partial \psi = 0 \text{ at } \psi = 0$$

since $v_1 = 0$ there and $p_1 \to 0$ as $\psi \to \infty$. Let

$$\alpha = x + \psi/a_0, \quad \beta = x - \psi/a_0 \qquad (4.4)$$

when

$$4[\partial^2 p_1'/(\partial\alpha\partial\beta)] = -\rho_0 a_0 R\{[(\alpha - \beta)/2]a_0\} v_E''(\beta)$$

so that

$$\frac{\partial p_1}{\partial \beta} = \frac{1}{2}\rho_0 v_E''(\beta)\int_{[(\alpha-\beta)/2]a_0}^{\infty} R(\psi)d\psi \qquad (4.5)$$

and

$$p_1 = -\int_\beta^\alpha \frac{\partial p_1}{\partial \beta}\alpha\beta + f(\alpha) \qquad (4.6)$$

where f is at present unknown. However, since

$$\left.\begin{aligned} \partial p_1/\partial \psi &= 0 \text{ at } \psi = 0 \\ \partial p_1/\partial \alpha &= \partial p_1/\partial \beta \text{ at } \alpha = \beta \end{aligned}\right\} \qquad (4.7)$$

and hence

$$f'(\alpha) = \rho_0 v_E''(\alpha)\int_0^\infty R(\psi)\, d\psi \qquad (4.8)$$

The value of $f(\alpha)$ is now found by noting that $p_1 \to 0$ as $\psi \to \infty$ so that on the plate

$$p_1 = \rho_0 v_E'(\alpha)\int_0^\infty R(\psi)\, d\psi \qquad (4.9)$$

Near $\psi = \infty$, $R \sim \psi^{-3/2}$ and near $\psi = 0$, $R \sim \psi^{-2/3\gamma}$ so that the integral in Eq. (4.9) is convergent. Further, when x is large $v_E(x) = 0.271\ M^2 U[\nu/(Ux)]^{1/2}[1 + o(1)]$, so that Eq. (4.9) becomes

$$-0.197 p_0 M^3 \left(\frac{\nu}{Ux}\right)^{1/2}\frac{1}{a_0 x}\int_0^\infty R(\psi)\, d\psi \qquad (4.10)$$

We may now check that all our assumptions are justified when x is large, and we conclude that the fourth term of Eq. (3.24) has a contribution from the entropy variation in the entire inviscid field. It cannot therefore be calculated without knowing the complete solution.

Acknowledgment

The author would like to thank Mr. Lester Lees for many long discussions on high-speed flow which he was privileged to have with him and for allowing him access to an unpublished monograph that provided the stimulus for this work. During the time it was done the author was at the California Institute of Technology on leave of absence from Bristol University, and it was supported by Contract N6 ONR-244, T.O. VIII.

References

[1] Eggers, A. J., Jr., and Syvertson, C. A., NACA TN 2646, March, 1952.

[2] Goldstein, S., *Modern Developments in Fluid Dynamics*, Vol. 1, Oxford University Press, pp. 156–160, 1938.

[3] Goldsworthy, F. A., Quart. J. of Mech. and App. Maths., Vol. 5, Part 1, p. 54, March, 1952.

[4] Hartree, D. R., Proc. Camb. Phil. Soc., Vol. 33, Part 2, p. 233, April, 1937.

[5] Howarth, L., *Modern Developments in Fluid Dynamics: High Speed Flow*, Vol. 1, Oxford University Press, p. 50, 1953.

[6] Lees, L., *On the Boundary-Layer Equations in Hypersonic Flow and Their Approximate Solutions*, Journal of the Aeronautical Sciences, Readers' Forum, Vol. 20, No. 2, February, 1953.

[7] Lees, L., and Probstein, Princeton Univ. Aero. Eng. Lab., Report No. 195, April 20, 1952 (unpublished).

[8] Lees, L., and Probstein, *Hypersonic Flows of a Viscous Fluid* (unpublished).

[9] Li, Ting-Yi, and Nagamatsu, H. T., *Shock-Wave Effects on the Laminar Skin Friction of an Insulated Plate at Hypersonic Speeds*, Journal of the Aeronautical Sciences, Vol. 20, No. 5, p. 345, May, 1953.

[10] Stewartson, K., *On the Motion of a Flat Plate at High Speed in a Viscous Compressible Fluid—I. Impulsive Motion*, Proc. Camb. Phil. Soc., Vol. 51, Part 1, p. 202, January, 1955.

[11] Tsien, H. S., *Superaerodynamics, Mechanics of Rarefied Gases*, Journal of the Aeronautical Sciences, Vol. 13, No. 12, p. 653, December, 1946.

Notice to Contributors

Manuscripts submitted for publication *must* be double- or triple-spaced originals. There should be wide margins on both sides of the sheets and triple spacing around formulas to allow for the marking of directions for the printer.

Original drawings (jet black India ink on white paper or tracing cloth) should accompany the manuscript. *(Blueprints are not acceptable.)* Photographs *must* be on glossy white paper. The smallest lettering on 8- by 10-in. figures should be no less than $^1/_4$ in. high.

Only the simplest formulas should be typewritten; all others should be carefully written in pen and ink. The difference between capital and lower-case letters and Greek symbols should be clearly distinguished.

See Inside Back Cover of this issue for further details

Methods for Computing Supersonic Aerodynamic Flutter Coefficients for Two-Dimensional Flow

ERNEST C. KENNEDY*

Convair, A Division of General Dynamics Corporation, Daingerfield, Texas

SUMMARY

The object of this paper is to collect and discuss some of the existing methods of calculating supersonic aerodynamic flutter coefficients and to exhibit a new method for evaluating certain associated integrals. The eight real and imaginary parts of the coefficients are expressed in terms of Mach Number and reduced frequency (ω) by means of convergent series involving the sine and cosine of ω. It is thought that this paper will be of value to engineers engaged in supersonic flutter analysis.

NOMENCLATURE

b	= semichord (ft.)
J_n	= standard Bessel function of order n
M	= Mach Number
V	= free-stream velocity (ft. per sec.)
θ	= $\sin^{-1}(1/M)$
λ	= identifying subscript; 0, 1, 2, 3
Ω	= circular flutter frequency (rad. per sec.)
ω	= reduced frequency = $2\Omega b/(V\cos^2\theta)$
$(-)$, $(*)$	= dash over symbol and asterisk denote real and imaginary parts of a complex quantity

INTRODUCTION

SINCE THE ADVENT of the high-speed plane, some intensive work has been done on the theory of supersonic flutter analysis. Pioneers in this field were Possio[1] and Borbely.[2] In 1936, the former set up and solved the linearized partial differential equation of motion of an airfoil oscillating in a supersonic air stream. Six years later, Borbely tackled the same problem and arrived at the same differential equation. Neither of these two men performed any numerical calculations in their papers. Both made simplifying assumptions which cause the theory to break down when the Mach Number is near one.

Borbely established the following relationships, taken from references 3 and 4:

$$\left.\begin{aligned}\omega^{\lambda+1}f_\lambda(M,\omega) &= \int_0^\omega e^{-iu}u^\lambda J_0(u/M)\,du, \qquad \lambda = 0, 1, 2, 3\\ &\qquad\qquad i = \sqrt{-1},\\ &= \int_0^\omega \cos uu^\lambda\, J_0(u/M)\,du - i\int_0^\omega \sin uu^\lambda\, J_0(u/M)\,du\end{aligned}\right\} \tag{1}$$

$$\begin{aligned}f_\lambda(M,\omega) = \frac{M^2}{\omega^2(M^2-1)}\Bigg\{&\Bigg[-\frac{\omega\cos\omega}{M}J_1(\omega/M) + (1-\lambda)\cos\omega J_0(\omega/M) +\\ &\omega\sin\omega J_0(\omega/M) - (1-2\lambda)\omega f_{\lambda-1}{}^*(M,\omega) + (1-\lambda)^2\bar{f}_{\lambda-2}(M,\omega)\Bigg] +\\ &i[\omega\cos\omega J_0(\omega/M) + (\omega/M)\sin\omega J_1(\omega/M) - (1-\lambda)\sin\omega J_0(\omega/M) +\\ &(1-2\lambda)\omega\bar{f}_{\lambda-1}(M,\omega) + (1-\lambda)^2 f_{\lambda-2}{}^*(M,\omega)]\Bigg\}\end{aligned} \tag{2}$$

$$(M,\omega) = e^{-i\omega}\sum_{n=0}^{\infty} A_n\,[J_n(\omega) + iJ_{n+1}(\omega)], \qquad \text{where } A_n = \frac{[\omega/2\cdot(M^2-1)/M^2]^n}{n!\,(2n+1)} \tag{3}$$

and showed that ωf_0 is the fundamental integral used in the evaluation of the forces and moments involved. Hence all of the eight aerodynamic lift and moment coefficients, as defined by Eqs. (49)–(52) of reference 3, can be expressed in terms of f_0, ω, and M. In this paper no attempt is made to develop the theory or to derive the fundamental equations of flutter analysis.

The method developed by the writer was used in calculating the table of aerodynamic force and moment coefficients listed in reference 5. These eight flutter coefficients were computed to high accuracy over a wide

Received June 12, 1954. Revised and received, October 7, 1954.

* Senior Research Engineer.

range of values of both Mach Number and frequency parameter and are available in the above publication.

Methods of Evaluating the Aerodynamic Coefficients

Method of Reference 3

Obviously, the f-functions of Eqs. (1), (2), and (3) are complex and may be written as $f_\lambda = \bar{f}_\lambda + i f_\lambda^*$, where the dash and the asterisk indicate real and imaginary components, respectively. The functions $\bar{f}_\lambda$ and f_λ^* can be expressed in terms of ω, M, and the f's of lower order by means of the recurrence formula (2).

The method of procedure is to first find $\bar{f}_0$ and f_0^* (by breaking Eq. (3) up into its real and imaginary parts) and then get f_λ, ($\lambda = 1, 2, 3$), by applying Eq. (2). The infinite series (3) converges rapidly for ω small and M near unity. However for such values of the two parameters, the factor $M^2/\omega^2(M^2 - 1)$ occurring in (2) is large and consequently these equations give poor results unless each term is evaluated to high accuracy—and this is a little awkward to do when ω/M is a number of more than three decimals. This method is not well adapted to IBM procedure, partly because of the J_n terms.

Method of Reference 4

Barton and Poindexter[4] devised a neat method for evaluating f_λ which does not necessitate the use of a J_n table. They expanded both the trigonometric functions and the Bessel functions into infinite series and integrated termwise. The resulting double series is broken up into two series—one a finite series in M and the other an infinite series in ω for a fixed M. These series converge rapidly for $M > 1$ and ω small, but if ω is large (>3, say) the convergence may be slow. Each f_λ is obtained independent of f_0. The method is useful in many cases, but it is not especially well adapted to IBM procedure.

The scheme described in reference 6 is very similar to that given in reference 4 six years earlier.

Method of the Author

In attempting to avoid some of the limitations of existing methods, the writer used the following scheme for evaluating the f_λ's.

As in the preceding methods we write

$$\omega^{\lambda+1}\bar{f}_\lambda = \int_0^\omega \cos u u^\lambda J_0(u/M)\, du \tag{4}$$

and illustrate the method by evaluating $\bar{f}_0$. Thus

$$\omega\bar{f}_0 = \int_0^\omega \cos u J_0(u/M)\, du = \int_0^\omega \cos u \left[1 - \frac{(u/M)^2}{4} + \frac{(u/M)^4}{64} - \frac{(u/M)^6}{2304} \ldots\right] du \tag{5}$$

Table 1

$$a_{n-2} = \frac{\omega^{n-2}}{2^n[(n/2)!]^2}$$

a_0	= 0.25	
a_2	= 1.5625	$(-2)\ \omega^{2*}$
a_4	= 4.3402 77778	$(-4)\ \omega^4$
a_6	= 6.7816 84028	$(-6)\ \omega^6$
a_8	= 6.7816 84028	$(-8)\ \omega^8$
a_{10}	= 4.7095 02797	$(-10)\ \omega^{10}$
a_{12}	= 2.4028 07549	$(-12)\ \omega^{12}$
a_{14}	= 9.3859 66989	$(-15)\ \omega^{14}$
a_{16}	= 2.8969 03391	$(-17)\ \omega^{16}$
a_{18}	= 7.2422 58480	$(-20)\ \omega^{18}$
a_{20}	= 1.4963 34396	$(-22)\ \omega^{20}$
a_{22}	= 2.5978 02772	$(-25)\ \omega^{22}$
a_{24}	= 3.8429 03509	$(-28)\ \omega^{24}$
a_{26}	= 4.9016 62638	$(-31)\ \omega^{26}$
a_{28}	= 5.4462 91819	$(-34)\ \omega^{28}$
a_{30}	= 5.3186 44355	$(-37)\ \omega^{30}$
a_{32}	= 4.6009 03424	$(-40)\ \omega^{32}$
a_{34}	= 3.5500 79802	$(-43)\ \omega^{34}$
a_{36}	= 2.4585 04018	$(-46)\ \omega^{36}$
a_{38}	= 1.5365 65019	$(-49)\ \omega^{38}$
a_{40}	= 8.7106 85999	$(-53)\ \omega^{40}$
a_{42}	= 4.4993 21278	$(-56)\ \omega^{42}$
a_{44}	= 2.1263 33308	$(-59)\ \omega^{44}$
a_{46}	= 9.2288 77205	$(-63)\ \omega^{46}$
a_{48}	= 3.6915 59881	$(-66)\ \omega^{48}$

* $1.5625\,(-2) = 1.5625 \times 10^{-2}$.

Making use of the reduction formula

$$\int u^m \cos u\, du = u^{m-1}[u \sin u + m \cos u] - m(m-1)\int u^{m-2}\cos u\, du \tag{6}$$

we get

$$\begin{aligned}
I_0 &= \int_0^\omega \cos u\, du = \sin\omega \\
I_1 &= \int_0^\omega u \cos u\, du = \omega\sin\omega + \cos\omega - 1 \\
I_2 &= \int_0^\omega u^2 \cos u\, du = \omega[\omega\sin\omega + 2\cos\omega] - 2I_0 \\
I_3 &= \int_0^\omega u^3 \cos u\, du = \omega^2[\omega\sin\omega + 3\cos\omega] - 6I_1 \\
&\cdots\cdots\cdots \\
I_n &= \int_0^\omega u^n \cos u\, du = \omega^{n-1}[\omega\sin\omega + n\cos\omega] - n(n-1)I_{n-2}
\end{aligned} \tag{7}$$

Only the even subscripts are used in evaluating $\bar{f}_0$, but the odd ones are included here for later use. Whence

$$\bar{f}_0 = D_0 - D_2/M^2 + D_4/M^4 - D_6/M^6 \ldots \tag{8}$$

where

$$\begin{aligned}
D_0 &= I_0/\omega = \frac{\sin\omega}{\omega} \\
D_2 &= I_2/4\omega = a_0[\omega\sin\omega + 2\cos\omega] - 0.5D_0 \\
D_4 &= I_4/64\omega = a_2[\omega\sin\omega + 4\cos\omega] - 0.75D_2 \\
&\cdots\cdots\cdots \\
D_n &= \frac{I_n}{2^n[(n/2)!]^2\omega} = a_{n-2}[\omega\sin\omega + n\cos\omega] - \frac{(n-1)}{n}D_{n-2},\ (n \text{ even})
\end{aligned} \tag{9}$$

where the coefficients $a_{n-2} = 2^{-n}\,[(n/2)!]^{-2}\omega^{n-2}$ are listed in Table 1. Note that D_n/M^n is not the nth term of series (8). This should cause no confusion. If ω is large it is usually convenient to transform Table 1 by setting $\omega = 10\omega'$, taking care to shift the decimal point properly.

A little study shows that the series (8) converges for all values of ω and M in which we are interested. It converges very rapidly for ω small and M large (e.g., for $\omega = 1$ and $M = 2$, five terms give f_0 correct to nine decimals; for $\omega = 10$ and $M = 2$, thirteen terms are necessary for the same accuracy).

Similarly, it can be shown that

$$f_1 = E_1 - E_3/M^2 + E_5/M^4 - E_7/M^6 \ldots \quad (10)$$

where

$$E_n = \frac{I_n}{2^{n-1}\left\{\left[\frac{n-1}{2}\right]!\right\}^2}\,\omega^2 = a_{n-3}(\omega \sin \omega + n \cos \omega) - [n/(n-1)]E_{n-2}, \qquad (n \text{ odd}) \quad (11)$$

$$f_2 = B_2 - B_4/M^2 + B_6/M^4 - B_8/M^6 \ldots \quad (12)$$

where

$$B_n = a_{n-4}\,(\omega \sin \omega + n \cos \omega) - \frac{n(n-1)}{(n-2)^2}\,B_{n-2} \qquad (n \text{ even}) \quad (13)$$

$$f_3 = G_3 - G_5/M^2 + G_7/M^4 - G_9/M^6 \ldots \quad (14)$$

where

$$G_n = a_{n-5}\,(\omega \sin \omega + n \cos \omega) - \frac{n(n-1)}{(n-3)^2}\,G_{n-2} \qquad (n \text{ odd}) \quad (15)$$

In using the above formulas note that D_n, E_n, B_n, and G_n are all functions of ω only and that all of the a_i coefficients have an even subscript, regardless of whether n is even or odd.

To get the imaginary components—the f^*'s—we write

$$\omega f_0^* = \int_0^\omega \sin uJ_0(u/M)\,du = \int_0^\omega \sin u[1 - u^2/4M^2 + u^4/64M^4 \ldots]\,du \quad (16)$$

Using the reduction formula

$$\int u^m \sin u\,du = u^{m-1}\,[m \sin u - u \cos u] - m(m-1)\int u^{m-2} \sin u\,du \quad (17)$$

and proceeding in a manner similar to that described above we get

$$f_0^* = P_0 - P_2/M^2 + P_4/M^4 - P_6/M^6 \ldots \quad (18)$$

$$P_n = a_{n-2}\,(n \sin \omega - \omega \cos \omega) - \frac{(n-1)}{n}\,P_{n-2} \qquad (n \text{ even}) \quad (19)$$

$$f_1^* = R_1 - R_3/M^2 + R_5/M^4 - R_7/M^6 \ldots \quad (20)$$

$$R_n = a_{n-3}\,(n \sin \omega - \omega \cos \omega) - \frac{n}{n-1}\,R_{n-2} \qquad (n \text{ odd}) \quad (21)$$

$$f_2^* = Q_2 - Q_4/M^2 + Q_6/M^4 - Q_8/M^6 \ldots \quad (22)$$

$$Q_n = a_{n-4}(n \sin \omega - \omega \cos \omega) - \frac{n(n-1)}{(n-1)^2}\,Q_{n-2} \qquad (n \text{ even}) \quad (23)$$

$$f_3^* = S_3 - S_5/M^2 + S_7/M^4 - S_9/M^6 \ldots \quad (24)$$

$$S_n = a_{n-5}\,(n \sin \omega - \omega \cos \omega) - \frac{n(n-1)}{(n-3)^2}\,S_{n-2} \qquad (n \text{ odd}) \quad (25)$$

Note that if ω is very small (≤ 0.1, say), it is necessary to evaluate I_1, I_2, I_3, quite accurately. However, in this case very few terms of the f-series will be needed regardless of the value of M—always recalling that M is larger than one, say $M \geq 1.1$.

Conclusion

The writer's method is especially useful when only a few values of ω and many values of M are concerned. It is applicable for either large or small ω and each f_λ is evaluated independently of f_0. Since most of the calculations for each f_λ involve a recurrence formula, the scheme works quite smoothly on a CPC-IBM machine using an eight-place floating decimal board. No tables of Bessel functions are required, but accurate trigonometric tables are necessary. Of course, if an IBM machine is available the trigonometric functions may be generated as needed.

References

[1] Possio, C., *L'azione Aerodinamica sul Profilo Ascillante alle Velocita ultransonica*, Acta Pont. Acad. Sci., Vol. 1, No. 11, pp. 93–105, 1937.

[2] v. Borbely, S., *Aerodynamic Forces on a Harmonically Oscillating Wing at Supersonic Velocity*, R.T.P. Translation No. 2019, British Ministry of Aircraft Production (from Z. Angew Math. Mech., Vol. 22, No. 4, August, 1942, pp. 190–205).

[3] Keller, E. G., Black, S., and Czuba, T., *Supersonic Airforce Coefficients for Flutter Analysis*, Curtiss-Wright Report No. P537-V-28, April, 1948.

[4] Barton, M. V., and Poindexter, Allen M., *Values of Some Aerodynamic Parameters Useful for Supersonic Flutter Studies*, CF-720, UT/DRL-125, July 10, 1947.

[5] *Handbook of Supersonic Aerodynamics*, NAVORD Report 1488 (Vol. 4, Sec. 12), January 1, 1952.

[6] Zartarian, G., and Voss, H. M., *On the Evaluation of the Function* $f_\lambda(M, \bar{\omega})$, Journal of the Aeronautical Sciences, Readers' Forum, Vol. 20, November 1953, p. 781.

Effect of Rotatory Inertia and Shear on Maximum Strain in Cantilever Impact Excitation

MARCEL K. NEWMAN*
University of Notre Dame

ABSTRACT

A solution of the Timoshenko beam equation is given for boundary and initial conditions similar to those obtaining in the drop test of a cantilevered beam. Curves are drawn for the amplification factor A and for $A\ (\omega/p_1)$ as a function of the relative impact duration ω/p_1. These show that for extremely short duration disturbances the effects of rotatory inertia and shear are of the same order of magnitude as those obtained from the Bernoulli-Euler theory with the addition of viscous internal damping on the constant Q hypothesis (Sezawa's equation).

INTRODUCTION

THE PROBLEM OF RESPONSE OF BEAMS to nonperiodic excitation has received considerable attention. In 1944, Symonds and Vigness[1] discussed effects of impact duration on the stresses at the root of a cantilever beam. The solution given was based on the Bernoulli-Euler equation.

Theory showed that when an elastic system is subjected to a nonperiodic disturbance, the response of the system is determined by the ratios of the frequency components of the disturbance to the fundamental frequency of natural vibrations of the beam. If the ratio of the dominant frequency component of the disturbance to the lowest natural frequency of the system is small, vibrations of the system at any of its natural frequencies are not excited appreciably, and the response may be found as if the excitation were static. As the dominant frequency component of the disturbance is increased and allowed to become equal to or greater than the fundamental frequency p_1 of the system, the fundamental mode of vibration of the system is excited, and this must be taken into account in calculating the maximum strains at the root of the cantilever. As the pulse duration is decreased still further, the Bernoulli-Euler theory predicts maximum strain at the clamped end which eventually increases without limit.

The defect in the results of the Bernoulli-Euler theory was of course attributed immediately to the omission of the effects of rotatory inertia and shear and also to the omission of damping.

In 1947, Mindlin, Stubner, and Cooper[2] discussed results of tests and also results of calculations using the Bernoulli-Euler theory, including viscous internal damping on the constant Q hypothesis, and concluded that the excessive strain predicted by the simple Bernoulli-Euler equation for extremely short duration impact excitation was due mainly to neglecting the effect of damping which normally provides a mechanism for the rapid dissipation of energy, particularly in the higher modes. This is in agreement with the suggestions made originally by Symonds and Vigness.[1]

The value of Q used in this case was $Q = 100$. It was found by observations on the decay of free vibrations of the first mode of cantilever specimens.

It is, therefore, of some interest to obtain solutions of the Timoshenko equation,[5, 6] which include the effects of rotatory inertia and shear with precisely the same or equivalent boundary conditions as those offered by Symonds and Vigness.[1]

There have been given a number of other solutions of the Timoshenko equation.[5, 6] Uflyand[3] treated the case of an infinite beam subjected to a concentrated load with a step function-time history. Dengler, Goland, and Wickersham[4, 11] solved the same problem using the unit impulse as the time function of disturbance.

In addition, a few studies have been made relating specifically to the effect of rotatory inertia and shear on the propagation of waves and on the natural frequencies of beams. Davies[7] considered the effect of rotatory inertia and shear on the wave and group velocities of flexural vibrations as they compare to those of dilatational disturbances. Ayre and Jacobsen[8] and Kruszewski[9] discussed effects of transverse shear and rotatory inertia on the natural frequencies of uniform beams. Recently, Schirmer[10] considered the problem of wave propagation of flexural vibrations in beams governed by the Timoshenko equation by analyzing separately the shear motion and the rotation.

More recently, Anderson[12] presented a general solution of the Timoshenko equation in terms of generalized orthogonal coordinates representing bending and shear deflections. He applied the solution to the case of a concentrated transient force at the midpoint of a hinged beam.

Also, Miklowitz[13] has given a general solution similar to that of Anderson. He also made comparisons with the Dengler and Goland[4] solution and with the Uflyand[3] solution and derived transforms for a number of boundary conditions both for finite and infinite beams.

Received May 27, 1954.

* Head, Department of Mechanical Engineering.

The object of this paper is to present a solution of the Timoshenko[5] equation for the case of half-period sine excitation applied to the root of a cantilever beam. This is the type of excitation normally considered typical of the drop test. The appropriate boundary conditions are obtained by means of the use of a variational principle. They are equivalent to those used by Symonds and Vigness[1] and Mindlin, Stubner, and Cooper.[2]

Results are plotted in a form similar to that used by earlier investigators. Amplification factor A for impact response is defined as the ratio of the maximum dynamic strain at the clamped end to the maximum static strain at the clamped end which would be obtained if the maximum acceleration were reached very slowly, as in a centrifuge test. Amplification factor is plotted versus frequency ratio p_1/ω, where p_1 is the fundamental frequency of the bar and ω is the dominant frequency of the disturbance.

Another set of coordinates is presented in order to make comparisons with earlier results. The ordinate $A(\omega/p_1)$ is plotted as function of ω/p_1 for two cases, that of a long bar and that of a short bar.

It will be shown that rotatory inertia and shear will lead to slightly different limits of maximum strain at the clamped end in the case of extremely short duration disturbances applied to slender bars as compared to thick bars. The distinction is made by means of nondimensional ratio L/K, where L is the length of the bar and K is the radius of gyration of the section with respect to the centroidal axis. All results are given in nondimensional form when such form appears to be indicated.

Specifically, numerical computations were carried out for the thick bar with $L/K = 30$ and for the slender bar with $L/K = 300$. These values were chosen with the intention to cover the approximate range of practical significance of values of L/K.

It was found that for short duration impact, the value of the ordinate $A(\omega/p_1)$ approaches a limit of 4.89 in the case of the slender bar and a limit of 4.08 in the case of the thick bar. These values compare to that reported by Mindlin, Stubner, and Cooper[2] in the case of a bar computed on the Bernoulli-Euler theory but with internal viscous damping according to the constant Q hypothesis. This value reported is $A(\omega/p_1) = 3.55$. It shows that effects of rotatory inertia and shear are of the same order of magnitude as those of constant Q damping.

(1) Equations of Motion and Boundary Conditions for Cantilever Bar

The equations of motion for the elastic system subjected to a drop test and the appropriate boundary conditions arising from consideration of rotatory inertia and shear are obtained conveniently by minimizing the integral

$$\int_{t_1}^{t_2} (T - U)dt \tag{1}$$

where $T - U$ is the Lagrangian function, T is the kinetic energy, and U is the potential energy of the beam.

The generalized coordinates chosen are w, the transverse displacement of the beam element, and Ψ, the angle of rotation of the element due to bending. The slope of the neutral axis of the beam is

$$\partial w/\partial x = \Psi + \gamma \tag{2}$$

where x is the coordinate parallel to the axis of the beam with origin at the free end and γ is the shearing strain.

The bending moment is

$$M = -EI(\partial\Psi/\partial x) \tag{3}$$

where EI is the flexural rigidity of the beam and $\partial\Psi/\partial x$ is a first approximation to the curvature for small values of Ψ.

The shearing force is

$$Q = K'AG\,\gamma = K'AG[(\partial w/\partial x) - \Psi] \tag{4}$$

where K' is a numerical constant depending on the shape of the cross section and on Poisson's ratio,[14] A is the cross-sectional area, and G is the shear modulus.

The kinetic energy is

$$T = \frac{1}{2}\rho A\int_0^L \left(\frac{\partial w}{\partial t}\right)^2 dx + \frac{1}{2}K^2\rho A\int_0^L \left(\frac{\partial \Psi}{\partial t}\right)^2 dx \tag{5}$$

The potential energy is

$$U = \frac{1}{2}EI\int_0^L \left(\frac{\partial \Psi}{\partial x}\right)^2 dx + \frac{1}{2}K'AG\int_0^L \left(\frac{\partial w}{\partial x} - \Psi\right)^2 dx \tag{6}$$

where K = radius of gyration with respect to horizontal principal axis through centroid of cross section of beam and ρ = mass density of beam material.

Definitions, Eqs. (5) and (6), exhibit the degree of approximation intended. Performing the operations indicated, Euler's differential equations of motion are obtained, together with the natural boundary conditions that must be satisfied in order to minimize integral (1)—namely,

$$-\rho A(\partial^2 w/\partial t^2) + K'AG[(\partial^2 w/\partial x^2) - (\partial\Psi/\partial x)] = 0 \tag{7}$$

$$-K^2\rho A(\partial^2\Psi/\partial t^2) + EI(\partial^2\Psi/\partial x^2) + K'AG[(\partial w/\partial x) - \Psi] = 0 \tag{8}$$

Eqs. (7) and (8) can be combined by eliminating the generalized coordinate Ψ. The result is the well-known equation

$$\frac{\partial^4 w}{\partial x^4} - \frac{\rho(1+\epsilon)}{E}\frac{\partial^4 w}{\partial x^2\partial t^2} + \frac{\rho^2\epsilon}{E^2}\frac{\partial^4 w}{\partial t^4} + \frac{\rho}{K^2E}\frac{\partial^2 w}{\partial t^2} = 0 \tag{9}$$

The natural conditions at the ends $x = 0$ and $x = L$ are

$$(\partial\Psi/\partial x)\delta\Psi = 0 \tag{10}$$

$$[(\partial w/\partial x) - \Psi]\delta w = 0 \tag{11}$$

where L is the length of the beam.

For arbitrary $\delta\Psi$ the condition of zero moment is obtained

$$\partial\psi/\partial x = 0 \tag{12}$$

Substitution in Eq. (7) leads to the form

$$(\partial^2 w/\partial x^2) - (\rho\epsilon/E)(\partial^2 w/\partial t^2) = 0 \tag{13}$$

If δw is arbitrary, the condition of zero shear is obtained

$$[(\partial w/\partial x) - \Psi] = 0 \tag{15}$$

Substituting this in Eq. (8) and using Eq. (7), the condition of zero shear takes the form

$$(\partial^3 w/\partial x^3) - [\rho(1 + \epsilon)/E](\partial^3 w/\partial x \partial t^2) = 0 \tag{16}$$

If the bending moment is arbitrary, Eq. (10) requires that

$$\delta\Psi = 0 \tag{17}$$

and for arbitrary shear, Eq. (11) requires that

$$\delta w = 0 \tag{18}$$

The quantity ϵ is a dimensionless constant defined as follows:

$$\epsilon = E/(K'G) = 2(1 + \nu)/K'$$

where ν is Poisson's ratio.

ϵ is adjusted in accordance with the suggestion made by Mindlin[14] so that the limiting transmission velocity for extremely short flexural waves approaches that of Rayleigh surface waves.

For a wave solution

$$w(x, t) = e^{i(\mu x + \omega t)}$$

Eq. (9) takes the form

$$c^4 - (c_s^2/K^2\mu^2)c^2 - (c_l^2 + c_s^2)c^2 + c_l^2 c_s^2 = 0 \tag{14}$$

where c_l is the velocity of long extensional waves $c_l^2 = E/\rho$; $c_s^2 = K'G/\rho$; $c_l^2/c_s^2 = E/(K'G) = \epsilon$; $\mu = 2\pi/\lambda$; and λ is the wave length.

Eq. (14) implies two modes of transmission[7,10] given by

$$\frac{c^2}{c_l^2} = \left[\left(1 + \frac{1}{K^2\mu^2} + \epsilon\right)\Big/ 2\epsilon\right] \times \left\{1 \pm \sqrt{1 - \left[4\epsilon\Big/\left(1 + \frac{1}{K^2\mu^2} + \epsilon\right)^2\right]}\right\} \tag{14a}$$

Confining attention to the lower transmission mode, the short wave-length limit with $1/(K^2\mu^2) = 0$ will be given by

$$c^2 = K'G/\rho$$

This corresponds to Mindlin's[14] equation $c^2 = K^2(G/\rho)$. For materials with Poisson's ratio $\nu = 0.2$, K^2 will be 0.828 and ϵ will be 2.9. For $\nu = 0.3$, $\epsilon = 3$.

(2) Cantilever Bar in Drop-Test Excitation

The initial conditions and end conditions for the case of excitation in a drop test of a cantilever bar of length L and with origin of coordinates at the free end are

$$[w]_{t=0} = 0 \tag{19a}$$

$$[\partial w/\partial t]_{t=0} = -V \tag{19b}$$

$$[w]_{x=L} = -\frac{V}{\omega}\sin\omega t\, u\left(\frac{\pi}{\omega} - t\right) + V\left(t - \frac{\pi}{\omega}\right) u\left(t - \frac{\pi}{\omega}\right) \tag{19c}$$

$$[\Psi]_{x=L} = 0 \tag{19d}$$

After some manipulation, the condition of zero angle of rotation Ψ at the clamped end of the bar $x = L$ takes the form

$$\left(\frac{\partial^2 w}{\partial x^3} - \frac{\epsilon}{c_l^2}\frac{\partial^3 w}{\partial x \partial t^2} + \frac{1}{\epsilon K^2}\frac{\partial w}{\partial x}\right)_{x=L} = 0 \tag{19e}$$

The boundary conditions at the free end of the bar are

$$\left(\frac{\partial^2 w}{\partial x^2} - \frac{\epsilon}{c_l^2}\frac{\partial^2 w}{\partial t^2}\right)_{x=0} = 0 \tag{19f}$$

$$\left[\frac{\partial^3 w}{\partial x^3} - \frac{(1 + \epsilon)}{c_l^2}\frac{\partial^3 w}{\partial x \partial t^2}\right]_{x=0} = 0 \tag{19g}$$

In the foregoing equations u is the unit step function

$$u[(\pi/\omega) - t] = 1 \quad \text{for } [(\pi/\omega) - t] > 0$$

$$u[(\pi/\omega) - t] = 0 \quad \text{for } [(\pi/\omega) - t] < 0$$

V is the initial velocity of the cantilever at the instant of impact. V is of such magnitude that the maximum acceleration $V\omega$ is large in comparison with the acceleration of gravity so that the latter may be neglected. This initial velocity corresponds to an initial kinetic-energy storage in the beam of $\frac{1}{2}mV^2$, where m is the mass of the beam.

Solution of this problem is accomplished readily by use of the Laplace transformation

$$Y = \int_0^\infty e^{-pt} w(x, t)dt \tag{20}$$

where p is a complex parameter.

The partial differential [Eq. (9)] and the conditions [Eqs. (19a) to (19g)] are thus converted to the following equations in Y.

$$\frac{d^4 Y}{dx^4} - \frac{1 + \epsilon}{c_l^2}p^2\frac{d^2 Y}{dx^2} + \left(\frac{\epsilon p^4}{c_l^4} + \frac{p^2}{K^2 c_l^2}\right)Y = -\left(\frac{\epsilon p^2}{c_l^4} + \frac{1}{K^2 c_l^2}\right)V \tag{21}$$

At $x = 0$

$$(d^2Y/dx^2) - [(\epsilon/c_t^2)p^2Y] = (\epsilon/c_t^2)V \quad (22a)$$

$$(d^3Y/dx^3) - [(1 + \epsilon)/c_t^2]p^2(dY/dx) = 0 \quad (22b)$$

At $x = L$

$$Y = Ve^{-(p\pi/\omega)}\{\omega/[p^2(p^2 + \omega^2)]\} - [V/(p^2 + \omega^2)] \quad (22c)$$

$$(d^3Y/dx^3) - [(\epsilon p^2/c_t^2) - (1/\epsilon K^2)](dY/dx) = 0 \quad (22d)$$

The complementary function of Eq. (21) can be written in the form

$$Y = c_1 \sinh \mu_1 x + c_2 \cosh \mu_1 x + c_3 \sin \mu_2 x + c_4 \cos \mu_2 x \quad (23)$$

provided the following quartic equations in μ_1, μ_2, and p are satisfied.

$$\mu_1^4 - [(1 + \epsilon)/c_t^2]p^2\mu_1^2 + (\epsilon p^4/c_t^4) + [p^2/(K^2c_t^2)] = 0 \quad (23a)$$

and

$$\mu_2^4 + [(1 + \epsilon)/c_t^2]p^2\mu_2^2 + (\epsilon p^4/c_t^4 + [p^2/(K^2c_t^2)] = 0 \quad (23b)$$

In general, each quartic has two roots in the squares of the parameters μ_1 and μ_2, respectively. These roots are

$$\mu_1^2 = \frac{(1 + \epsilon)}{2c_t^2}p^2 \pm \frac{(1 + \epsilon)}{2c_t^2}p^2 \times \sqrt{1 - \frac{4\epsilon}{(1 + \epsilon)^2} - \frac{4c_t^2}{(1 + \epsilon)^2K^2p^2}} \quad (24a)$$

$$\mu_2^2 = -\frac{(1 + \epsilon)}{2c_t^2}p^2 \pm \frac{(1 + \epsilon)}{2c_t^2}p^2 \times \sqrt{1 - \frac{4\epsilon}{(1 + \epsilon)^2} - \frac{4c_t^2}{(1 + \epsilon)^2K^2p^2}} \quad (24b)$$

It will be noted that μ_1^2 and μ_2^2 are of opposite sign. This means that the corresponding values of μ_1 and μ_2 are at quadrature in the complex plane. Because of the symmetry of Eq. (23), one of the double signs in Eqs. (24a) and (24b) is redundant. They are dropped since they will contribute no new solutions in Eq. (23). Eqs. (24a) and (24b) are therefore given as follows:

$$\mu_1^2 = \frac{1 + \epsilon}{2c_t^2}p^2 - \frac{1 + \epsilon}{2c_t^2}p^2 \times \sqrt{1 - \frac{4\epsilon}{(1 + \epsilon)^2} - \frac{4c_t^2}{(1 + \epsilon)^2K^2p^2}} \quad (24c)$$

$$\mu_2^2 = -\frac{1 + \epsilon}{2c_t^2}p^2 - \frac{1 + \epsilon}{2c_t^2}p^2 \times \sqrt{1 - \frac{4\epsilon}{(1 + \epsilon)^2} - \frac{4c_t^2}{(1 + \epsilon)^2K^2p^2}} \quad (24d)$$

The signs of μ_1^2 and μ_2^2 in Eqs. (24c) and (24d) reflect the fact that Eq. (23) is chosen hyperbolic in $\mu_1 x$ and harmonic in $\mu_2 x$ for positive real values of μ_1 and μ_2.

The solution of the differential Eq. (21) with boundary conditions (22a) to (22d) leads to the Laplace transform $Y(x, p)$ of the solution $w(x, t)$.

$$Y(x, p) = \frac{V\omega^2(1 + e^{-p\pi/\omega})\Phi(x, p)}{p^2(p^2 + \omega^2)\Delta(L, p)} - \frac{V}{p^2} \quad (25)$$

where

$$\Phi(x, p) = \mu_1\mu_2\{(c_t^2/K^2)[\cosh \mu_1(L - x) + \cos \mu_2(L - x)] + [(\epsilon - 1)(\mu_1^2c_t^2 - \epsilon p^2) + (c_t^2/K^2)] \cosh \mu_1 L \cos \mu_2 x + [-(\epsilon - 1)(\mu_2^2c_t^2 + \epsilon p^2) + (c_t^2/K^2)] \cos \mu_2 L \cosh \mu_1 x\} - (\mu_2^2c_t^2/K^2) \sinh \mu_1 L \sin \mu_2 x + (\mu_1^2c_t^2/K^2) \sin \mu_2 L \sinh \mu_1 x \quad (26)$$

and

$$\Delta(L, p) = \mu_1\mu_2\{(2c_t^2/K^2) + [(2c_t^2/K^2) - (\epsilon - 1)^2p^2] \cosh \mu_1 L \cos \mu_2 L\} + [(1 + \epsilon)p^2/K^2] \sinh \mu_1 L \sin \mu_2 L \quad (27)$$

It can be shown that

$$\Phi(L, p) = \Delta(L, p)$$

The use of two parameters μ_1 and μ_2 in the Laplace transform $Y(x, p)$ [Eq. (25)] insures that $Y(x, p)$ [Eq. (25)] is a single valued function of p at the branch points of μ_1 and μ_2.

The branch points of μ_1 are

$$p = 0, \qquad p = \pm 2c_t/[(1 - \epsilon)K]$$

The branch points of μ_2 are

$$p = 0, \qquad p = \pm 2c_t/[(1 - \epsilon)K]$$

This can be shown by writing μ_1 and μ_2 in the form

$$\mu_1 = Mp^{1/2}[p - N(p^2 - a^2)^{1/2}]^{1/2} \quad (24e)$$

$$\mu_2 = iMp^{1/2}[p + N(p^2 - a^2)^{1/2}]^{1/2} \quad (24f)$$

where

$$M = [(1 + \epsilon)/2c_t^2]^{1/2}$$

$$N = (1 - \epsilon)/(1 + \epsilon)$$

$$a = 2c_t/[(1 - \epsilon)K]$$

The point $p = \pm i(c_t/K\sqrt{\epsilon})$, which is a zero of the function

$$z = [p \pm N(p^2 - a^2)]^{1/2}$$

is not a branch point of μ_1 and μ_2. This is shown by performing a circuit in the complex plane around this point and noting upon completing the circuit that z is single valued.

A single circuit in the complex plane around any one of the branch points of μ_1 and μ_2 either changes sign or changes the value of μ_1 and μ_2 in such a way that $Y(x, p)$ [Eq. (25)] remains single valued. It is concluded that the only singularities of $Y(x, p)$ [Eq. (25)] are poles.

It remains to find the solution $w(x, t)$ of the problem, of which $Y(x, p)$ is the Laplace transform. This solution is the Laplace Inverse of $Y(x, p)$. Since the inversion process is unique, $w(x, t)$ will be the solution of Eq. (9). The inversion is accomplished by means of the contour integral

$$w(x, t) = \frac{1}{2\pi i} V\omega^2 \oint_{Br_1} \frac{e^{pt}(1 + e^{-(p\pi/\omega)})\Phi(x,p)dp}{p^2(p^2 + \omega^2)\Delta(L, p)} - \frac{1}{2\pi i} V \oint_{Br_1} \frac{e^{pt}dp}{p^2} \quad (28)$$

The solution is the sum of the residues at the poles of the integrands of Eq. (28). In addition to the double pole at $p = 0$ and to the poles $p = \pm i\omega$, there exist zeros of $\Delta(L, p)$.

An analysis of the equation

$$\Delta(L, \mu_1 L, \mu_2, p) = 0 \quad (29)$$

shows that these roots are $\mu_1 L = \mu_{1n} L$ and $\mu_2 L = \mu_{2n} L$. They represent the characteristic values of the problem. The values $\mu_{1n} L$ and $\mu_{2n} L$ occur in a one-to-one correspondence. They are related to a set of values of p governed by Eqs. (24c) and (24d). The values of p that correspond to the roots $\mu_{1n} L$ and $\mu_{2n} L$ of the equation $\Delta(L, \mu_1 L, \mu_2 L, p) = 0$ are poles of the integrand of Eq. (28). These poles are located on the imaginary axis. They represent the natural frequencies $p = \pm ip_n$ of the modes of free vibrations of the bar.

Introducing now the circular frequency

$$\omega = c_1\alpha/(K\sqrt{\epsilon})$$

and

$$p_n = c_1\alpha_n/(K\sqrt{\epsilon})$$

where α and α_n are real positive numbers $0 \leq \alpha \leq \infty$, the equations for μ_1^2 and μ_2^2 may be written in a convenient nondimensional form.

If $p = i\omega = i[(c_1\alpha)/(K\sqrt{\epsilon})]$ is substituted in Eqs. (24c) and (24d) the following is obtained:

$$K^2\mu_1^2 = -\frac{(1 + \epsilon)}{2\epsilon}\alpha^2 + \frac{(1 + \epsilon)}{2\epsilon} \times \alpha^2\sqrt{\frac{(1 - \epsilon)^2}{(1 + \epsilon)^2} + \frac{4\epsilon}{(1 + \epsilon)^2\alpha^2}} \quad (24g)$$

$$K^2\mu_2^2 = \frac{(1 + \epsilon)}{2\epsilon}\alpha^2 + \frac{(1 + \epsilon)}{2\epsilon} \times \alpha^2\sqrt{\frac{(1 - \epsilon)^2}{(1 + \epsilon)^2} + \frac{4\epsilon}{(1 + \epsilon)^2\alpha^2}} \quad (24h)$$

$K\mu_1$ will be real for $0 \leq \alpha < 1$ and imaginary for $1 < \alpha \leq \infty$. $K\mu_2$ will be real for all values of α, $0 \leq \alpha \leq \infty$.

The roots were obtained by computation of $\Delta(L, \mu_1 L, \mu_2 L, i\alpha)$, using appropriate values of $\mu_1 L$, $\mu_2 L$, and α. All roots in p of $\Delta(L, \mu_1 L, \mu_2 L, i\alpha) = 0$ are simple poles.

The first six roots are listed in Table 1 as function of α_n for the short beam, $L/K = 30$, and for the long beam, $L/K = 300$.

The solution is written for the period of the disturbance $0 \leq t \leq \pi/\omega$ and for the time after the disturbance has ceased to exist, $\pi/\omega \leq t \leq \infty$.

For the period $0 \leq t \leq \pi/\omega$, the displacement is

$$w(x, t) = -\frac{V}{\omega}\frac{\Phi(x, i\omega)}{\Delta(L, i\omega)}\sin \omega i + 2V\omega^2 \times \sum_n \frac{\Phi(x, ip_n)\sin p_n t}{p_n^2(p_n^2 - \omega^2)\Delta'(L, ip_n)} \quad (30)$$

For $\pi/\omega \leq t \leq \infty$

$$w(x, t) = V\left(t - \frac{\pi}{\omega}\right) - 4V\omega^2 \times \sum_n \frac{\Phi(x, ip_n)\cos[(\pi p_n)/(2\omega)]\sin p_n[t - (\pi/2\omega)]}{p_n^2(p_n^2 - \omega^2)\Delta'(L, ip_n)} \quad (31)$$

where ω = frequency of impact and p_n = natural frequency of nth mode of vibration. $\Delta(L, i\omega)$ is obtained from Eq. (27) by substituting $p = i\omega$; $\Phi(x, i\omega)$ is obtained from Eq. (26) by substituting $p = i\omega$; $\Phi(x, ip_n)$ is obtained from Eq. (26) by substituting $p = ip_n$; and $\Delta'(L, ip_n)$ is the derivative of $\Delta(L, p)$ with respect to p for values of $p = ip_n$. It takes the form

$$\begin{aligned}\Delta'(L, ip_n) = A_n(\mu_{1n}, \mu_{2n}, p_n)\,\{&(2c_1^2/K^2) + [(\epsilon - 1)^2 p_n^2 + (2c_1^2/K^2)]\cosh \mu_{1n}L \cos \mu_{2n}L\} - \\ &2\mu_{1n}\mu_{2n}(\epsilon - 1)^2 p_n \cosh \mu_{1n}L \cos \mu_{2n}L + [2(1 + \epsilon)/K^2]p_n \sinh \mu_{1n}L \sin \mu_{2n}L + \\ &\{\mu_{1n}\mu_{2n}[(\epsilon - 1)^2 p_n^2 + (2c_1^2/K^2)]B_n - [(1 + \epsilon)p_n^2/K^2]C_n\}\sinh \mu_{1n}L \cos \mu_{2n}L - \\ &\{\mu_{1n}\mu_{2n}[(\epsilon - 1)^2 p_n^2 + (2c_1^2/K^2)]C_n + [(1 + \epsilon)p_n^2/K^2]B_n\}\cosh \mu_{1n}L \sin \mu_{2n}L\end{aligned}$$

where u_{1n} is the value of μ_1 for the nth mode, μ_{2n} is $2\pi/\lambda_n$, proportional to the wave number of the nth mode.

$$A_n(\mu_{1n}, \mu_{2n}, p_n) = -\frac{2\mu_{1n}\mu_{2n}}{p_n} + \frac{\mu_{2n}p_n}{K^2\mu_{1n}[2\mu_{1n}^2c_l^2 + (1 + \epsilon)p_n^2]} + \frac{\mu_{1n}p_n}{K^2\mu_{2n}[2\mu_{2n}^2c_l^2 - (1 + \epsilon)p_n^2]}$$

$$B_n = \lim_{p = p_n} L\frac{\partial u_1}{\partial p} = L\left\{-\frac{u_{1n}}{p_n} + \frac{p_n}{K^2\mu_{1n}[2\mu_1^2c_l^2 + (1 + \epsilon)p_n^2]}\right\}$$

$$C_n = \lim_{p = p_n} L\frac{\partial \mu_2}{\partial p} = L\left\{-\frac{\mu_{2n}}{p_n} + \frac{p_n}{K^2\mu_{2n}[2\mu_{2n}^2c_l^2 - (1 + \epsilon)p_n^2]}\right\}$$

Solutions (30) and (31) satisfy the differential Eq. (9) and the initial conditions and boundary conditions (19a) to (19g) inclusive.

(3) The Amplification Factor

The results obtained may be expressed conveniently in the form of an amplification factor for strain at the clamped end of the cantilever. It is defined as the ratio of the extreme dynamic fiber strain at the clamped end of the bar to the extreme fiber strain at the same location that would result if the maximum acceleration $V\omega$ were reached very slowly, as in a centrifuge test.

The extreme fiber strain at the clamped end of the bar is given by

$$\epsilon_m = d/2(\partial\Psi/\partial x)_{x=L} \tag{32}$$

where d is the depth of the beam.

The extreme fiber strain, at the clamped end, that would result if the maximum acceleration $V\omega$ were reached very slowly, as in a centrifuge test, is

$$\epsilon_{st} = (V\omega L^2 d)/(4c_l^2 K^2) \tag{33}$$

The amplification factor for strain at the clamped end is here defined as the maximum value of ϵ_m/ϵ_{st}.

$$A = \{[2K^2c_l^2(\partial\Psi/\partial x)_{x=L}]/(V\omega L^2)\}_{max}. \tag{34}$$

The amplification factor, Eq. (34), is plotted against p_1/ω in Fig. 1 for values of $L/K = 30$ and $L/K = 300$.

The amplification factor for the Bernoulli-Euler system is also plotted on the same figure.

Differences between the curves for $L/K = 30$ and $L/K = 300$ were found almost imperceptible and arise primarily in the range of extremely low frequency ratios p_1/ω.

It may be seen that the Bernoulli-Euler theory is close to the more exact theory over most of the range of frequency ratios. However, in the range of extremely small frequency ratios p_1/ω, the Bernoulli-Euler theory predicts infinite strains, not in agreement with the more exact theory which takes into account effects of rotatory inertia and shear. This lack of agreement for extremely short duration impact is not apparent from Fig. 1.

This is an inherent shortcoming of the amplification-factor curves. In order to bring out clearly the characteristic dynamic behavior in the range of short duration impacts, it is preferred to discuss the quantity $A(\omega/p_1)$ as function of ω/p_1. This quantity is proportional to the maximum dynamic strain at the clamped end

$$A(\omega/p_1) = \{(4\sqrt{\epsilon}/\alpha_1)\ (K^2/L^2)\ [(a\epsilon_m)/(Vd)]\} \tag{35}$$

where

$$a^2 = EK^2/\rho = K^2c_l^2$$

α_1 is defined by fundamental frequency of bar as

$$p_1 = (c_l\alpha_1)/(K\sqrt{\epsilon})$$

V = initial velocity of bar at moment of impact; d = depth of the bar; and K/L = nondimensional ratio of radius of gyration of cross section to length of bar.

It will be noted that $A(\omega/p_1)$ depends on $(K/L)^2$—i.e., its value will be different for a slender bar than for a thick bar. In the case of $L/K = 30$

$$A(\omega/p_1) = 1.18[(a\epsilon_m)/(Vd)] \tag{36a}$$

and in the case of $L/K = 300$

$$A(\omega/p_1) = 1.13\ [(a\epsilon_m)/(Vd)] \tag{36b}$$

$A(\omega/p_1)$ was computed from values of $w(x, t)$, Eq. (30), for the period of duration of impact $0 \leq t \leq \pi/\omega$, and from the values of $w(x, t)$, Eq. (31), for the period $\pi/\omega \leq t \leq \infty$, after the disturbance has ceased.

Curves of $A(\omega/p_1)$ were plotted as function of ω/p_1 for $L/K = 30$ and for $L/K = 300$, a range that covers most practical cases.

Equations for $A(\omega/p_1)$ have the following form.

During impact, for $0 \leq t \leq \dfrac{\pi}{\omega}$

$$A\frac{\omega}{p_1} = 2\sqrt{\epsilon}\frac{K^2\alpha}{L^2\alpha_1}\left(\sqrt{\epsilon}\left\{\frac{[\partial^2\Phi_1(i\alpha)/\partial x^2]_{x=L}}{\Delta_1(i\alpha)} - 1\right\}\sin\omega t - \frac{2\alpha[\partial^2\Phi_1(i\alpha_1)/\partial x^2{}_{x=L}}{(\alpha_1^2 - \alpha^2)\Delta_1'(i\alpha_1)}\sin p_1 t\right) - 4\sqrt{\epsilon}\frac{K^2}{L^2}\frac{1}{\alpha_1}\sum_2^n \frac{[\partial^2\Phi_1(i\alpha_n)/\partial x^2]_{x=L}}{\left(\dfrac{\alpha_n^2}{\alpha^2} - 1\right)\Delta_1'(i\alpha_n)}\sin p_n t \tag{37}$$

After impact for $\pi/\omega \leq t \leq \infty$

$$A\frac{\omega}{p_1} = 8\sqrt{\epsilon}\frac{K^2}{L^2}\frac{1}{\alpha_1}\sum_1^n \frac{[\partial^2\Phi_1(i\alpha_n)/\partial x^2]_{x=L}\cos[(\pi/2)\ (\alpha_n/\alpha)]}{[1 - (\alpha_n^2/\alpha^2)]\Delta_1'(i\alpha_n)}\sin p_n\left(t - \frac{\pi}{2\omega}\right) \tag{38}$$

TABLE 1
Characteristic Values for Cantilever

$L/K = 30$ short beam			$L/K = 300$ long beam		
α_n	$\mu_{1n}L$	$\mu_{2n}L$	α_n	$\mu_{1n}L$	$\mu_{2n}L$
0.0064242	1.8336	1.881	0.00006720	1.875	1.875
0.0390157	4.446	4.644	0.00042708	4.688	4.688
0.1014267	6.864	7.743	0.00116583	7.860	7.860
0.1819940	8.760	10.791	0.00224506	10.860	10.905
0.273441	10.029	13.836	0.00375991	13.950	14.145
0.3723474	10.890	16.875	0.00557713	17.010	17.220

where

$$\Delta_1(i\alpha) = (K\mu_1)\,(K\mu_2)\,\{2\epsilon + [(\epsilon-1)^2\alpha^2 + 2\epsilon]\cosh\mu_1 L\cos\mu_2 L\} - (1+\epsilon)\alpha^2\sinh\epsilon\mu_1 L\sin\mu_2 L$$

$$[\partial^2\Phi_1(i\alpha)/\partial x^2]_{x=L} = (K\mu_1)\,(K\mu_2)\,\{(1+\epsilon) + [(\epsilon-1)^2\alpha^2 + (3\epsilon-1)]\cosh\mu_1 L\cos\mu_2 L\} - \{[(1+\epsilon^2)/\epsilon]\alpha^2 + 2\}\sinh\mu_1 L\sin\mu_2 L$$

$$[\partial^2\Phi_1(i\alpha_n)/\partial x^2]_{x=L} = (K\mu_{1n})\,(K\mu_2)_n\,\{(1+\epsilon) + [(\epsilon-1)^2\alpha_n^2 + (3\epsilon-1)]\cosh\mu_{1n}L\cos\mu_{2n}L\} \{[(1+\epsilon^2)/\epsilon]\,\alpha_n^2 + 2\}\sinh\mu_{1n}L\sin\mu_{2n}L$$

$$\Delta_1'(i\alpha_n) = \sqrt{1-\alpha_n^2}\,E_n\left\{2 + \left[(\epsilon-1)^2\frac{\alpha_n^2}{\epsilon} + 2\right]\cosh\mu_{1n}L\cos\mu_{2n}L\right\} - \frac{2(\epsilon-1)^2\alpha_n^2\sqrt{1-\alpha_n^2}}{\epsilon}\cosh\mu_{1n}L\cos\mu_{2n}L + \frac{(1+\epsilon)\,\alpha_n}{\sqrt{\epsilon}}\sinh\mu_{1n}L\sin\mu_{2n}L + \frac{L}{K}\left\{(K\mu_{1n})\sqrt{1-\alpha_n^2}\left[(\epsilon-1)^2\frac{\alpha_n^2}{\epsilon} + 2\right]F_n - \frac{(1+\epsilon)\alpha_n(K\mu_{2n})}{\sqrt{\epsilon}}G_n\right\}\sinh\mu_{1n}L\cos\mu_{2n}L - \frac{L}{K}\left\{(K\mu_{2n})\sqrt{1-\alpha_n^2}\left[(\epsilon-1)^2\frac{\alpha_n^2}{\epsilon} + 2\right]G_n + \frac{(1+\epsilon)\alpha_n(K\mu_{1n})}{\sqrt{\epsilon}}F_n\right\}\cosh\mu_{1n}L\sin\mu_{2n}L$$

where

$$E_n = \left(\frac{2\epsilon}{\alpha_n^2\{[(1-\epsilon)^2 + (4\epsilon/\alpha_n^2)] - (1+\epsilon)\sqrt{(1-\epsilon)^2 + (4\epsilon/\alpha_n^2)}\}} + \frac{2\epsilon}{\alpha_n^2\{[(1-\epsilon)^2 + (4\epsilon/\alpha_n^2)] + (1+\epsilon)\sqrt{(1-\epsilon)^2 + (4\epsilon/\alpha_n^2)}\}} - 2\right)$$

$$F_n = \frac{2\epsilon}{\alpha_n^2\{[(1-\epsilon)^2 + (4\epsilon/\alpha_n^2)] - (1+\epsilon)\sqrt{(1-\epsilon)^2 + (4\epsilon/\alpha_n^2)}\}} - 1$$

$$G_n = \frac{2\epsilon}{\alpha_n^2\{[(1-\epsilon)^2 + (4\epsilon/\alpha_n^2)] + (1+\epsilon)\sqrt{(1-\epsilon)^2 + (4\epsilon/\alpha_n^2)}\}} - 1$$

$A(\omega/p_1)$ is a continuous function of ω/p_1 for the period of impact $0 \le t \le \pi/\omega$ and for the period after impact $\pi/\omega \le t \le \infty$. At the time $t = \pi/\omega$, both Eqs. (37) and (38) assume equal values.

When $\omega = p_n$ or $\alpha = \alpha_n$—i.e., when the frequency of the half-period of impact is equal to any one of the natural frequencies of the bar—Eqs. (37) and (38) cannot be used. The form of these equations is such that cases of "resonance" lead to indeterminacies that can be determined by means of a limit calculation. There are obvious physical reasons why strains in such cases must be finite and determinate. When α_p represents any one of the natural modes of the bar, the form of Eq. (37) changes as follows.

During impact, for $0 \le t \le \pi/\omega$

$$A\frac{\omega}{p_1} = -2\frac{c_l}{K}\frac{K^2}{L^2}\frac{\alpha}{\alpha_1}\frac{[\partial^2\Phi_1(i\alpha_p)/\partial x^2]_{x=L}}{\Delta_1'(i\alpha_p)}\,t\cos\omega t - \frac{4}{\alpha_1}\sqrt{\epsilon}\frac{K^2}{L^2}\sum_{\alpha_n\neq\alpha_p}^{\infty}\frac{[\partial^2\Phi_1(i\alpha_n)/\partial x^2]_{x=L}}{[(\alpha_n^2/\alpha^2) - 1]\Delta_1'(i\alpha_n)}\sin p_n t - 2\epsilon\frac{K^2}{L^2}\frac{\alpha}{\alpha_1}\sin\omega t \quad (39)$$

where

$$v = (c_l\,\alpha_p)/(K\sqrt{\epsilon})$$

After impact, for $\pi/\omega \le t \le \infty$

$$A\frac{\omega}{p_1} = -2\sqrt{\epsilon}\frac{K^2}{L^2}\frac{1}{\alpha_1}\frac{[\partial^2\Phi_1(i\alpha_p)/\partial x^2]_{x=L}}{\Delta_1'(i\alpha_p)}\,\pi\cos\omega t + 8\sqrt{\epsilon}\frac{K^2}{L^2}\frac{1}{\alpha_1}\sum_{\alpha_n\neq\alpha_p}^{\infty}\frac{[\partial^2\Phi_1(i\alpha_n)/\partial x^2]_{x=L}\cos[(\pi/2)(\alpha_n/\alpha)]}{[1 - (\alpha_n^2/\alpha^2)]\Delta_1'(i\alpha_n)}\sin p_n\left(t - \frac{\pi}{2\omega}\right) \quad (40)$$

Again it easily can be shown that Eqs. (39) and (40) give the same value for $A(\omega/p_1)$ at $t = \pi/\omega$. For

$$\omega = (c_l\,\alpha_p)/(K\sqrt{\epsilon})$$

this value is

$$A\frac{\omega}{p_1} = 2\sqrt{\epsilon}\frac{K^2}{L^2}\frac{\pi}{\alpha_1}\frac{[\partial^2\Phi_1(i\alpha_p)/\partial x^2]_{x=L}}{\Delta_1'(i\alpha_p)} - 4\sqrt{\epsilon}\frac{K^2}{L^2}\frac{1}{\alpha_1}\sum_{\alpha_n\neq\alpha_p}^{\infty}\frac{[\partial^2\Phi_1(i\alpha_n)/\partial x^2]_{x=L}}{[(\alpha_n^2/\alpha^2) - 1]\Delta_1'(i\alpha_n)}\sin\left(\frac{\pi p_n}{\omega}\right) \quad (41)$$

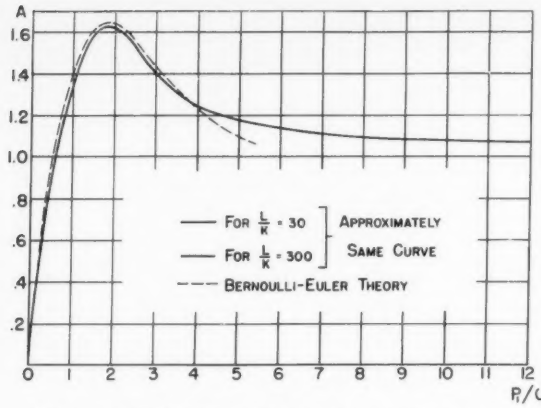

FIG. 1. Amplification factor "A" as a function of p_1/ω.

The series in Eqs. (37) to (41) appear highly convergent for small values of ω/p_1. Convergence is satisfactory for extremely large values of ω/p_1.

The nature of the convergence of the strains is best illustrated in terms of contributions to $A(\omega/p_1)$ by the various individual modes. This is shown in Table 2 for three typical values of ω/p_1 and for $L/K = 30$.

It will be noted that one value of ω/p_1 chosen is small and another is extremely large. The small value represents a condition arising during the half-period of impact. The first figure listed in that case as contribution by the first mode contains the effects of the forced response as indicated by Eq. (37). It is the maximum value arising due to beats between the forced response and the fundamental.

The final value of $A(\omega/p_1)$ in each case is obtained by summation of the contributions by the individual modes in their proper phase.

TABLE 2
Values of $A(\omega/p_1)$ as Contributed by the First Six Modes for Three Typical Values of ω/p_1, $L/K = 30$

Mode	$\omega/p_1 = 0.221$	$\omega/p_1 = 10$	$\omega/p_1 = 10^6$
1	−0.25121086	−1.8217899	−1.8260538
2	+0.00065495	−0.9050575	−0.9875643
3	+0.00005248	−0.2829975	−0.5353914
4	+0.00001042	−0.1264207	−0.3424051
5	+0.00000309	+0.0123078	−0.2290035
6	+0.00000112	+0.0044955	−0.1543817
$A(\omega/p_1)$	−0.25048880	−3.1194623	−4.0747998

Curves of $A(\omega/p_1)$ were plotted as functions of ω/p_1 for $L/K = 30$ and for $L/K = 300$. In each case the first six terms were included in the series, and it was found that little was gained by carrying more terms. The results are shown in Fig. 2.

In the case of the short and thick bar $L/K = 30$, it will be noted that the limiting value of $A(\omega/p_1)$ for large values of ω/p_1 is 4.08. Similarly, the limit of $A(\omega/p_1)$ for large values of ω/p_1 in the case of the slender and long bar $L/K = 300$ is 4.89.

$A(\omega/p_1)$ is proportional to the maximum strain ϵ_m at the clamped end. In the case of the short bar, $L/K = 30$

$$A\,\frac{\omega}{p_1} = \frac{4\sqrt{\epsilon}}{\alpha_1}\left(\frac{K^2}{L^2}\right)\frac{a\epsilon_m}{Vd} = 1.18\,\frac{a\epsilon_m}{Vd} \qquad (42a)$$

In the case of the long bar, $L/K = 300$

$$A\,\frac{\omega}{p_1} = \frac{4\sqrt{\epsilon}}{\alpha_1}\left(\frac{K^2}{L^2}\right)\frac{a\epsilon_m}{Vd} = 1.13\,\frac{a\epsilon_m}{Vd} \qquad (42b)$$

where

$$a^2 = \frac{EK^2}{\rho} = K^2 c_l^2$$

V = initial velocity on impact

d = depth of bar

From Eq. (42a) the maximum strain for impact of extremely short duration at the clamped end of a short bar will be

$$\epsilon_m = (4.08/1.18)\,(Vd/a) = 3.46(Vd/a) \qquad (43a)$$

For the long slender bar, the maximum strain will be

$$\epsilon_m = (4.89/1.13)\,(Vd/a) = 4.34(Vd/a) \qquad (43b)$$

In the case of the constant Q hypothesis in the Bernoulli-Euler theory

$$\epsilon_m = (3.55/1.138)\,(Vd/a) = 3.12(Vd/a) \qquad (43c)$$

This shows then that the effect of rotatory inertia and shear on the maximum strain at the clamped end of a bar in short duration impact is of approximately the same order of magnitude as viscous damping would be on the constant Q hypothesis. It is instructive to note that a thin slender bar will be subjected to approximately 25.5 per cent higher strain than the thick short bar at the clamped end in short duration impact.

REFERENCES

[1] Symonds, P., and Vigness, I., *Influence of Impact on Damage of Some Elastic Systems*, Report No. 0-2293, Naval Research Laboratory, Bellevue, D.C., May 15, 1944.

[2] Mindlin, R. D., Stubner, F. W., Cooper, H. L., *Response of Damped Elastic Systems to Transient Disturbances*, Proceedings of the Society for Experimental Stress Analysis, Vol. 5, pp. 69–87, 1948.

(*Continued on page 348*)

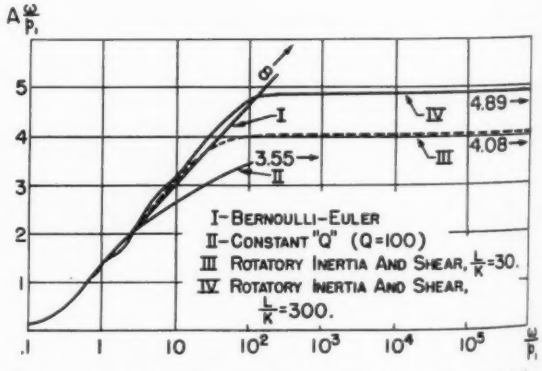

FIG. 2. Relation between maximum dynamic strain and relative impact duration.

The Buckling of Isosceles Triangular Plates

HUGH L. COX* AND BERTRAM KLEIN*

Douglas Aircraft Company, Inc.

SUMMARY

Approximate solutions are presented for the elastic critical buckling loads of isosceles triangular plates that have either clamped or simply supported edges. Loading conditions of uniform axial compression along all edges of the plate and of compression along the base edge and shear along the other two edges are treated. The results of the calculations are presented in graphical form so that an engineer may determine rapidly the lowest critical buckling load.

(1) INTRODUCTION

FREQUENTLY IN THE ANALYSIS of aircraft structures it is necessary to determine the buckling load of a triangular plate. Usually the plate is either uniformly axially compressed along all edges, Fig. 1(a), or compressed along the base edge with the load taken out in shear along the other two edges, Fig. 1(b). The approximate solution presented in this paper is based essentially upon the method of collocation—i.e., for an assumed deflection function, which satisfies the boundary conditions, the governing differential equation for the plate is satisfied at a finite number of points. Comparisons are made for certain cases with other known solutions, and the agreement appears to be satisfactory for most engineering purposes.

(2a) SIMPLY SUPPORTED PLATES UNDER THRUST

Let x and y be coordinates in the middle surface of the plate as shown in Fig. 1(a). The differential equation for a uniform plate subjected to thust is

$$D\Delta^2\Delta^2 w = N_x(\partial^2 w/\partial x^2) + N_y(\partial^2 w/\partial y^2) \qquad (1)$$

where

D = plate stiffness
w = deflection of plate, positive downward
N_x = load per unit length acting parallel to x axis
N_y = load per unit length acting parallel to y axis

The boundary conditions are

$$(w)_{y=h} = (w)_{x=\pm(a/h)y} = 0 \qquad (2)$$

$$\left(\frac{\partial^2 w}{\partial y^2} + \nu\frac{\partial^2 w}{\partial t^2}\right)_{y=h} = \left(\frac{\partial^2 w}{\partial n^2} + \nu\frac{\partial^2 w}{\partial t^2}\right)_{x=\pm(a/h)y} = 0 \qquad (3)$$

where n is the normal direction to the lines

$$x = \pm(a/h)y$$

and t is the tangential direction of any line. Along a rectilinear edge the term $\partial^2 w/\partial t^2$ is equal to zero.

Received July 20, 1954.

* Strength Engineer, Santa Monica Division.

The deflection function

$$w = (\alpha_1 F_1 + \alpha_2 F_2 + \alpha_3 F_3)\cos k\frac{\pi}{2}\frac{h}{a}\frac{x}{y} \qquad (4)$$

where

$F_1 = 2\sin^2(\pi y/2h)\sin(\pi y/h)$
$F_2 = 2\sin^2(\pi y/2h)\sin(2\pi y/h)$
$F_3 = 2\sin^2(\pi y/2h)\sin(3\pi y/h)$
α = generalized coefficient
k = odd integer

satisfies Eq. (2) exactly and the condition

$$(\partial^2 w/\partial n^2)_{x=\pm(a/h)y} = 0$$

from Eq. (3) at some point in the region of $(h/2) \leq y \leq (3h/4)$; the condition that

$$\left(\frac{\partial^2 w}{\partial y^2}\right)_{y=h} = 0$$

is satisfied exactly only when $x = 0$. Selected points for collocation will be on the line $x = 0$; therefore, no serious error should result from not satisfying completely the boundary conditions. The first term of the deflection function given by Eq. (4) appears physically to have the shape that one might expect for a triangular plate buckled into one wave.

It will be necessary to differentiate the deflection function given in Eq. (4) and substitute the proper derivatives into Eq. (1).

Let

$$F(y) = \alpha_1 F_1 + \alpha_2 F_2 + \alpha_3 F_3 \qquad (5)$$

Eq. (4) may be written as

$$w = F(y)\cos k(\pi/2)(h/a)(x/y) \qquad (6)$$

Derivatives of w at $x = 0$ are

$$\left(\frac{\partial^2 w}{\partial x^2}\right)_{x=0} = -F(y)\left(k\frac{\pi}{2}\frac{h}{ay}\right)^2 \qquad (7)$$

$$\left(\frac{\partial^4 w}{\partial x^4}\right)_{x=0} = F(y)\left(k\frac{\pi}{2}\frac{h}{ay}\right)^4 \qquad (8)$$

$$(\partial^2 w/\partial y^2)_{x=0} = \partial^2 F(y)/\partial y^2 \qquad (9)$$

$$(\partial^4 w/\partial y^4)_{x=0} = \partial^4 F(y)/\partial y^4 \qquad (10)$$

$$\left(\frac{\partial^4 w}{\partial x^2\partial y^2}\right)_{x=0} = -\frac{k^2\pi^2}{4y^2}\left(\frac{h}{a}\right)^2\frac{\partial^2 F(y)}{\partial y^2} + \frac{k^2\pi^2}{y^3}\left(\frac{h}{a}\right)^2\frac{\partial F(y)}{\partial y} - \frac{3k^2\pi^2}{2y^4}\left(\frac{h}{a}\right)^2 F(y) \qquad (11)$$

The derivatives of $F(y)$ are written as

$$\left.\begin{aligned}
F_1' &= (\pi/h)\,[\cos(\pi y/h) - \cos(2\pi y/h)] \\
F_1'' &= (\pi/h)^2\,[-\sin(\pi y/h) + 2\sin(2\pi y/h)] \\
F_1'''' &= (\pi/h)^4\,[\sin(\pi y/h) - 8\sin(2\pi y/h)] \\
F_2' &= \frac{\pi}{h}\left[2\cos\frac{2\pi y}{h} - \frac{3}{2}\cos\frac{3\pi y}{h} - \frac{1}{2}\cos\frac{\pi y}{h}\right] \\
F_2'' &= \left(\frac{\pi}{h}\right)^2\left[-4\sin\frac{2\pi y}{h} + \frac{9}{2}\sin\frac{3\pi y}{h} + \frac{1}{2}\sin\frac{\pi y}{h}\right] \\
F_2'''' &= \left(\frac{\pi}{h}\right)^4\left[16\sin\frac{2\pi y}{h} - \frac{81}{2}\sin\frac{3\pi y}{h} - \frac{1}{2}\sin\frac{\pi y}{h}\right] \\
F_3' &= \frac{\pi}{h}\left[3\cos\frac{3\pi y}{h} - 2\cos\frac{4\pi y}{h} - \cos\frac{2\pi y}{h}\right] \\
F_3'' &= \left(\frac{\pi}{h}\right)^2\left[-9\sin\frac{3\pi y}{h} + 8\sin\frac{4\pi y}{h} + 2\sin\frac{2\pi y}{h}\right] \\
F_3'''' &= \left(\frac{\pi}{h}\right)^4\left[81\sin\frac{3\pi y}{h} - 128\sin\frac{4\pi y}{h} - 8\sin\frac{2\pi y}{h}\right]
\end{aligned}\right\} \tag{12}$$

If Eqs. (12) are substituted into Eqs. (7) through (11) and the resulting derivatives are substituted into Eq. (1), there results

$$\left.\begin{aligned}
A\alpha_1 + B\alpha_2 + C\alpha_3 &= 0, \qquad \text{at } y = h/2 \\
J\alpha_1 + E\alpha_2 + F\alpha_3 &= 0, \qquad \text{at } y = 2h/3 \\
G\alpha_1 + H\alpha_2 + I\alpha_3 &= 0, \qquad \text{at } y = 3h/4
\end{aligned}\right\} \tag{13}$$

where

$$\left.\begin{aligned}
A &= \pi^2\left(k\frac{h}{a}\right)^4 + \pi^2 + 22.00490\left(k\frac{h}{a}\right)^2 - \beta\left[\left(k\frac{h}{a}\right)^2 + 1\right] \\
B &= 394.7860 - 21.5740[k(h/a)]^2 - 4\beta \\
C &= -\pi^2\left(k\frac{h}{a}\right)^4 - 799.4416 - 179.9193\left(k\frac{h}{a}\right)^2 + \beta\left[\left(k\frac{h}{a}\right)^2 + 9\right] \\
J &= 2.3421\left(k\frac{h}{a}\right)^4 + 44.41342 + 5.26442\left(k\frac{h}{a}\right)^2 - \beta\left[0.42187\left(k\frac{h}{a}\right)^2 + 1.5\right] \\
E &= -2.34211\left(k\frac{h}{a}\right)^4 - 81.42461 - 41.13184\left(k\frac{h}{a}\right)^2 + \beta\left[0.42187\left(k\frac{h}{a}\right)^2 + 2.25\right] \\
F &= -592.1790 + 21.78418[k(h/a)]^2 + 3\beta \\
G &= 2.35332\left(k\frac{h}{a}\right)^4 + 85.93610 + 1.77300\left(k\frac{h}{a}\right)^2 - \beta\left[0.53649\left(k\frac{h}{a}\right)^2 + 2.70711\right] \\
H &= -3.32809\left(k\frac{h}{a}\right)^4 - 444.04924 - 60.45476\left(k\frac{h}{a}\right)^2 + \beta\left[0.75871\left(k\frac{h}{a}\right)^2 + 7.53553\right] \\
I &= 2.35332\left(k\frac{h}{a}\right)^4 + 644.24798 + 123.31292\left(k\frac{h}{a}\right)^2 - \beta\left[0.53649\left(k\frac{h}{a}\right)^2 + 8.36396\right]
\end{aligned}\right\} \tag{14}$$

and where

$$\beta = Nh^2/D \tag{15}$$

Values of β for various ratios of h/a may be determined from the condition

$$\begin{vmatrix} A & B & C \\ J & E & F \\ G & H & I \end{vmatrix} = 0 \tag{16}$$

Fig. 2 shows in graphical form, on semilog paper, the relationship between β and h/a for a practical range of h/a values. For an equilateral triangle, from Eq. (16), $\beta = 35.6$. The exact answer[1] is $\beta = 4\pi^2$. The above solution is somewhat conservative for an equilateral triangular plate; for the case of $h/a = 1.0$, the value of β given in Fig. 2 differs by less than one-half of one per cent from a value obtained by Wittrick.[3] In general, the curve in Fig. 2 affords a rapid approximate answer, which appears to be on the safe side for plates having various ratios of h/a.

(2b) Simply Supported Plates Under Shear and Thrust

For the load conditions shown in Fig. 1(b)

$$\left.\begin{aligned} N_x &= -N\left(\frac{a}{h}\right)^2 \\ N_y &= N \end{aligned}\right\} \tag{17}$$

If the first terms in brackets in Eqs. (14) are multiplied by $-(a/h)^2$, the resulting equations will be sufficient for determining the lowest critical value of N. Fig. 3 gives values of β for different ratios of h/a. When $h/a = 1.0$, the value of β given in Fig. 3 differs by less than 1 per cent from the value obtained by Wittrick.[3]

(3a) Clamped Plates Under Thrust

Consider the plate shown in Fig. 1(a). The boundary conditions are

$$\left.\begin{aligned} (w)_{y=h} &= (w)_{x=\pm(a/h)y} = 0 \\ (\partial w/\partial y)_{y=h} &= (\partial w/\partial n)_{x=\pm(a/h)y} = 0 \end{aligned}\right\} \tag{18}$$

The deflection function

$$w = (\alpha_1 F_1 + \alpha_2 F_2) F_3 \tag{19}$$

where

$$F_1 = y^2 \sin^2(\pi y/h)$$

$$F_2 = y^2 \sin(\pi y/h) \sin(2\pi y/h)$$

$$F_3 = \left[1 - \left(\frac{h}{a}\frac{x}{y}\right)^2\right] \cos k \frac{\pi}{2}\frac{h}{a}\frac{x}{y}$$

satisfies the boundary conditions. It is necessary to differentiate Eq. (19) and substitute the proper derivatives into Eq. (1). Let

$$F(y) = \alpha_1 F_1 + \alpha_2 F_2 \tag{20}$$

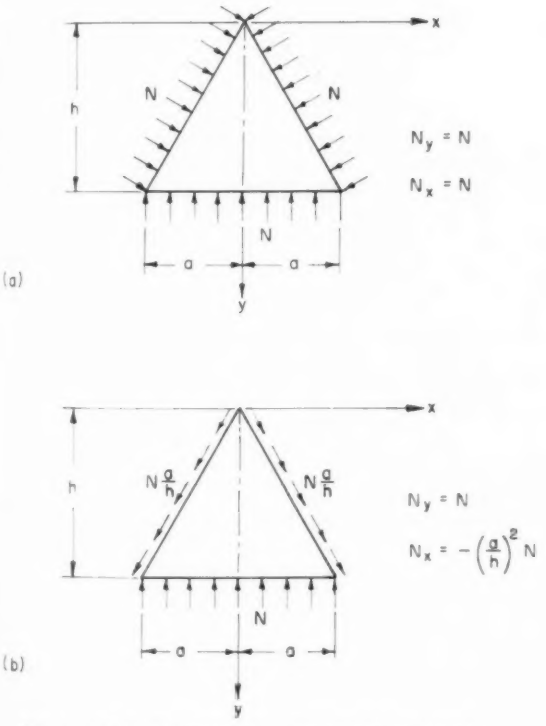

FIG. 1 LOAD CONDITIONS CONSIDERED FOR TRIANGULAR PLATES

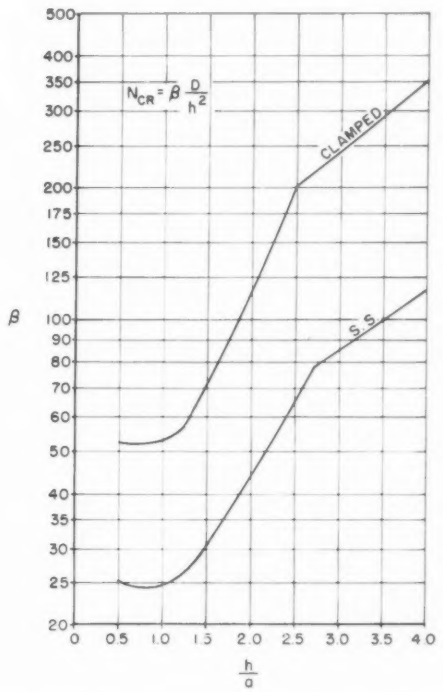

FIG. 2 BUCKLING COEFFICIENT FOR PLATE SUBJECTED TO UNIFORM THRUST (FIG. 1a)

Derivatives of w at $x = 0$ become

$$\left(\frac{\partial^2 w}{\partial x^2}\right)_{x=0} = -F(y)\left(\frac{h}{a}\right)^2 \frac{1}{y^2}\left[2 + \frac{k^2\pi^2}{4}\right]$$

$$\left(\frac{\partial^4 w}{\partial x^4}\right)_{x=0} = F(y)\left(\frac{h}{a}\right)^4 \frac{k^2\pi^2}{y^4}\left[3 + \frac{k^2\pi^2}{16}\right]$$

$$(\partial^2 w/\partial y^2)_{x=0} = \partial^2 F(y)/\partial y^2 \qquad (21)$$

$$(\partial^4 w/\partial y^4)_{x=0} = \partial^4 F(y)/\partial y^4$$

$$\left(\frac{\partial^4 w}{\partial x^2 \partial y^2}\right)_{x=0} = \left(\frac{h}{a}\right)^2 \left\{-\frac{\partial^2 F(y)}{\partial y^2}\frac{1}{y^2}\left[2 + \frac{k^2\pi^2}{4}\right] + \frac{\partial F(y)}{\partial y}\frac{4}{y^3}\left[2 + \frac{k^2\pi^2}{4}\right] - 6F(y)\frac{1}{y^4}\left[2 + \frac{k^2\pi^2}{4}\right]\right\}$$

The derivatives of $F(y)$ are written as

$$F_1' = \frac{\pi}{h} y^2 \sin\frac{2\pi y}{h} + 2y\sin^2\frac{\pi y}{h}$$

$$F_1'' = 4\frac{\pi}{h} y \sin\frac{2\pi y}{h} + \frac{2\pi^2}{h^2} y^2 \cos\frac{2\pi y}{h} + 2\sin^2\frac{\pi y}{h}$$

$$F_1'''' = 24\frac{\pi^2}{h^2}\cos\frac{2\pi y}{h} - 32\frac{\pi^3}{h^3} y\sin\frac{2\pi y}{h} - 8\frac{\pi^4}{h^4} y^2\cos\frac{2\pi y}{h} \qquad (22)$$

$$F_2' = y\left[\cos\frac{\pi y}{h} - \cos\frac{3\pi y}{h}\right] + \frac{y^2}{2}\left[-\frac{\pi}{h}\sin\frac{\pi y}{h} + \frac{3\pi}{h}\sin\frac{3\pi y}{h}\right]$$

$$F_2'' = \frac{2\pi y}{h}\left[-\sin\frac{\pi y}{h} + 3\sin\frac{3\pi y}{h}\right] + \left[\cos\frac{\pi y}{h} - \cos\frac{3\pi y}{h}\right] - \frac{y^2\pi^2}{2h^2}\left[\cos\frac{\pi y}{h} - 9\cos\frac{3\pi y}{h}\right]$$

$$F_2'''' = \frac{6\pi^2}{h^2}\left[-\cos\frac{\pi y}{h} + 9\cos\frac{3\pi y}{h}\right] + 4y\frac{\pi^3}{h^3}\left[\sin\frac{\pi y}{h} - 27\sin\frac{3\pi y}{h}\right] + \frac{y^2\pi^4}{2h^4}\left[\cos\frac{\pi y}{h} - 81\cos\frac{3\pi y}{h}\right]$$

If Eqs. (22) are substituted into Eqs. (21) and the resulting derivatives are substituted into Eq. (1), there results

$$\begin{aligned} P\alpha_1 + Q\alpha_2 &= 0, \qquad \text{at } y = h/2 \\ R\alpha_1 + S\alpha_2 &= 0, \qquad \text{at } y = 2h/3 \end{aligned} \qquad (23)$$

where

$$P = 118.435\left(\frac{h}{a}\right)^4 k^2 T - 42.052 + 39.478\left(\frac{h}{a}\right)^2 W - \beta\left[\left(\frac{h}{a}\right)^2 W + 2.9348\right]$$

$$Q = 1736.350 - 12.566\beta$$

$$R = 49.965\left(\frac{h}{a}\right)^4 k^2 T + 627.583 + 19.742\left(\frac{h}{a}\right)^2 W - \beta\left[\frac{3}{4}\left(\frac{h}{a}\right)^2 W + 10.1417\right] \qquad (24)$$

$$S = -49.965\left(\frac{h}{a}\right)^4 k^2 T - 1130.014 - 93.761\left(\frac{h}{a}\right)^2 W - \beta\left[-\frac{3}{4}\left(\frac{h}{a}\right)^2 W - 15.7082\right]$$

and where

$$\beta = Nh^2/D$$
$$W = 2 + (\pi^2 k^2/4)$$
$$T = 1 + 0.20562k^2.$$

Values of β for various ratios of h/a may be obtained from the condition

$$\begin{vmatrix} P & Q \\ R & S \end{vmatrix} = 0$$

Fig. 2 gives values of β for practical ranges of the parameter h/a. In the case of an equilateral triangle

$$\beta = 88.2 \qquad (25)$$

(3b) Clamped Plates Under Shear and Thrust

For the load condition shown in Fig. 1(b)

$$N_x = -N(a/h)^2, \qquad N_y = N$$

If the first terms in brackets in Eqs. (24) are multiplied by $-(a/h)^2$, the resulting equations will be sufficient for determining the critical value of N. Fig. 3 gives values of β for different ratios of h/a.

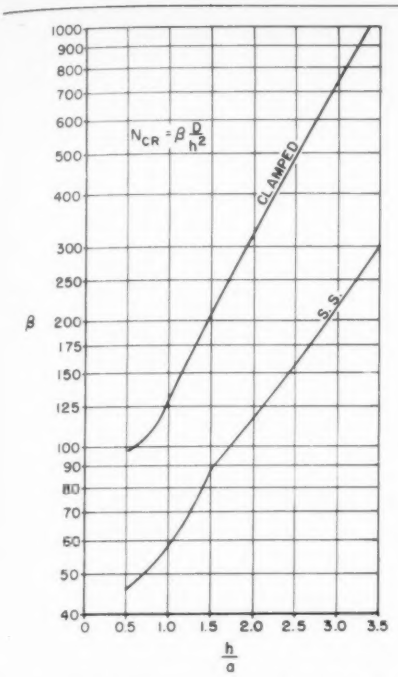

FIG. 3 BUCKLING COEFFICIENT FOR PLATE SUBJECTED TO THRUST AND SHEAR (FIG. 1b)

(3) Finite Difference Solution for Clamped Plate Under Thrust

In order to check the results presented in Part (3a) of this paper, the lowest critical buckling load of a uniformly compressed equilateral triangular plate is determined. Twenty-four interior points are selected. An equilateral triangular mesh is used.[2]

The difference equations that result from writing Eq. (1) in difference form may be written matrically as

$$(A + \lambda B)W = 0 \tag{26}$$

where

A = matrix of coefficients of $\Delta^2\Delta^2 w$ terms
B = matrix of coefficients of terms on right side of Eq. (1)
$\lambda = Nh^2/50D$

Eq. (26) is in standard eigen-value form and the solution for λ may be obtained easily by using an Electronic Digital Computor. The value of λ was found to be 1.949. Therefore

$$N_{CR} = 97.45(D/h^2) \tag{27}$$

This value is about 10 per cent higher than the value obtained in Eq. (25).

(4) Concluding Remarks

The curves presented in Figs. 2 and 3 should enable the engineer to obtain a rapid approximate answer for the lowest critical buckling load of isosceles triangular plates. It appears that the values of N_{Cr} given by the curves are on the safe side in the practical range of the values of h/a.

References

[1] Timoshenko, S., *Theory of Elastic Stability*, McGraw-Hill Book Company, Inc., 1st Ed., p. 371; 1936.

[2] Jensen, V. P., *Analyses of Skew Slabs*, Eng. Exp. Sta. Bull. No. 332, University of Ill., p. 53, 1941.

[3] Wittrick, W. H., *Buckling of a Simply Supported Triangular Plate in Combined Compression and Shear*, A.R.L. Rep. No. SM 197, Melbourne, July, 1952.

[4] Wittrick, W. H., *Buckling of a Right-Angled Isosceles Triangular Plate in Combined Compression and Shear (Perpendicular Edges Clamped, Hypotenuse Simply Supported)*, A.R.L. Rep. No. SM 211, Melbourne, June, 1953.

[5] Wittrick, W. H., *Buckling of a Right-Angled Isosceles Triangular Plate in Combined Compression and Shear (Perpendicular Edges Simply Supported, Hypotenuse Clamped)*, A.R.L. Rep. No. SM 220, Melbourne, November, 1953.

IAS Twenty-Fourth Annual Meeting

Hotel Astor, New York City, January 23–27, 1956

The Meetings Committee is planning sessions on Aerodynamics, Aeroelasticity, Structures, Rotating Wing, Aircraft Design, Meteorology, etc.

Authors wishing to have papers considered for presentation at this meeting should submit outlines or short abstracts to the Meetings Committee, 2 East 64th St., New York 21, N.Y., no later than September 1, 1955.

A Fraction Series Solution for Characteristic Values Useful in Some Problems of Airplane Dynamics

E. L. LEPPERT, JR.*

Lockheed Aircraft Corporation

ABSTRACT

Means for solving the determinantal equation $D(\lambda) = |A - k\lambda|$ for its characteristic values is described. The method has been developed with particular regard for its use in solution of flutter problems and to its use with punch-card or high-speed electronic computing equipment.

The roots are obtained by evaluation of a function consisting of a series of fractions and having the same roots as the polynomial of the determinant. The fraction series is formed in such a manner that its coefficients are readily calculated such that the roots may be obtained to a high degree of accuracy. A simple example illustrates the procedures.

The method has been adapted to the IBM 701. Evaluation of the 15 complex roots and their corresponding eigen-vectors for a 16 degree of freedom (one body mode without stiffness) complex flutter determinant is accomplished in 59 min., including a complete check. Evaluation of the roots without check requires 29 min.

INTRODUCTION

SOLUTION FOR THE eigen-values of the determinantal equation

$$D(\lambda) = |A - k\lambda| = \begin{vmatrix} a_{11} - k_1\lambda & a_{12} & a_{13} & a_{1n} \\ a_{21} & a_{22} - k_2\lambda & a_{23} & a_{2n} \\ a_{31} & a_{32} & a_{33} - k_3\lambda & a_{3n} \\ \cdots & \cdots & \cdots & \cdots \\ a_{n1} & a_{n2} & a_{n3} & a_{nn} - k_n\lambda \end{vmatrix} = 0$$

having real or complex coefficients a_{ij} is required in the solution of many physical problems. Wayland[1] describes a number of methods for expansion into polynomial form preliminary to solving for the roots. The relative merits of the methods described are compared by him on the basis of the number of operations required. The important question of the requisite accuracy is not resolved.

In the following development, a function consisting of a series of fractions[2]

$$f(\lambda) = \sum_{j=1}^{n+1} \frac{C_j}{\lambda - \lambda_j} = \frac{C_1}{\lambda - \lambda_1} + \frac{C_2}{\lambda - \lambda_2} + \frac{C_3}{\lambda - \lambda_3} + \cdots \frac{C_{n+1}}{\lambda - \lambda_{n+1}} = 0 \quad (1)$$

is utilized to determine all the roots to the same accuracy. The λ_j are arbitrary values for substitution into, and subsequent evaluation of, $D(\lambda)$; the values of the C_j coefficients are determined such that the roots of $D(\lambda)$ and $f(\lambda)$ are the same.

The fraction series is the quotient of two polynomials. The numerator is the polynomial of the determinant; the denominator is a polynomial having as roots the arbitrary λ_j. Evaluation of the coefficients C_j is made according to Peirce.[3] In general form,

$$C_j = \frac{D(\lambda_j)}{\prod_{\substack{i=1 \\ (i \neq j)}}^{n+1} (\lambda_j - \lambda_i)} \quad (2)$$

For the special case where the substitution λ_i is a root, so that $\Pi(\lambda_r - \lambda_i) = 0$; $D(\lambda_r) = 0$ and $C_r = 0$. The function $f(\lambda)$ then has the same roots as the determinant with one root divided out. While selection of the λ_i may be completely arbitrary, evaluation of the series to determine the roots is improved if the substitution values approximate the roots as closely as possible. In the absence of any knowledge of the distribution of roots, selection of a geometric progression has been found advantageous for some vibration problems.

EXAMPLE

An example illustrates the simplicity of the operations. A determinant having the eigen-values 0.2, 1.7, and 7.0 is assumed. The polynomial to which such determinant expands is

$$D(\lambda) = (\lambda - 0.2)(\lambda - 1.7)(\lambda - 7.0) = 0 \quad (3)$$

Presuming no information other than the order of the polynomial, the arbitrary values λ are chosen—0, 1, 2, 4, and 8. Evaluation of the coefficients for the

Received November 8, 1950. Revised and received July 8, 1954.

* Research Specialist.

TABLE 1

λ_i \ $\lambda_j - \lambda_i$	1	2	4	8	$\Pi(\lambda_j-\lambda_i)$ $i \neq j$	$D(\lambda_j)$	$C_j = \frac{D(\lambda_j)}{\Pi(\lambda_j-\lambda_i)}$
1	0	-1	-3	-7	-21	3.36	-.1600
2	1	0	-2	-6	12	-2.70	-.2250
4	3	2	0	-4	-24	-26.22	1.0925
8	7	6	4	0	168	49.14	.2925
0						-2.38	

fraction series is shown in Table 1 from which

$$f(\lambda) = -\frac{0.1600}{\lambda - 1} + \frac{-0.2250}{\lambda - 2} + \frac{1.0925}{\lambda - 4} + \frac{0.2925}{\lambda - 8} = 0 \quad (4)$$

Examination of the values of the determinant $D(\lambda)$ reveals changes in sign between 0 and 1, between 1 and 2, and between 4 and 8. Three methods for obtaining the roots are shown

(1) Substitution of assumed values of λ_A, calculation of the corresponding values of $f(\lambda)$ (see Table 2) and plotting the resultant curve as in Fig. 1 until a crossing is obtained is rapid and well suited to desk calculation.

(2) An iterative solution, wherein an assumed λ_A is substituted in all the fractions but one and a value λ_C obtained for that one such that $f(\lambda) = 0$, is often possible. Substitution of λ_C into the fractions in place of λ_A and solution for a new λ_C generally results in rapid convergence to a root. Table 3 lists values of λ_C for a number of λ_A to illustrate rapidity of convergence toward the root from widely separated assumed values.

(3) A modified iteration procedure requiring calculation of the λ_C for two trial values of λ_A in the vicinity of the root and assuming linearity of the function has been developed by E. E. Postel for use by the IBM Card Programmed Calculator to solve for the eigenvalues of the complex flutter determinant. Corresponding to the two trial values, two calculated λ_C values, C_1 and C_2, are obtained. A third trial value, λ_3, is then obtained with the linearity formula

$$\lambda_3 = \lambda_2 + \frac{C_2 - \lambda_2}{1 - \frac{C_1 - C_2}{\lambda_1 - \lambda_2}} \quad (5)$$

and a corresponding C_3 is calculated. The linearity formula is then again applied to obtain a fourth trial for which the corresponding C_4 is calculated. The procedure is repeated until sufficient convergence of

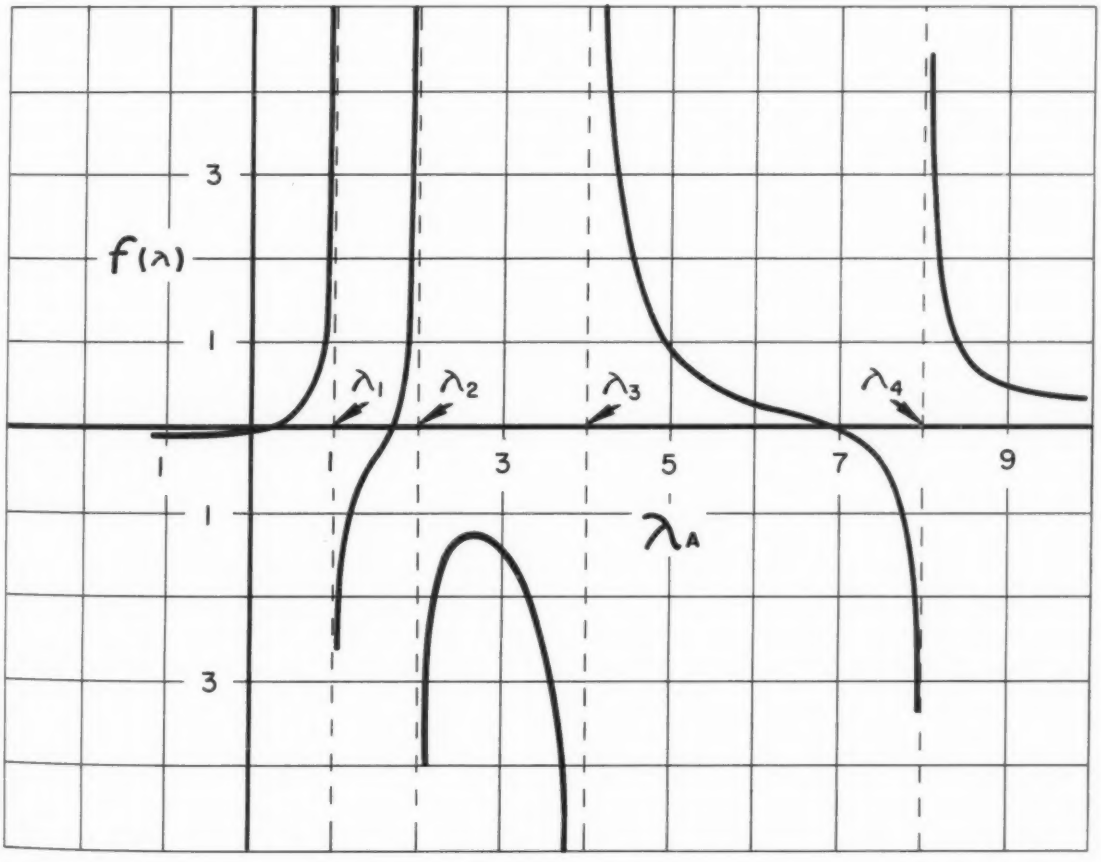

FIG. 1 $f(\lambda)$ vs. λ_A

TABLE 2

λ_A	(1)	(2)	(3)	(4)	$f(\lambda)$
0	+0.1600	+0.1125	−0.2731	−0.0366	−0.0372
0.1	+0.1778	+0.1184	−0.2801	−0.0369	−0.0208
0.5	+0.3200	+0.1500	−0.3150	−0.0390	+0.1160
$1-\epsilon$	$+\infty$				$+\infty$
$1+\epsilon$	$-\infty$				$-\infty$
1.3	−0.5333	+0.3214	−0.4046	−0.0437	−0.6516
1.5	−0.3200	+0.4500	−0.4370	−0.0450	−0.3520
1.8	−0.2000	+1.1250	−0.4960	−0.0472	+0.3818
$2-\epsilon$		$+\infty$			$+\infty$
$2+\epsilon$		$-\infty$			$-\infty$
2.2	−0.1333	−1.1250	−0.6100	−0.0505	−1.9188
2.4	−0.1140	−0.5625	−0.6850	−0.0523	−1.4138
3.0	−0.0800	−0.2250	−1.0925	−0.585	−1.4560
3.7	−0.0593	−0.1325	−3.6600	−0.0681	−3.9199
3.8	−0.0572	−0.1250	−5.4800	−0.0696	−5.7318
$4-\epsilon$			$-\infty$		$-\infty$
$4+\epsilon$			$+\infty$		$+\infty$
6.0	−0.0320	−0.0750	+0.5480	−0.1461	+0.2949
6.5	−0.0291	−0.0500	+0.4380	−0.1950	+0.1639
7.5	−0.0246	−0.0409	+0.3130	−0.5850	−0.3375
7.25	−0.0256	−0.0429	+0.3370	−0.3900	−0.1215

TABLE 3

λ_A	$f(\lambda)$	λ_C
0	$\frac{-0.1600}{\lambda_C - 1} + 0.1125 - 0.273125 - 0.0365625 = 0$	+0.1886
0.5	$\frac{-0.1600}{\lambda_C - 1} + 0.1500 - 0.31214 - 0.0390 = 0$	+0.2045
0.1	$\frac{-0.1600}{\lambda_C - 1} + 0.11842 - 0.280128 - 0.037025 = 0$	+0.195
0.2015	$\frac{-0.1600}{\lambda_C - 1} + 0.1251 - 0.2876 - 0.0375 = 0$	0.2000
1.3	$-0.5333 + \frac{-0.2250}{\lambda_C - 2} - 0.4046 - 0.0437 = 0$	1.77
1.5	$-0.3200 + \frac{-0.2250}{\lambda_C - 2} - 0.4370 - 0.0450 = 0$	1.718
1.8	$-0.2000 + \frac{-0.2250}{\lambda_C - 2} - 0.4966 - 0.0472 = 0$	1.697
1.673	$-0.2377 + \frac{-0.2250}{\lambda_C - 2} - 0.4695 - 0.0462 = 0$	1.7014
1.7	$-0.2286 + 0.7500 - 0.4750 - 0.0464 = 0$	

λ_n and C_n is obtained. An example utilizing numerical values from Table 3 follows:

$$\lambda_1 = 1.30, \quad C_1 = 1.77$$
$$\lambda_2 = 1.50, \quad C_2 = 1.718$$
$$\lambda_3 = 1.673, \quad C_3 = 1.7014 \qquad \lambda_4 = 1.699$$

DISCUSSION

The procedure is used at Lockheed as one of several methods of solution of the flutter determinant. In many cases, all the eigen-values are obtained by it with the same amount of computation as is required to obtain two or three roots by other methods. Utilization of the latest available IBM equipment to evaluate the determinants is a basic premise of the method.

An important feature of the method is the accuracy of the solutions. Each coefficient of the fraction series is obtained to the same accuracy as the evaluation of the determinant. They are not obtainde by differences of large numbers, a condition that requires computation with an exorbitant number of significant figures in other methods. The resultant eigen-values, whether large or small, are thus obtainable to the same accuracy as the value of the determinant.

Solution for the eigen-values of all real determinants of 16th order, and of complex flutter determinants of 8th order, is readily accomplished with presently available punched card equipment. Routine evaluation of each 8th order complex determinant requires 1 hour for each starring reduction on the IBM 604. From 1.8 to 2.0 hours on the Card Programmed Calculator are needed to form the fraction series and to iterate to all the roots.

The Lockheed Mathematical Analysis Department has programmed the method for the IBM 701 "Defense Calculator." Evaluation of an 8th order complex determinant requires 15 sec. In an application to 16th order complex flutter determinants, the 15 eigen-values and their corresponding eigen-vectors are obtained in an average elapsed time of 59 min. for each set. The modes include one body mode with no stiffness. The time includes a complete check. Evaluation of the roots without check requires 29 min.

Improvements on the 701, which will be available on production within a year, will allow evaluation of the larger degree of freedom problems in about one quarter the time.

The method has been utilized to explore the effect of variation of tip tank parameters on all of the wing flutter modes of a large military airplane. By utilizing primitive modes having motion of the tip tank in only one twist and one bending degree of freedom, it is possible to economically determine values of the determinants for a wide range of tip-tank conditions, utilizing a single set of assumed λ. Formation of the corresponding fraction series and solution for its eigen-values thus represents almost all the additional work required to obtain a complete set of solutions for each tip-tank condition.

CONCLUSIONS

A means for solving the determinantal equation for all its eigen-values is described. The method is of particular value in solution of flutter problems with punch-card equipment. A particular feature is its ability to obtain all roots with good accuracy. It has been found particularly useful in the study of the effect of variation of parameters in a problem having a large number of degrees of freedom.

REFERENCES

[1] Wayland, Harold, *Expansion of Determinantal Equations*, Quarterly of Applied Mathematics, Vol. II, No. 4, January, 1945.

[2] Lucas, Felix, *Comtes Rendes Hebdomainer de l'Academie Francaise*, 1888 pages, 1072 and 1073.

[3] Peirce, B. O., *A Short Table of Integrals*, page 14, 3rd Rev. Ed., Ginn and Company, 1929.

Stability of Compressible Laminar Boundary Layer with Internal Heat Sources or Sinks

GEORGE M. LOW*

Lewis Flight Propulsion Laboratory, NACA

SUMMARY

A solution of the equations of the compressible laminar boundary layer with heat sources or heat sinks is presented. The solution is limited to the flow over a flat plate with arbitrary surface temperature and constant Prandtl Number. It is assumed that the additional mass associated with the heat sources or sinks is negligible.

Stability calculations indicate that the boundary layer can be stabilized by heat withdrawal near the aircraft surface (e.g., by evaporation of liquid droplets) or by heat addition near the outer edge of the boundary layer (e.g., by condensation of a vapor). In addition, heat withdrawal near the surface is shown to provide an effective means of surface cooling.

INTRODUCTION

THE AERODYNAMIC HEATING of high-speed aircraft and missiles leads to many new design problems. If flight speeds continue to increase at the present rate, the steady-state skin temperatures encountered will soon exceed the allowable temperatures for metals used in aircraft construction (see Fig. 1). If the use of these metals is to be continued, adequate means of cooling will have to be provided.

Coexistent with the cooling problem is the problem of boundary-layer transition. If the boundary layer becomes turbulent, approximately ten times the amount of coolant is required to maintain a given surface temperature than that needed if the boundary layer remains laminar. As yet, little is known about the mechanism of transition from laminar to turbulent flow; presumably, if the turbulence level is low (as it will be in flight), transition is a result of the instability of the laminar boundary layer to small disturbances.

The stability of the laminar boundary layer in a compressible fluid has received a great deal of attention in recent years. In particular, Lees and Lin[1] and Lees[2] have established criteria for the determination of stability limits. In these papers it is suggested that, if sufficient heat is withdrawn at the surface, the boundary layer can be stabilized for all Reynolds Numbers. Detailed calculations by Van Driest[3] show that complete stability to two-dimensional disturbances can be attained at Mach Numbers between 1 and 9. The amount of cooling required for stability was found to be of the same order of magnitude as required to maintain the wall temperature at a reasonable level. These results have been at least qualitatively substantiated by Sternberg,[4] who observed laminar boundary layers at Reynolds Numbers as high as 50×10^6.

In the past, two methods of cooling, and thereby of stabilizing the laminar boundary layer, have been suggested: surface cooling, accomplished by passing a coolant along the inside of the skin, and transpiration cooling, accomplished by passing the coolant through the skin. In the present report a third method will be investigated—that of cooling by heat sinks within the boundary layer. The possibility of stabilizing the boundary layer by use of heat sources will also be investigated. Physically, the evaporation of liquid droplets in the boundary layer will act as a heat sink; whereas condensation of vapor or burning of fuel will be a source of heat.

A prerequisite for the calculation of stability limits is a solution of the applicable boundary-layer equations. These equations are therefore derived and solved for several particular distributions of heat sinks or sources. The Lees-Lin stability criteria are then applied to these solutions.

SYMBOLS

The following symbols are used in this report:

$a_N x^{*N}$	=	polynomial describing wall temperature distribution ($a_N x^{*N} \equiv a_0 + a_1 x^* + a_2 x^{*2} + \ldots$)
C	=	constant of proportionality in viscosity temperature relation
C_F	=	average friction drag coefficient
C_w	=	the factor $\sqrt{t_w/t_\infty}\,(t_\infty + S)/(t_w + S)$, a function of x
c	=	phase velocity of disturbance, divided by u_∞
c_f	=	local skin-friction coefficient
c_p	=	specific heat at constant pressure
f	=	solution of momentum equation
g	=	function describing temperature deviation due to heat sources (Eq. 18)

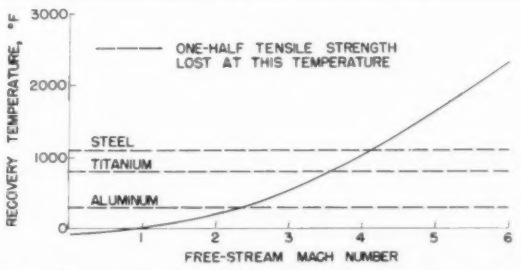

FIG. 1. Recovery temperature as function of free-stream Mach Number ($t_\infty = -67°$F.).

Presented at the Aerodynamics Session, National Summer Meeting, IAS, June 21–24, 1954, Los Angeles.

* Head, Fluid Mechanics Section, Supersonic Propulsion Division.

k = thermal conductivity
L = reference length
M = Mach Number
Pr = Prandtl Number, $\mu c_p/k$
p = static pressure
Q = heat addition per unit mass per unit time by source (or withdrawal by sink)
Q^* = $QL/c_p t_\infty u_\infty$
q = local rate of heat transfer
R = gas constant
Re = Reynolds Number, $\rho_\infty x u_\infty/\mu_\infty$
r = temperature function (see reference 5)
S = Sutherland's constant ($S = 216°$R.)
t = static temperature
t^* = t/t_∞
u = velocity in x-direction
u^* = u/u_∞
v = velocity in y-direction
w = coolant flow rate
x = distance along surface measured from leading edge
x^* = x/L
V_N = temperature function (see reference 5)
y = distance from surface measured perpendicular to surface
γ = ratio of specific heats
η = characteristic variable defined by Eq. (9)
η_0 = variable defining heat source location
μ = coefficient of viscosity
μ^* = μ/μ_∞
ν = kinematic viscosity, μ/ρ
ρ = mass density
τ = shearing stress

Subscripts

e = local conditions at outer edge of boundary layer
iw = insulated wall
w = conditions at wall or surface
∞ = conditions at $x = 0$, $y = \infty$
x, y, η = partial differentiation with respect to x, y, or η

Superscripts

$*$ = dimensionless quantities
$'$ = total differentiation with respect to η
A bar over a quantity indicates integration from zero to η

Boundary-Layer Analysis

Differential Equations and Boundary Conditions.—The steady laminar flow of a viscous compressible fluid in a boundary layer on a flat plate is governed by the momentum equation

$$uu_x + vu_y = (1/\rho)\,(\mu u_y)_y \tag{1}$$

the equation of continuity

$$(\rho u)_x + (\rho v)_y = 0 \tag{2}$$

the energy equation

$$c_p u t_x + c_p v t_y = (1/\rho)\,(k t_y)_y + \nu (u_y)^2 + Q \tag{3}$$

and the equation of state

$$\rho R t = p = \text{constant} \tag{4}$$

The last term in the energy equation describes the heat addition (or withdrawal) per unit mass per unit time.

These equations are subject to the following boundary conditions:

$$\left.\begin{aligned} u(x, 0) &= 0 \qquad u(x, \infty) = u_\infty \\ v(x, 0) &= 0 \qquad t(x, \infty) = t_e \\ t(x, 0) &= t_w(x) \quad \text{(for a noninsulated wall)} \\ \text{or} & \\ t_y(x, 0) &= 0 \quad \text{(for an insulated wall)} \end{aligned}\right\} \tag{5}$$

Assumption and Limitations.—The following assumptions and limitations are imposed in order to simplify the solution of Eqs. (1) to (4):

(1) The viscosity and temperature are linearly related as follows:

$$\mu^* = Ct^* \tag{6}$$

(Asterisks denote dimensionless quantities as defined under the section, Symbols.) Chapman and Rubesin[5] have shown that solutions of the boundary-layer equations based on this viscosity-temperature law agree well with more exact solutions at Mach Numbers up to about 5 if the constant C is determined by matching Eq. (6) with Sutherland's relation at the solid boundary:

$$C = \sqrt{t_w^*}\,[(1 + S/t_\infty)/(t_w^* + S/t_\infty)] \tag{7}$$

This assumption should also be reasonable for flows with heat sources, provided the resulting temperature deviation is not large.

(2) The additional mass associated with the heat sources has a negligible effect on the boundary-layer development. The validity of this assumption is demonstrated *a posteriori*.

(3) The surface temperature can be represented by a polynomial in x:

$$t_w^* = t_{iw}^* + a_N x^{*N} \tag{8}$$

where t_{iw}^* is the dimensionless wall temperature for zero heat transfer and the repeated index N indicates a summation.

Solution of Equations.—The present problem and the problem solved by Chapman and Rubesin[5] differ only in the last term in the energy equation. It is therefore only natural that the solution of the equations presented herein follows along the same line as given in reference 5. Briefly, the procedure is as follows: The system of four equations [Eqs. (1) to (4)] is reduced to two equations by absorption of the continuity equation and the equation of state into the other two equations. The dependent variables in the remaining equations are a newly defined stream function and a temperature. Further reduction of these equations is obtained by introducing new independent variables x^* and η, defined as follows:

$$\left.\begin{aligned} x^* &= x^* \\ \eta &= \frac{1}{2}\sqrt{\frac{u_\infty}{\nu_\infty x C}}\int_0^y \frac{1}{t^*}\,dy \end{aligned}\right\} \tag{9}$$

The dependent variables in this coordinate system are f and t and are defined by

$$\left.\begin{aligned} u^* &= (1/2)f'(\eta) \\ t^*(x^*, y) &= t^*(x^*, \eta) \end{aligned}\right\} \tag{10}$$

The resulting equations and associated boundary conditions are

$$\left.\begin{aligned} &f''' + ff'' = 0 \\ &f'(0) = f(0) = 0 \\ &f'(\infty) = 2 \end{aligned}\right\} \tag{11}$$

$$\left.\begin{aligned} &t_{\eta\eta}^* + Prft_\eta^* - 2Prf'x^*t_{x^*}^* = \\ &\qquad -\frac{\gamma - 1}{4} M_\infty^2 Pr(f'')^2 - 4Prx^*Q^* \\ &t^*(x^*, 0) = t_{iw}^* + a_N x^{*N} \\ &t^*(x^*, \infty) = 1 + \int_0^{x^*} Q^*(x^*, \infty)\, dx^* \end{aligned}\right\} \tag{12}$$

The momentum equation [Eq. (11)] is, of course, the well-known Blasius equation. The energy equation [Eq. (12)] is, with the exception of the last term on the right-hand side, identical to the energy equation solved by Chapman and Rubesin. Because the equation is linear, only a particular solution satisfying Eq. (12) need be added to the temperature function of reference 5 in order to obtain the complete solution.

Up to this point the derivation has been quite general. Before a solution of the energy equation can be obtained, however, a particular form for the heat-source distribution need be assumed. At this time, therefore, the assumption is made that Q^* is a function of η alone. In order to solve Eq. (12), it is divided into two linearly related parts,

$$t^* = t_1^* + t_2^* \tag{13}$$

where t_1^* and t_2^* satisfy the following equations:

$$\left.\begin{aligned} &t_{1\eta\eta}^* + Prft_{1\eta}^* - 2Prf'x^*t_{1x^*}^* = \\ &\qquad -\frac{\gamma - 1}{4} M_\infty^2 Pr(f'')^2 \\ &t_1^*(x^*, 0) = t_{iw}^* + a_N x^{*N} - t_2^*(x, 0) \\ &t_1^*(x^*, \infty) = 1 \end{aligned}\right\} \tag{14}$$

$$\left.\begin{aligned} &t_{2\eta\eta}^* + Prft_{2\eta}^* - 2Prf'x^*t_{2x^*}^* = -4Prx^*Q^* \\ &t_{2\eta}^*(x^*, 0) = 0 \\ &t_2^*(x^*, \infty) = x^*Q^*(\infty) \end{aligned}\right\} \tag{15}$$

Eq. (14) therefore describes the temperature distribution caused by wall heat transfer and by frictional heating. Eq. (15) describes the temperature increment due to heat sources or sinks. The wall heat transfer in Eq. (15) can be taken as zero without loss of generality, because arbitrary heat-transfer conditions are included in Eq. (14). The solution of Eq. (14), as given in reference 5, is

$$t_1^*(x^*, \eta) = 1 + \frac{\gamma - 1}{2} M_\infty^2 r(\eta) + a_N x^{*N} Y_N(\eta) \tag{16}$$

The solution to Eq. (15) is found to be

$$t_2^* = 4PrQ_0^* x^* g(\eta) \tag{17}$$

where g is the solution of the ordinary differential equation

$$\left.\begin{aligned} &g'' + Prfg' - 2Prf'g = -(Q^*/Q_0^*) \\ &g'(0) = 0, \quad g(\infty) = Q^*(\infty)/4PrQ_0^* \end{aligned}\right\} \tag{18}$$

and where Q_0^* is a measure of the total source or sink strength, defined by

$$Q_0^* = \int_0^\infty Q^*\, d\eta \tag{19}$$

The functions f, r, and Y_N and, where required, their derivatives and integrals, are presented graphically in reference 5. When more accuracy is desired, tabulated values of f and r can be found in reference 6, while numerical values of Y_N can be obtained from the following relations:

$$\left.\begin{aligned} Y_0(\eta) &= s(\eta)/s(0) \\ Y_N(\eta) &= \frac{h_{N1}(\eta) - H_{N1}(\eta)}{h_{N1}(0)} \qquad (N = 1, 2, 3) \end{aligned}\right\} \tag{20}$$

where the functions on the right-hand side are tabulated in reference 6. The function $g(\eta)$ was obtained on an electromechanical differential analyzer for nine specified distributions $Q^*(\eta)$. These distributions can be classified as "broad-band" distributions, defined by

$$\begin{aligned} Q^* &= 1 \quad (0 < \eta < \eta_0) \\ Q^* &= e^{-[6(\eta - \eta_0)]^2} \qquad (\eta > \eta_0) \end{aligned} \tag{21}$$

and as "narrow-band" distributions, defined by

$$Q^* = e^{-[6(\eta - \eta_0)]^2} \tag{22}$$

Sketches of these distributions appear as inserts in Fig. 2. Values of g, g', and $\bar{g} = \int_0^\eta g\, d\eta$ are presented in Figs. 2, 3, and 4. ($Pr = 0.72$.)

Boundary-Layer Characteristics.—Because the boundary-layer characteristics are obtained in the same manner as shown in reference 5, only final results will be presented herein.

Velocity and temperature profiles are obtained as functions of η by

$$u^* = (1/2)f'(\eta) \tag{23}$$

$$t^* = t_1^* + t_2^* = 1 + \frac{\gamma - 1}{2} M_\infty^2\, r(\eta) + a_N x^{*N} Y_N(\eta) + 4PrQ_0^* x^* g(\eta) \tag{24}$$

where the coefficients a_N are obtained by fitting a polynomial to the wall temperature distribution

$$a_N x^{*N} = t_w^* - t_{iw}^* \tag{25}$$

The insulated wall temperature is

$$t_{iw}^* = 1 + \frac{\gamma - 1}{2} M_\infty^2\, r(0) + 4PrQ_0^* x^* g(0) \tag{26}$$

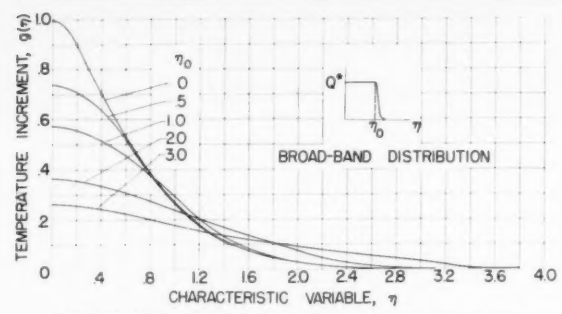

(a) BROAD-BAND DISTRIBUTION OF SOURCES OR SINKS.

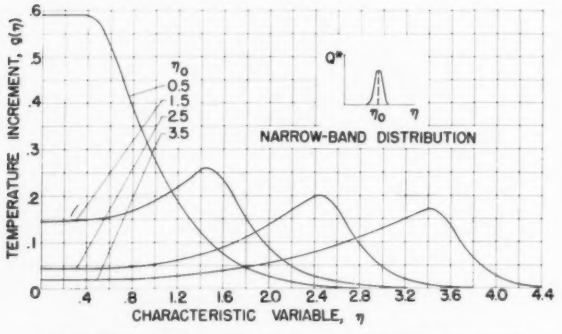

(b) NARROW-BAND DISTRIBUTIONS OF SOURCES OR SINKS.

FIG. 2. Variation of temperature increment due to heat sources or sinks.

If it is desired to obtain profiles in the physical x-, y-coordinate system, then the following relation between y and η is required:

$$y = 2\sqrt{\frac{\nu_\infty x C}{u_\infty}}\left[\eta + \frac{\gamma - 1}{2} M_\infty{}^2 \bar{f}(\eta) + a_N x^{*N} \bar{Y}_N(\eta) + 4 Pr Q_0{}^* x^* \bar{g}(\eta)\right] \quad (27)$$

(A bar over a quantity denotes integration from zero to η.) The wall shearing stress is

$$\tau_w \equiv \left(\mu \frac{\partial u}{\partial y}\right)_w = \frac{f''(0)}{4} u_\infty C_w \sqrt{\frac{\rho_\infty u_\infty \mu_\infty}{Cx}} \quad (28)$$

where $C_w(x^*) = \mu_w{}^*/t_w{}^*$ is equal to C for the special case of constant wall temperature. Local and average skin-friction coefficients are defined as follows:

$$c_f = \frac{\tau_w}{(1/2)\rho_\infty u_\infty{}^2} = \frac{f''(0)}{2} \frac{C_w}{\sqrt{CRe}} \quad (29)$$

$$C_F = \frac{1}{(1/2)\rho_\infty u_\infty{}^2 x} \int_0^x \tau_w \, dx$$

which, for constant wall temperature, becomes

$$C_F = 1.328\sqrt{C}/\sqrt{Re} \quad (30)$$

Thus it can be seen that heat sources affect skin friction only indirectly. In general, heating will alter the wall temperature, which in turn affects the constant C. The resulting change in skin friction is expected to be small.

The local rate of heat transfer is found from the temperature gradient by the following expression:

$$q \equiv -k_w (t_y)_w = -\frac{k_\infty t_\infty}{2} C_w \sqrt{\frac{u_\infty}{\nu_\infty x C}} a_N x^{*N} Y_N'(0) \quad (31)$$

The effect of heat sources or sinks on heat transfer is expected to be appreciable, because they have a first-order effect on $t_{iw}{}^*$, which is directly related to $a_N x^{*N}$. For example, it is expected that the transient heating of a missile could be reduced appreciably by the use of heat sinks in the boundary layer.

Use of Heat Sinks to Cool the Surface

The use of a broad-band distribution of heat sinks to cool the surface was investigated. In particular, the amount of heat withdrawn by heat sinks over an insulated surface [Fig. 5(b)] was compared with the amount of heat withdrawn at a wall [Fig. 5(a)] with the same surface temperature. The relative heat-transfer rates are shown in Fig. 6. The significance of these rates of heat transfer can be interpreted in terms of two alternate methods of cooling. If, for example, water is used as a coolant and if it is fully evaporated in both systems, then the relative coolant flow rates will be the same as the heat-transfer rates; under these conditions, wall cooling is slightly more efficient than cooling with heat sinks.

On the other hand, conditions may be such that evaporation can take place within the boundary layer,

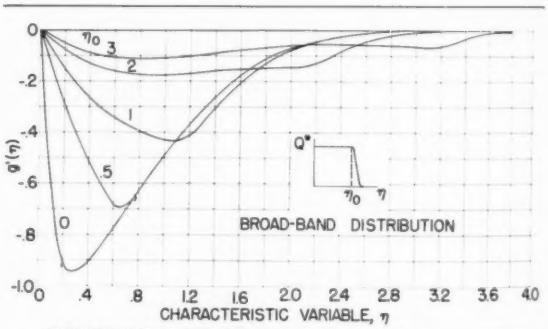

(a) BROAD-BAND DISTRIBUTION OF SOURCES OR SINKS.

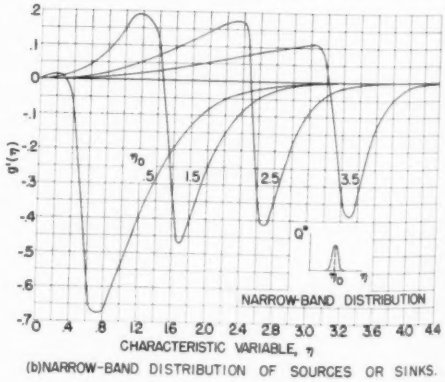

(b) NARROW-BAND DISTRIBUTION OF SOURCES OR SINKS.

FIG. 3. Variation of function $g'(\eta)$.

whereas within the wall the coolant cannot boil. When compared on the basis of coolant weight required, the heat sinks then provide a much more efficient cooling system than that provided by wall cooling (Fig. 7).

Stability Analysis

The stability of the laminar boundary layer on a flat plate in a compressible fluid has been investigated by Lees and Lin. As for the incompressible case, the stability differential equations are obtained by linearizing the equations of motion and energy for a flow with time-dependent fluctuating components superposed on the steady mean-flow quantities. These equations, in general, lead to a characteristic value problem relating the wave velocity and wave length of a disturbance to the parameters that govern the shape of the velocity and temperature profiles.

There is, however, one difference between the incompressible and the compressible stability problem. In the compressible case, distinction must be made between supersonic and subsonic disturbances. By definition, the x-component of the phase velocity of a supersonic disturbance relative to the free-stream velocity is greater than the free-stream speed of sound, and conversely. When a disturbance is supersonic, the characteristic value problem does not arise, and Lees and Lin have reasoned that amplified supersonic disturbances cannot exist. It therefore follows that only subsonic disturbances—that is, disturbances for which the dimensionless phase velocity c is greater than $1 - (1/M_e)$—are relevant in boundary-layer stability calculations.

Lees[2] suggested the possibility that, if sufficient heat is withdrawn from a supersonic laminar boundary layer, the flow will be stable at all Reynolds Numbers. This means that no self-excited disturbances can exist which satisfy the stability differential equations, their boundary conditions, and the requirement that c be greater than $1 - (1/M_e)$. In the present report only conditions for this "complete stability" are investigated.

Solutions of the stability problem fall in two general categories—inviscid solutions and viscous solutions. In the inviscid solutions, as the name implies, the effect of viscosity is neglected; these solutions apply only at infinite Reynolds Numbers. In the viscous solutions, the effect of viscosity is considered to the first order; these solutions therefore apply at large, but finite, Reynolds Numbers. In general, the inviscid solutions are much easier to obtain than the viscous solutions. However, care must be taken in interpreting inviscid results. A flow that is stable at $Re = \infty$ will usually not be stable at all Reynolds Numbers. It was found in reference 3 that, as far as complete stability is concerned, the viscous and inviscid solutions yield similar results at Mach Numbers greater than about 1.5. In the present report, therefore, only the inviscid solution is considered.†

The inviscid stability is determined by the shape of the velocity and temperature profiles in the boundary layer. In particular, amplified disturbances will not exist if

$$(\partial/\partial y)\ [\rho(\partial u/\partial y)] < 0 \tag{32}$$

when

$$c = u^* > 1 - (1/M_e) \tag{33}$$

In terms of the coordinates used in the present report, Eq. (32) becomes

$$(u_{\eta\eta}{}^*/u_\eta{}^*) - (2l_\eta{}^*/l^*) < 0 \tag{34}$$

or, by use of Eqs. (23), (24), and (11),

$$-f - \frac{(\gamma - 1)M_\infty{}^2 r' + 2a_N x^{*N} Y_N' + 8PrQ_0{}^* x^* g'}{1 + [(\gamma - 1)/2]M_\infty{}^2 r + a_N x^{*N} Y_N + 4PrQ_0{}^* x^* g} < 0 \tag{35}$$

The following procedure was employed in the determination of stability limits: For a given wall temperature distribution, a value of $Q_0{}^*$ was found such that the left-hand side of inequality (35) vanishes when $c = 1 - (1/M_e)$. This value of $Q_0{}^*$ was then used to determine whether the criterion was satisfied when $c > 1 - (1/M_l)$. In general, it was found that this was the case. In the few cases when the criterion was not satisfied, $Q_0{}^*$ was adjusted by trial and error until the correct value was determined.

The basic stability criteria, Eqs. (32) and (33), were derived for the flow without heat sources or sinks. It has been shown in the past[7] that stability criteria derived for flat-plate flows apply equally well to flows with pressure gradients, provided the local velocity and temperature profiles are considered. In other words, previous history of the flow is important only insofar as it affects the profile shapes. By analogy, it is assumed herein that the stability equations derived for flows without heat sources apply also to the flows treated in the present analysis if the proper velocity and temperature profiles are used.

It should also be noted that instability to two-dimensional disturbances only is considered. It was shown by Squire[8] that, for incompressible flow, two-dimensional disturbances are always more destabilizing than three-dimensional disturbances. Dunn and Lin[9] have recently shown that Squire's theorem cannot be extended to supersonic flows; at sufficiently high speeds, the boundary layer can never be completely stabilized with respect to all three-dimensional disturbances. However it has been shown experimen-

† One point in Fig. 10(a) was calculated by use of the viscous solution This point is seen to yield essentially the same result as the corresponding inviscid result.

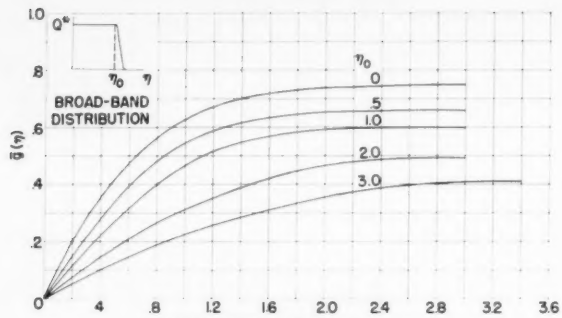

(a) BROAD-BAND DISTRIBUTIONS OF SOURCES OR SINKS.

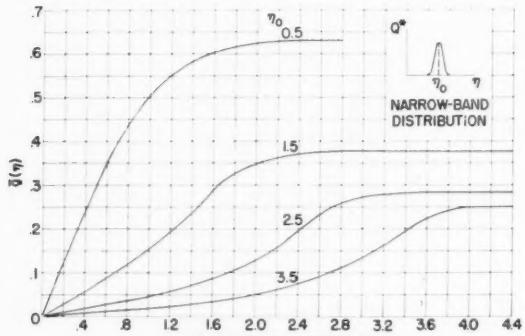

(b) NARROW-BAND DISTRIBUTION OF SOURCES OR SINKS.

FIG. 4. Variation of function $\bar{g}(\eta)$.

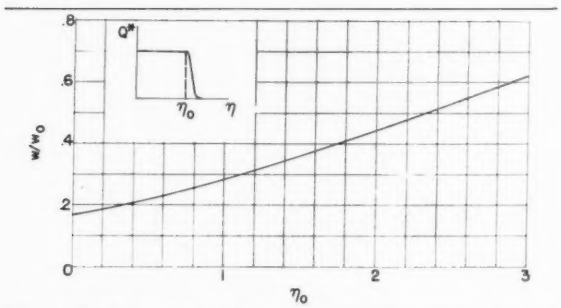

FIG. 7. Relative coolant flow rates required to maintain given surface temperature. w, cooling with sinks; w_0, wall cooling.

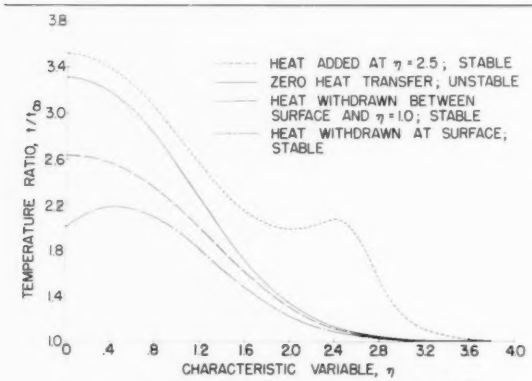
HEAT ADDED AT η = 2.5; STABLE
ZERO HEAT TRANSFER; UNSTABLE
HEAT WITHDRAWN BETWEEN SURFACE AND η = 1.0; STABLE
HEAT WITHDRAWN AT SURFACE; STABLE
TEMPERATURE RATIO, T/T_∞
CHARACTERISTIC VARIABLE, η

FIG. 8. Typical temperature profiles, M_∞, 3.69.

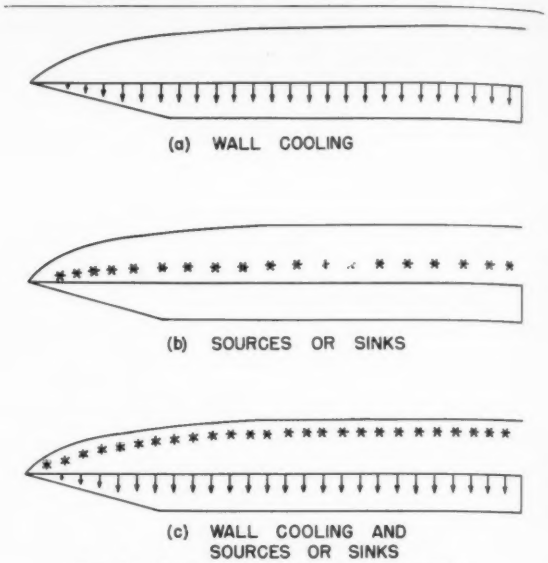

FIG. 5. Configurations discussed in examples.

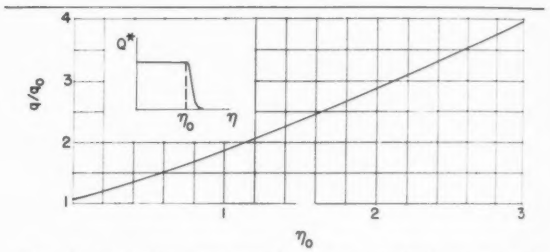

FIG. 6. Relative heat-transfer rates required to maintain given surface temperature. q, heat withdrawn by heat sinks; q_0, heat withdrawn at wall.

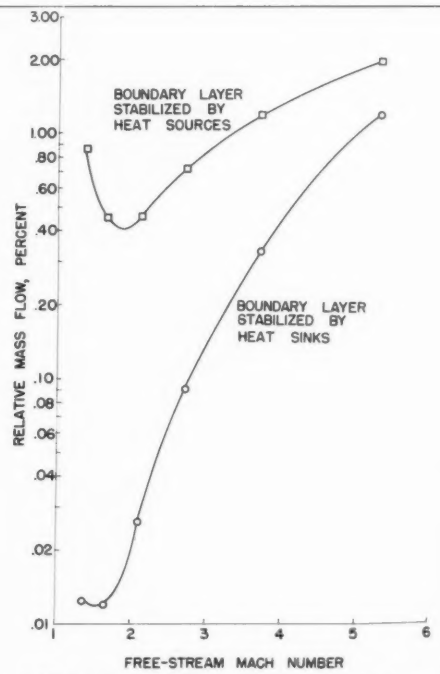
BOUNDARY LAYER STABILIZED BY HEAT SOURCES
BOUNDARY LAYER STABILIZED BY HEAT SINKS
RELATIVE MASS FLOW, PERCENT
FREE-STREAM MACH NUMBER

FIG. 9. Additional mass flow due to sources or sinks, x = 5 ft.

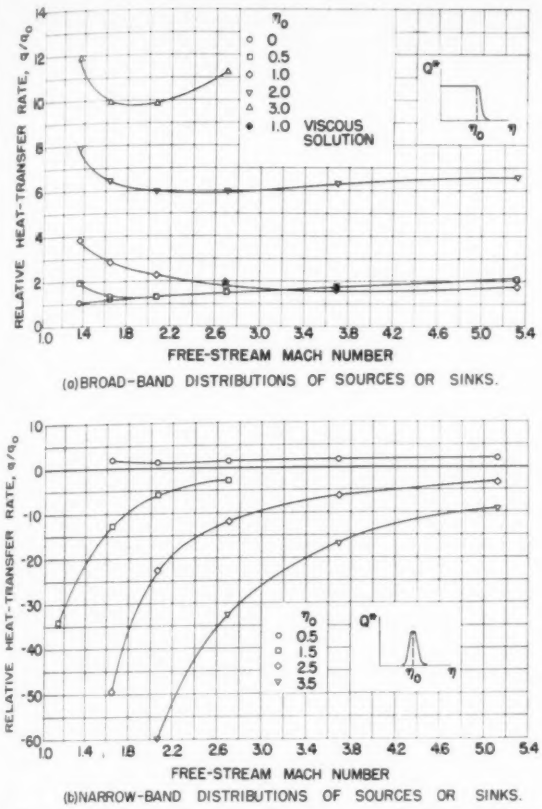

FIG. 10. Relative heat-transfer rates required to stabilize boundary layer. q, heat withdrawn by heat sinks or added by heat sources; q_0, heat withdrawn at wall.

tally[4] that surface cooling has a large effect on stability. It is believed, therefore, that the present results at least qualitatively describe the effect of heat sources and sinks on boundary-layer stability.

EFFECT OF HEAT SOURCES AND SINKS ON STABILITY

The stability of the laminar boundary layer is governed to a large extent by the distribution of angular momentum throughout the layer. The theory states that, if the angular momentum increases with y in that portion of the boundary layer where $u^* > 1 - (1/M_e)$, disturbances may be amplified. At supersonic speeds such an increase in $\rho(\partial u/\partial y)$ can be caused by the large negative temperature gradient in the central part of the boundary layer [see Eq. (34)]. If the temperature gradient can be kept small enough so that

$$2t^{*\prime}/t^* > -f \tag{36}$$

the flow will be stable. This distortion of the temperature profile could be accomplished by withdrawing heat at or near the wall or by adding heat at a distance from the wall.

In Fig. 8 are shown three temperature profiles that will just stabilize the boundary layer at a Mach Number of 3.69. Also shown in this figure is the profile for the unstable flow over an insulated surface. It is apparent that whether the stabilizing is done by wall cooling, by heat sinks, or by heat sources, the effect is always the same: The central part of the stable profiles is less steep than the central part of the unstable profiles. The outer portion of the profile with heat addition is fairly steep, but there the value of f is also large, so that condition (36) is not violated.

It was stated in the section entitled "Assumptions and Limitations" that the additional mass associated with heat sources or sinks is negligible. The mass flow of water or steam required to stabilize completely the boundary layer is shown in Fig. 9 as a percentage of the total boundary-layer mass flow. The addition of mass flow ranges between 0.01 and 2.00 per cent. By assuming that the additional mass is diffused like the temperature, it was found that the maximum percentage change in u''/u' is about three times as large as the percentage change in mass flow. Thus the effect of neglecting mass addition appears to be small.

Stability with Heat Sources and Sinks.—In Fig. 10 with heat sources or sinks on an insulated plate as compared with stability by wall cooling are presented. The broad-band distributions of heat sinks [Fig. 10(a)] are effective only if they are at or near the wall; at a distance from the wall the heat-transfer rate becomes prohibitive. Narrow-band distributions of heat sinks are effective only when they are extremely near the wall [Fig. 10(b)]. When the narrow-band distributions are placed at a distance from the surface, then heat addition is required, as indicated by the negative sign of the quantity q/q_0.

When the narrow-band distributions are placed in a critical layer in the central portion of the boundary layer, an infinite amount of heat addition or withdrawal is required to stabilize the boundary layer. The location of this critical layer will, in general, depend on the Mach Number and the exact shape of the distribution. From Eq. (35) it is seen that an infinite amount of heating or cooling is required for an insulated surface when

$$2g' + gf = 0 \tag{37}$$

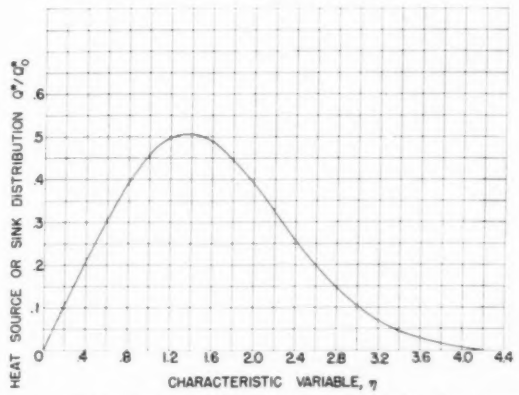

FIG. 11. Distribution of heat sources or sinks that cannot stabilize boundary layer at any Mach Number.

at that point in the boundary layer where

$$u^* = 1 - (1/M_e)$$

If Eq. (37) is solved for g and the result is substituted into Eq. (18), a distribution is obtained which cannot stabilize the boundary layer at any Mach Number. This distribution is shown in Fig. 11.

The relative efficiency of the stabilizing systems depends upon the method of cooling or heating. When water is used as a coolant, heat sinks can be much more effective than wall cooling if evaporation can only be realized within the boundary layer but not beneath the skin. If, on the other hand, evaporation can take place both within the wall and in the boundary layer, then wall cooling appears to be the more efficient method. Another possible system of stabilizing involves the simultaneous use of wall cooling and heat addition in the boundary layer [Fig. 5(c)]. The following example of this system was calculated: Water at 40°F. and at sea-level pressure is passed along the inside of the skin, where it is evaporated and the resulting steam is raised to the surface temperature. The steam is then ejected in the outer portion of the boundary layer ($\eta_0 = 2.5$), where it reaches the local velocity by a constant total-enthalpy process. Finally, condensation of the steam takes place. A ratio of w/w_0 was calculated, where w is the coolant flow rate for this system and where w_0 is the amount of water required to stabilize the boundary layer through evaporation within the wall. The following results were found for an altitude of 50,000 ft.:

M_∞	w/w_0
3.1	0.90
5.3	0.74

At high Mach Numbers, therefore, a sizable reduction in coolant weight can be realized by reusing the evaporated coolant as a source of heat in the outer portion of the boundary layer.

When the boundary layer is stabilized by wall cooling, complete stability cannot be attained at Mach Numbers greater than about nine.[3] This limitation does not exist when the boundary layer is stabilized by use of heat sinks, although the amount of heat that must be withdrawn at high Mach Numbers becomes extremely large. For example, at $M_\infty = 13$, eight times the amount of heat removal is required for stability than that required when $M_\infty = 6.5$. This result, of course, is only approximate, because neither the stability theory nor the boundary-layer equations used herein apply at these high Mach Numbers.

Practical Aspects

In all calculations it was assumed that the heat sources or sinks are evenly distributed in the direction of the flow and that their strength varies essentially as $\sqrt{x}$. In practice it would probably be desirable to inject the sources or sinks at one, or several, distinct stations and to obtain the proper distribution through the time lag inherent in the process of evaporation or condensation. It is not known how closely the theoretical problem duplicates the practical conditions.

The question naturally arises as to whether it is feasible to inject the heat sources or sinks without the injecting mechanism itself being the cause for transition. It appears possible that, if the injecting mechanism is placed in a stable part of the boundary layer and if it does not generate a large wake, all disturbances originating there will be damped. If this possibility is confirmed experimentally, the relative advantage of heat sinks for cooling purposes and of sinks or sources for stability purposes will depend primarily on the possible weight-savings.

A comparison on a weight basis with other systems was not undertaken, because it is difficult to define a system without having a specific airplane in mind. Circulation of fuel past the surface, circulation of an expendable coolant past the surface, and transpiration cooling have all been suggested in the past. The aforementioned systems would be rather complex, because the airplane skin would have to be either a complicated heat exchanger for purposes of surface cooling, or porous, for transpiration cooling. The use of heat sinks might therefore represent a substantial weight-saving, because neither a double shell structure nor a porous structure would be required.

References

[1] Lees, Lester, and Lin, Chia Chiao, *Investigation of the Stability of the Laminar Boundary Layer in a Compressible Fluid*, NACA TN No. 1115, 1946.

[2] Lees, Lester, *The Stability of the Laminar Boundary Layer in a Compressible Fluid*, NACA Report No. 876, 1947. (Supersedes NACA TN No. 1360.)

[3] Van Driest, E. R., *Calculation of the Stability of the Laminar Boundary Layer in a Compressible Fluid on a Flat Plate with Heat Transfer*, Journal of the Aeronautical Sciences, Vol. 19, No. 12, pp. 801–812, December, 1952.

[4] Sternberg, Joseph, *A Free-Flight Investigation of the Possibility of High Reynolds Number Supersonic Laminar Boundary Layers*, Journal of the Aeronautical Sciences, Vol. 19, No. 11, pp. 721–733, November, 1952.

[5] Chapman, Dean R., and Rubesin, Morris W., *Temperature and Velocity Profiles in the Compressible Laminar Boundary Layer with Arbitrary Distribution of Surface Temperature*, Journal of the Aeronautical Sciences, Vol. 16, No. 9, pp. 547–565, September, 1949.

[6] Low, George M., *The Compressible Laminar Boundary Layer with Heat Transfer and Small Pressure Gradient*, NACA TN No. 3028, 1953.

[7] Laurmann, J. A., *Stability of the Compressible Laminar Boundary Layer with an External Pressure Gradient*, Rep. No. 48, the College of Aeronautics (Cranfield), September, 1951.

[8] Squire, H. B., *On the Stability for Three-Dimensional Disturbances of Viscous Fluid Flow Between Parallel Walls*, Proc. Roy. Soc. (London), Ser. A, Vol. 142, No. A 847, pp. 621–628, November 1, 1933.

[9] Dunn, D. W., and Lin, C. C., *On the Stability of the Laminar Boundary Layer in a Compressible Fluid, Pt. I*, Dept. of Math., M.I.T., December, 1953.

Readers' Forum

BRIEF REPORTS of investigations in the aeronautical sciences and discussions of papers published in the JOURNAL are presented in this special department. Publication is completed as soon as possible after receipt of the material. The Editorial Committee does not hold itself responsible for the opinions expressed by the correspondents.

Note on the Unsteady Heat Regenerator

R. E. Meyer and T. A. d'Ews Thomson
Department of Aeronautical Engineering, University of Sydney, Sydney, Australia
December 7, 1954

IN MOST SUPERSONIC TUNNELS, control of stagnation pressure suffices for the control of Reynolds Number, but in blow-down tunnels of large working section and small running time, control of stagnation temperature is similarly important. The provision of such control by passing the air, upstream of the nozzle, through porous material has been discussed by Pillow,[1] assuming that (1) the material is packed uniformly into a cylindrical duct with heat-insulated walls, (2) heat conduction in the air and in the material is negligible compared with the heat transfer between the two, and (3) the density is uniform throughout. Pillow shows that with finely constituted material a satisfactory approximation for the purpose of stagnation temperature control is obtained by neglecting the difference between the temperatures of the air and the material at any fixed station, x, and time, t.

On the other hand, since the stagnation pressure needs to be similarly controlled, it is in general not the density, but the pressure, which is constant in the regenerator, except for a small pressure drop through the porous material, which will be neglected in the following. The equation of continuity is

$$\partial\rho/\partial t + \partial(\rho u)/\partial x = 0 \tag{1}$$

where ρ is the air density and u the air velocity. The heat balance for the segment of the duct between x and $x + dx$ is

$$(hs + \rho c_p)\partial T/\partial t + c_p\partial(\rho u T)/\partial x = 0 \tag{2}$$

where T is the temperature, h is the density of the porous material, and c_p and s are the specific heats of air and material, respectively. With the pressure constant, $\partial(\rho T)/\partial t = 0$ and from Eqs. (1) and (2),

$$\partial[(\rho u)^2/(\lambda + 2/T)]/\partial x = 0$$

where $\lambda = hsR/(pc_p)$, p being the pressure and R the gas constant. In general, the mass-flow rate $\dot{m}$ at the outlet will be constant and known, and, if A is the area of cross section and $\theta_2(t)$ the value at the outlet of

$$\theta = \lambda + 2/T$$

then

$$(\rho u)^2 = (\dot{m}/A)^2\theta/\theta_2$$

and from Eq. (2),

$$(p/R)\partial\theta/\partial t + (\dot{m}/A)\,(\theta/\theta_2)^{-1/2}\partial\theta/\partial x = 0$$

or in terms of θ and t as independent variables,

$$(p/R)\partial x/\partial t = (\dot{m}/A)\,(\theta\theta_2)^{-1/2} \tag{3}$$

Here $\partial x/\partial t$ is the local rate at which any given temperature is transmitted through the duct.

For stagnation temperature control it is desirable that the initial temperature distribution, $T_0(x)$, of the porous material be uniform. Then the solution of Eq. (3) is $T(x, t) \equiv T_0$ as long as $t \leq xt_*/l$, where l is the length of the duct and

$$t_* = p\theta_0 Al/(R\dot{m}) = hAl\,[(s/c_p) + (2\rho_0/h)]/\dot{m} \tag{4}$$

This is the duration of the run at constant outlet temperature, and it is *longer* by a factor $(s/c_p + 2\rho_0/h)/(s/c_p + \rho_0/h)$ than that for incompressible flow. Since $\theta_2(t) = \theta_0$ during this period, Eqs. (3) and (4) give the equation

$$x/l = (\theta_0/\theta)^{1/2}[1 - t_1(T)/t_*]$$

for the temperature distribution in the porous material at time t_*, where $t_1(T)$ is the time at which the temperature T occurs at the inlet. From this the regeneration required between runs can be estimated.

After this initial period, the rate of transmission of temperature decreases not only with the temperature but also falls during the transmission. Integration of Eq. (3) at constant θ gives

$$t_*\theta^{1/2}/\theta_0 = \int_{t_1(T)}^{t_2(T)} \frac{d\tau}{\theta_2(\tau)}$$

by Eq. (4), where $t_2(T)$ is the time at which the temperature T occurs at the outlet; therefore,

$$dt_2/d\theta = [\theta/\theta_2(t_1)]^{1/2}dt_1/d\theta + (1/2)t_*/\theta_0$$

For $t_1 \leq t_*$, which includes the period of interest for wind-tunnel operation, $\theta_2(t_1) = \theta_0$, and, hence,

$$t_2 - t_1 = t_* + {}^1/_2t_*(\theta/\theta_0 - 1) + \int_0^{t_1}[(\theta_1/\theta_0)^{1/2} - 1]dt$$

where $\theta_1(t)$ is the value of θ at the inlet. This shows how the delay in the transmission of temperature from inlet to outlet increases as the temperature at the inlet falls.

REFERENCE

[1] Pillow, A. F., *The Theory of Heat Regenerators in the Unsteady State*, Report A.78, Aeronautical Research Lab., Melbourne, Australia, January, 1952.

A Procedure for the Approximate Analysis of Buckled Plates

Sara R. Boley
Department of Civil Engineering and Engineering Mechanics, Columbia University, New York, N.Y.
December 8, 1954

A METHOD FOR OBTAINING approximate solutions to the von Kármán plate equations,[1] and in particular the effective width of buckled plates is presented below. It is an extension of a method introduced by von Mises[2] for the case of a buckled column. The procedure involves a set of successive approximations in dealing with the nonlinear terms of the governing equations; the first approximation has the form of the linear solution.

The illustrative problem presented here, a rectangular plate with all edges simply supported and under constant edge dis-

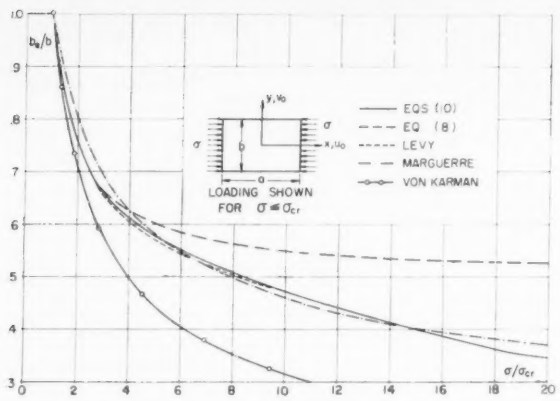

FIG. 1. Nondimensional variation of effective width with applied stress.

placements u_0 and v_0 (see Fig. 1 inset), was chosen because previous approximations (for example, references 3 and 4) and an exact solution[5] are available for comparison. The values of the effective width are in good agreement with those given by the exact solution (Fig. 1).

For a plate with large deflections, the stress function F and the deflection w can be obtained from the von Kármán equations:

$$\nabla^4 F = E(w_{xy}^2 - w_{xx}w_{yy}) \tag{1a}$$

$$\nabla^4 w = (h/D)\,(w_{xx}F_{yy} + w_{yy}F_{xx} - 2w_{xy}F_{xy}) \tag{1b}$$

and the edge conditions for the problem stated above are

$$\left.\begin{aligned} w &= 0 \text{ at all edges} \\ w_{xx} &= 0 \text{ at } x = \pm(a/2) \\ w_{yy} &= 0 \text{ at } y = \pm(b/2) \\ \tau_{xy} &= -F_{xy} = 0 \text{ at all edges} \\ u_0 &= \int_{-a/2}^{+a/2} [(1/E)\,(F_{yy} - \nu F_{xx}) - (1/2)w_x^2]\,dx = \text{constant} \\ v_0 &= \int_{-b/2}^{+b/2} [(1/E)\,(F_{xx} - \nu F_{yy}) - (1/2)w_y^2]\,dy = \text{constant} \end{aligned}\right\} \tag{2}$$

in the usual notation.

The linear solution, with indeterminate amplitude A,

$$F = \sigma(y^2/2) \tag{3a}$$

$$w = A \cos \mu x \cos \eta y \tag{3b}$$

is the first approximation, where σ is the average edge stress in the x-direction and

$$\left.\begin{aligned} \mu &= m\pi/a \\ \eta &= n\pi/b \end{aligned}\right\} \tag{3c}$$

Eq. (3b) is substituted in the nonlinear terms of Eq. (1a), and the stress function F, obtained by solving the resulting linear equation, is

$$F = \sigma(y^2/2) - (EA^2/32)\,[(\eta^2/\mu^2)\cos 2\mu x + (\mu^2/\eta^2)\cos 2\eta y] \tag{4}$$

Expressions (3b) and (4) satisfy conditions (2). It may be noted that the constant v_0 may be made equal to zero by the introduction of an edge stress $\sigma_y = F_{xx}$ at the edges $y = \pm(b/2)$; in the present case the resultant $\int_{-a/2}^{a/2} \sigma_y\,dx = 0$. The stress in the x-direction is (taken positive in tension):

$$\sigma_x = F_{yy} = \sigma + (\mu^2 EA^2/8)\cos 2\eta y \tag{4a}$$

and it may be seen that, as expected, the greater part of the load is taken by the portions of the plate close to the edges $y = \pm(b/2)$.

To determine the amplitude A, Eqs. (4) and (3b) are substituted in the right-hand side of Eq. (1b) with the result

$$\nabla^4 w = -(hA\mu^4/D)\left\{[(\sigma/\mu^2) + (EA^2/16)\,(1+\beta^4)]\cos\mu x\cos\eta y + (EA/16)\,(\beta^4\cos 3\mu x\cos\eta y + \cos\mu x\cos 3\eta y)\right\} \tag{5}$$

The solution, satisfying the boundary conditions of Eqs. (2) to terms of the order of A^4 is

$$w = A\cos\mu x\cos\eta y + B\cos 3\mu x\cos\eta y + C\cos\mu x\cos 3\eta y \tag{6}$$

where

$$\left.\begin{aligned} (A/h)^2 &= 4/[3(1-\nu^2)]\,[(1+\beta^2)2/(1+\beta^4)]\,[(\sigma/\sigma_{cr}) - 1] \text{ for } |\sigma| > \sigma_{cr} \\ B &= -EhA^3/(16D)\,[\beta^4/(9+\beta^2)^2] \\ C &= -EhA^3/(16D)\,[1/(1+9\beta^2)^2] \\ \sigma_{cr} &= [\pi^2 D/(hb^2)]\,[\beta + (1/\beta)]^2 \\ D &= Eh^3/[12(1-\nu^2)];\ \beta = \mu/\eta \end{aligned}\right\} \tag{6a}$$

It is shown in reference 1 that for $(a/b) > 1$, the approximation $\beta = 1$ can effectively be used; this value is therefore employed in the remainder of this note.

The effective width b_e is defined by the relation

$$b_e\sigma_{(b/2)}\,h = h\int_{-b/2}^{+b/2} \sigma_x\,dy \tag{7}$$

Use of Eqs. (4) and (6a) gives the first approximation as

$$(b_e/b) = (1/2)\,[1 + (\sigma_{cr}/\sigma_{b/2})] \tag{8}$$

It is interesting to note, incidentally, that this expression is identical with the first two terms of a binomial expansion as obtained from von Kármán's effective-width formula[3]—i.e.,

$$(b_e/b) = (\sigma_{cr}/\sigma_{b/2})^{1/2} = \left\{1 + [(\sigma_{cr}/\sigma_{b/2}) - 1]\right\}^{1/2} = 1 + (1/2)\,[(\sigma_{cr}/\sigma_{b/2}) - 1] + \ldots \tag{8a}$$

Eq. (8), however, is not sufficiently accurate except for stresses close to the critical (see Fig. 1), and the next approximation is therefore required. It was obtained by the procedure described above, using in the right-hand side of Eq. (1a) the expression for w given by Eqs. (6) rather than that of Eq. (3b). The new function F, obtained after much algebraic manipulation, is then

$$F = (\sigma y^2/2) + (EA^2/25600)\,[d_1(\cos 2\mu x + \cos 2\mu y) + d_2\cos 2\mu x\cos 2\mu y + d_3(\cos 4\mu x + \cos 4\mu y) + d_4(\cos 2\mu x\cos 4\mu y + \cos 2\mu y\cos 4\mu x)] \tag{9}$$

where

$$\left.\begin{aligned} d_1 &= -800 - 12\alpha + 81\alpha^2/200 \\ d_2 &= 24\alpha - 9\alpha^2/25 \\ d_3 &= 3\alpha \\ d_4 &= (48\alpha - 9\alpha^2)/100 \end{aligned}\right\} \tag{9a}$$

in terms of the dimensionless amplitude parameter

$$\alpha = (1-\nu^2)(A/h)^2 \tag{9b}$$

The relationship between α and $\sigma_{(b/2)av}$, analogous to that given by Eqs. (6a) and again obtained from Eq. (1b), is

$$(\sigma_{(b/2)av}/\sigma_{cr}) = 1 + 0.375\alpha(2 - 0.0225\alpha + 0.001314\alpha^2 - 0.0000219\alpha^3) \tag{10a}$$

where $\sigma_{(b/2)av}$ is the average stress along either unloaded edge.

The final expression for the new approximation to the effective width is

$$(b_e/b) = 1 - (\sigma_{cr}/\sigma_{(b/2)av})\,(0.375\alpha)\,(1 + 0.00950625\alpha^2) \tag{10b}$$

The variation of the effective width with the average edge stress can now be obtained by solving simultaneously Eqs. (10a) and (10b); this was done numerically. The resulting values for the effective width are plotted in Fig. 1 and are in good agreement with the exact solution given in reference 5 and with the approximation given in reference 4.

The application of this method to the solution of other plate problems of this nature (for example, considering the effects of thermal stress[6] or of different boundary conditions) would appear useful and is being studied.

References

[1] Timoshenko, S., *Theory of Elastic Stability*, McGraw-Hill, New York, 1936.

[2] von Mises, R., *Ausbiegung eines auf Knicken beanspruchten Stabes*, Z. angew. Math. Mech., Vol. 4, p. 435, 1924.

[3] von Kármán, Th., Sechler, E. E., and Donnell, L. H., *The Strength of Thin Plates in Compression*, Trans. Am. Soc. Mech. Eng., Vol. 54, p. 53, 1932.

[4] Marguerre, K., *Die mittragende Breite der gedruckten Platte*, Luftfahrtforschung, Vol. 14, p. 121, 1937, also NACA TN 833, 1937.

[5] Levy, S., *Bending of Rectangular Plates with Large Deflections*, NACA TN 846, 1942.

[6] Gossard, M. L., Seide, P., and Roberts, W. M., *Thermal Buckling of Plates*, NACA TN 2771, August, 1952.

On Distributed Roughness as a Means of Fixing Transition at High Supersonic Speeds

William B. Fallis

Senior Aerodynamics Engineer, Convair, Ft. Worth, A Division of General Dynamics Corporation, Fort Worth, Texas

December 13, 1954

A WELL-KNOWN WIND-TUNNEL TECHNIQUE for fixing the boundary-layer transition location at subsonic and low supersonic speeds has been developed through the use of distributed roughness. Recent Convair experiments in the Jet Propulsion Laboratory 20-in. supersonic wind tunnel at the California Institute of Technology have shown that distributed roughness may be used effectively as a boundary-layer trip at higher Mach Numbers than generally anticipated.[1]

The experiments were carried out on an approximately parabolic body of revolution of fineness ratio 10. The nose of the model was contoured to a slight radius. Distributed roughness, applied to the model nose, extended approximately $3^1/_2$ per cent of the body length aft of the stagnation point. The roughness particles were aluminum oxide and were of grain sizes 320, 220, 150, 100, 80, and 60. A coating of "Trivar" baking varnish approximately 0.0005 in. in thickness, was used to fix the particles to the model surface.

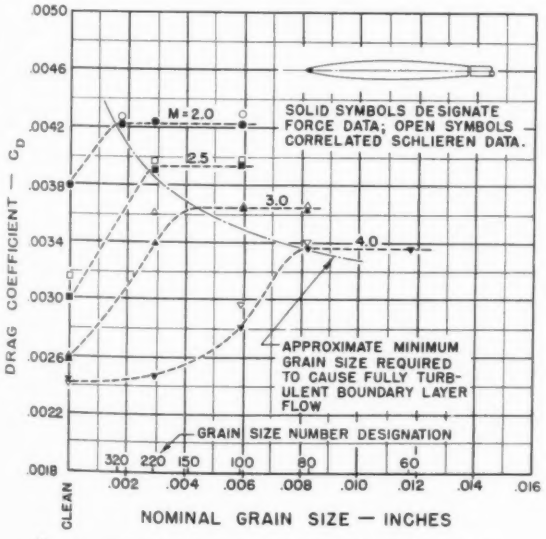

FIG. 1. Variation of zero lift drag with roughness size.

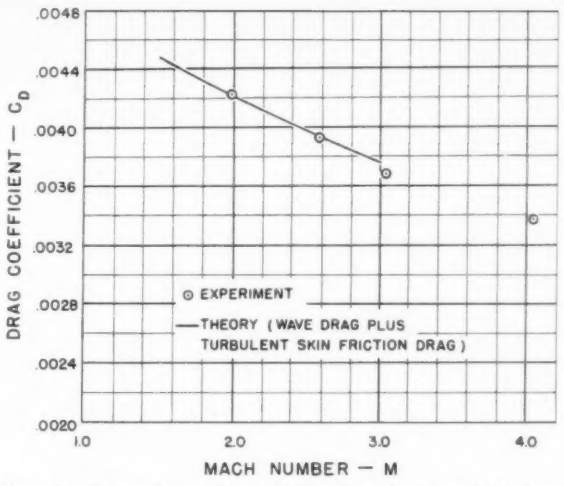

FIG. 2. Comparison of experimental and theoretical drag variation with Mach Number.

Force data were obtained as a function of grain size at Mach Numbers 2.0, 2.5, 3.0, and 4.0 and for Reynolds Numbers in the range 6.80×10^6 to 10.5×10^6; a minimum of three force measurements were taken for each surface condition. Schlieren photographs were also obtained to enable a visual study of transition location.

The zero lift drag coefficient referenced to the frontal area of the body (3.142 sq. in.) is plotted against grain size in Fig. 1. As the roughness size was increased at a given Mach Number, the drag increased from a low value, corresponding to the "clean" model with partial laminar flow, to a constant value independent of grain size. The constant drag level indicates that the boundary layer was effectively fully turbulent from the nose aft and that the wave drag was insensible to changes in grain size. The grain size required to produce fully turbulent flow increased as the Mach Number increased. The upper boundary of the curves, where the drag again became a function of grain size, was not determined in the present tests.

The interpretation of the force data was further substantiated through examination of the schlieren photographs. An estimate was made of the body wave drag variation with Mach Number for the cases with fully turbulent boundary-layer flow, by taking the difference between the constant drag levels and the corresponding theoretical turbulent skin-friction drags. The open symbols in Fig. 1 represent the sum of the wave drag increment and the computed skin-friction drag, accounting for the location of transition as shown by the schlieren pictures. Satisfactory correlation with the force measurements is evident.

A theoretical calculation of the body wave drag at Mach Numbers 1.5 to 3.0 was performed using Van Dyke's second-order theory and neglecting the slight nose radius. Fig. 2 shows the drag coefficient plotted as a function of Mach Number. The symbols represent force measurements obtained with transition induced at the roughness strip; the solid curve represents the aggregate of the theoretical wave drag and skin-friction drag increments. It is concluded from the results that the distributed roughness as applied to the model provided a convenient and satisfactory method of producing fully turbulent boundary-layer flow throughout the Reynolds and Mach Number range of the tests.

Reference

[1] Coles, Donald, *Measurement of Turbulent Skin Friction on a Smooth Flat Plate in Supersonic Flow*, Journal of the Aeronautical Sciences, Vol. 21, No. 7, pp. 433–448, July, 1954.

Stagnation Temperature Control for a Blow-Down Supersonic Wind Tunnel

T. A. d'Ews Thomson
Department of Aeronautics, University of Sydney, Sydney, Australia
December 14, 1954

A METHOD OF MAINTAINING constant stagnation temperature during operation of an intermittent, blow-down, supersonic wind tunnel of short running time has been tested at the University of Sydney. Pillow[1] has treated theoretically the process that occurs when a fluid with nonuniform temperature distribution passes through porous material. He assumed that the material was contained in a cylindrical, heat-insulated duct, that conditions were uniform over any of its cross sections, and that the conductive transfer of heat in both media was negligibly small. If the rate of heat transfer between the two media is sufficiently large that the temperature difference between them is negligible at any point, and the porous material is initially at uniform temperature, T_0, then the temperature, T_2, of the emerging fluid remains constant and equal to T_0 until

$$m = M[(s/c) + (\rho/h)] \tag{1}$$

where m is the mass of fluid which has passed through the porous material, c is the specific heat of the fluid, and ρ is its density; M is the mass of the porous material, s is its specific heat, and h is its apparent density. The temperature of further fluid leaving the material is

$$T_2(m) = T_1(m - M[(s/c) + (\rho/h)]) \tag{2}$$

if $T_1(m)$ is the temperature of the entering fluid.

The theory was used to design a unit for the 6- by 3-in. wind tunnel at the University of Sydney. The air was passed on its way from the high-pressure storage to the nozzle, through glass wool. This was packed between gauzes into a number of open-ended cells arranged, in honeycomb fashion, in a container. Inlet and outlet valves were operated to maintain constant both the rate of mass-flow through the container and the pressure in it. The temperatures of the air entering and leaving the glass wool were recorded and corrected approximately for some small fluctuations of pressure.

The results of these tests (Fig. 1) show the effectiveness of the method. The outlet temperature was constant, within ±0.5 per cent, until a mass of air, $M[(s/c) + (\rho/h)]$, had passed through the glass wool, and this result was independent of the rate of mass-flow.

With further flow, however, the results did not agree with the prediction of Eq. (2). The initial, sudden drop of temperature, due to the Joule-Thomson effect, which is conspicuous in the distribution of inlet temperature, was not observed at the outlet. A number of factors were examined, which are neglected in reference 1, and all were shown to have negligible influence on the performance of the system tested except the effects of (a) nonuniform packing density of the glass wool and (b) a possible error in the value of its specific heat. It appears likely that the discrepancy between the experimental results and the prediction of Eq. (2) was due to a combination of these two effects.

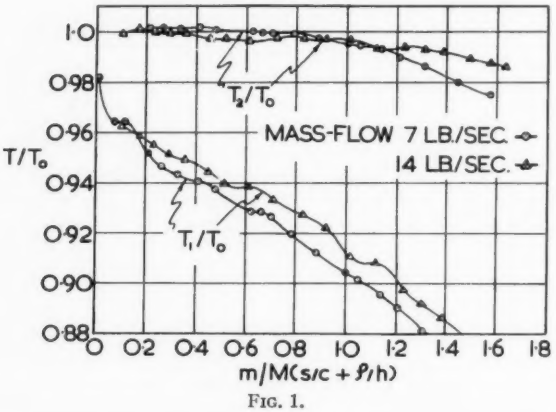

FIG. 1.

Experiments and theoretical estimates also showed that even small amounts of leakage past the glass wool impair seriously the performance of the system. Breaking up of the glass wool, causing choking and leakage, was noted after frequent tests, and a more robust porous material appears desirable.

Initial uniformity of temperature of the porous material is important, and this can be obtained by the inverse process of passing air of uniform temperature through the material between tunnel tests.

REFERENCE

[1] Pillow, A. F., *The Theory of Heat Regenerators in the Unsteady State*, Report A78, Dept. of Supply, Aeronautical Research Lab., Australia, 1952.

Aerodynamic Coefficients for Cambering and Aileron Motions

E. F. Tyler
Douglas Aircraft Company, Inc., El Segundo Division, El Segundo, Calif.
November 30, 1954

THE AERODYNAMIC FORCE COEFFICIENTS for an airfoil undergoing changes in camber, translation, and pitch (two-dimensional incompressible flow) were derived by Spielberg.[1] This note adds the extra coefficients that are necessary if the airfoil also has a control surface hinged about the nose. The notation of Spielberg will be used. Let the airfoil be oscillating in the following motions:

$$z_3 = \zeta(1 - x^2)e^{i\omega t}$$

which denotes parabolic change in camber of the mean chord with amplitude ζ feet, measured at the mid-chord point, positive down.

$$z_4 = 0 \quad x < c$$
$$= \beta b(x - c)e^{i\omega t} \quad x \geq c$$

which denotes rotation of the control surface about its hinge line with angular amplitude β radians (relative to the main surface).

In the foregoing equations x is the dimensionless coordinate of a point on the chord measured from the mid-chord and referred to b, the semichord. $c = -\cos\varphi$ is the value of x for the hinge line. The aerodynamic coefficient of the generalized cambering force due to control surface rotation is

$$N_\beta = -[C(k)/k^2]N_1 - (i/k)C(k)N_2 - (1/k^2)N_3 - (i/k)N_4 + N$$

where

$$N_1 = (1/\pi)(\pi - \varphi + \sin\varphi)$$

$$N_2 = (1/\pi)\{[(\pi - \varphi)/2](1 + 2\cos\varphi) + (\sin\varphi/2)(2 + \cos\varphi)\}$$

$$N_3 = (2/3\pi)\sin^3\varphi$$

$$N_4 = (1/\pi)[\pi - \varphi + (4/3)\sin\varphi\cos\varphi - (\sin\varphi\cos^3\varphi/3)]$$

$$N_5 = (1/\pi)\{(3/4)(\pi - \varphi)\cos\varphi + (\sin\varphi/2)[1 + (\cos^2\varphi/2)] - (\sin^5\varphi/30)\}$$

The coefficient of control surface moment about its hinge line due to cambering is

$$T_\zeta = -[C(k)/k^2]T_1 - (i/k)C(k)T_2 - (1/k^2)T_3 - (i/k)T_4 + T_5$$

where

$$T_1 = (1/\pi)[(\pi - \varphi)(1 - 2\cos\varphi) + \sin\varphi(\cos\varphi - 2)]$$

$$T_2 = -T_1/2$$

$$T_3 = (1/\pi)\,[-\cos\varphi \sin\varphi - (\pi - \varphi) + (2/3)\sin^3\varphi]$$

$$T_4 = (1/\pi)\,\{-(\cos\varphi \sin\varphi/2) - (\cos\varphi \sin^3\varphi/3) - [(\pi - \varphi)/2]\}$$

$$T_5 = (1/\pi)\,\{(3/4)(\pi - \varphi)\cos\varphi + (\sin\varphi/2)[1 + (\cos^2\varphi/2)] - (\sin^5\varphi/30)\} = N_5$$

REFERENCE

[1] Spielberg, Irvin N., *The Two-Dimensional Incompressible Aerodynamic Coefficients for Oscillatory Changes in Airfoil Camber*, Wright Air Development Center TN WCNS 52-7, 1952.

The Lift of a Blowing Wing in a Parallel Stream*

Heinrich B. Helmbold
Staff Engineer, University of Wichita, School of Engineering, Wichita, Kan.

December 13, 1954

WHEN A JET IS ISSUED THROUGH a blowing slot in the downstream direction tangentially to the surface or at the trailing edge of the wing as shown by Fig. 1, an additional lift, ΔL, will result. Let ρ denote the air density, b the span of wing and jet, h the thickness of the jet at the trailing edge, V the undisturbed velocity, and v the excess velocity in the jet.

Experience shows that the additional lift ΔL of a blowing wing is considerably higher, say 5 times, than the vertical component

$$\Delta I_y = \rho b h[(V + v)^2 - V^2]_{te} \sin\delta_{te} \tag{1}$$

of the excess-momentum flux of the jet at the trailing edge (te). This fact in itself says that an additional circulation must be produced by the turning action of the basic flow on the jet.

Integration of the pressure gradient in curved flow across the thin jet sheet in the manner of Fig. 2 gives the pressure increase as

$$p_2 - p_1 = \rho(V + v)^2(h/r) \tag{2}$$

where $V + v$ now denotes the local average velocity in the jet. The pressure increase across a thin sheet of the basic flow with the same geometrical shape would be

$$p_2' - p_1 = \rho V^2(h/r) \tag{3}$$

Thus an additional pressure increase across the thin sheet of the jet is produced by the excess of centrifugal acceleration in the jet

$$p_2 - p_2' = \rho[(V + v)^2 - V^2]\,(h/r) \tag{4}$$

The radial pressure distribution in the basic flow on the convex side of the jet is shifted by this amount with reference to the analytical continuation of the radial pressure distribution in the basic flow on the concave side (see Fig. 2). Since the total pressure in the basic flow is constant in any case, the pressure increase of Eq. (4) is connected by Bernoulli's law to the velocities at opposite points of the thin sheet under consideration.

$$p_2 - p_2' = \rho[(V_2'^2 - V_2^2)/2] \tag{5}$$

This pressure increase may be interpreted as the pressure discontinuity at a lifting surface where the velocity jumps from V_2 to V_2'. Then

$$\epsilon \equiv V_2' - V_2 = \frac{2}{\rho}\frac{p_2 - p_2'}{V_2' + V_2} = 2\frac{(V + v)^2 - V^2}{V_2' + V_2}\frac{h}{r} \tag{6}$$

is the lifting vorticity (circulation per unit length) of the discontinuous surface that simulates the action of the thin jet on the basic flow. Because the static pressure is continuous through the jet surface, the excess of total pressure in the jet is

* This research was sponsored by the Air Branch of the Office of Naval Research under Contract No. N-onr 201(01).

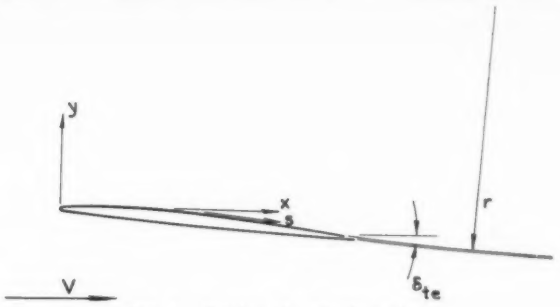

FIG. 1. Section of a blowing wing.

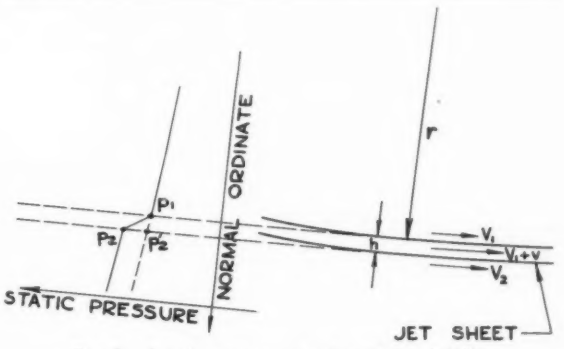

FIG. 2. Jet sheet pressure and vorticity details.

$$\Delta p_t = \rho\{[(V + v)^2 - V^2]/2\} \tag{7}$$

Hence, by Eq. (4),

$$p_2 - p_2' = 2\Delta p_t(h/r) \tag{8}$$

and by Eq. (6)

$$\epsilon = (4/\rho)\,[\Delta p_t/(V_2' + V_2)]\,(h/r) \tag{9}$$

The vorticity ϵ must vanish at infinity downstream where the jet is completely turned in the direction of undisturbed velocity and where the radius of curvature has become infinite.

Now let x and y_j denote the coordinates of a point on the vortex sheet substituted for the jet and assume that the slope dy_j/dx and the curvature $1/r = d^2y_j/dx^2$ are small of the first order everywhere. Then the vorticity ϵ is small of the same order if $\Delta p_t/(V_2' + V_2)$ is of the zero order of magnitude. In this order of approximation

$$(V_2' + V_2)/2 = V_\infty$$

if V_∞ denotes the undisturbed velocity and

$$\epsilon = 2(\Delta p_t/\rho V_\infty)h(d^2y_j/dx^2) \tag{10}$$

At the trailing edge the distribution $\epsilon(x)$ is continuously connected with the distribution $\gamma(x)$ of lifting vorticity on the airfoil, which means that the lifting vorticity γ at the trailing edge does not vanish as with the airfoil with no jet. At the x-axis the whole vorticity distribution, γ together with ϵ, induces a stream slope

$$-\frac{w_j(x)}{V_\infty} = \frac{1}{2\pi V_\infty}\left[\int_0^c \frac{\gamma(x')}{x' - x}\,dx' + \int_c^\infty \frac{\epsilon(x')}{x' - x}\,dx'\right] =$$

$$\frac{1}{2\pi V_\infty}\int_0^c \frac{\gamma(x')}{x' - x}\,dx + \frac{1}{2\pi}\frac{\Delta p_t}{\rho V_\infty^2/2}\,h\int_c^\infty \frac{d^2y_j(x')}{dx'^2}\frac{dx'}{x' - x} \tag{11}$$

where $w_j(x)$ denotes the local downwash velocity and c the chord of the airfoil. The boundary conditions are

$$-w_j(x)/V_\infty = dy_m(x)/dx \tag{12}$$

for $0 \leq x \leq c$ and

$$-w_j(x)/V_\infty = dy_j(x)/dx \tag{13}$$

for $x \geq c$. In other words, at the airfoil, the flow must follow the slope of the airfoil mean line $y_m(x)$, and, behind the airfoil, it must coincide with the slope of the jet mean line $y_j(x)$. Elimination of $w_j(x)/V_\infty$ from Eqs. (11) to (13) yields two integral equations that determine the unknown functions $\gamma(x)$ and $y_j(x)$ or $\gamma(x)$ and $\epsilon(x)$, since $\epsilon(x)$ is connected with $y_j(x)$ by Eq. (10).

At the airfoil, the vorticity ϵ induces an upwash angle $\Delta\alpha$ and an increase ΔV_x of the x-component of the velocity, because with reference to the x-direction the jet is situated below the trailing edge. In order to compensate for the induced upwash angle, the original vorticity γ_0, with no jet, must be increased by an additional vorticity $\Delta\gamma$.

It is supposed that the air quantity of an airfoil blowing jet is taken from the general flow and not from within the airfoil. Furthermore, it is assumed that a thin stream leaving it at the trailing edge will not influence the lift of the airfoil, provided the flow passing the interior of the airfoil experiences neither gain nor loss of energy; this is the case with no jet, $v = 0$. With a blowing jet, the concern is only with the jet vertical excess-momentum flux ΔI_y at the trailing edge, which must be in equilibrium with the integral of the additional pressure forces of Eq. (4).

$$0 = \int_c^\infty \rho(V_\infty + \Delta V_x)\epsilon \, ds - (\Delta I_y/b) \tag{14}$$

Here s is the curvilinear distance from the leading edge measured along the lifting surfaces, and ΔV_x is the x-component of the induced velocity; hence

$$V_\infty + \Delta V_x = [(V_2' + V_2)/2]\,(dx/ds)$$

The lift of the airfoil with blowing jet results from applying the momentum theorem to a control surface tightly enclosing the airfoil and crossing the jet normally at the trailing edge.

$$L/b = \int_0^c \rho(V_\infty + \Delta V_x)\,(\gamma_0 + \Delta\gamma)\,ds + (\Delta I_y/b) \tag{15}$$

From Eq. (14) this becomes

$$L/b = \int_0^c \rho(V_\infty + \Delta V_x)\,(\gamma_0 + \Delta_\gamma)\,ds + \int_c^\infty \rho(V_\infty + \Delta V_x)\epsilon \, ds \tag{16}$$

The lift of the airfoil with a blowing jet can also be determined by applying the momentum theorem to a control surface enclosing the wing and jet far from the wing everywhere and crossing the jet at a right angle (Kutta-Joukowski),

$$L/b = \rho V_\infty \left[\int_0^c (\gamma_0 + \Delta\gamma)\,ds + \int_c^\infty \epsilon \, ds\right] \tag{17}$$

Since Eqs. (16) and (17) must be compatible,

$$\int_0^c \Delta V_x(\gamma_0 + \Delta\gamma)\,ds + \int_c^\infty \Delta V_x \cdot \epsilon \, ds = 0 \tag{18}$$

By subtracting the lift of the airfoil with no jet from the lift of the airfoil with blowing jet, we get the *additional lift* produced by the jet

$$\Delta L/b = \rho V_\infty \left[\int_0^c \Delta\gamma \cdot ds + \int_c^\infty \epsilon \, ds\right] \tag{19}$$

According to Eqs. (14) and (18) this additional lift exceeds the vertical component of the excess-momentum flux of the jet at the trailing edge by an amount

$$\frac{\Delta L - \Delta I_y}{b} = \rho \int_0^c [(V_\infty + \Delta V_x)\Delta\gamma + \Delta V_x \cdot \gamma_0]\,ds \tag{20}$$

Therefore, *the additional lift is greater than the downward component of the excess-momentum flux of the jet at the trailing edge*, at least if the additional quantities ΔV_x and $\Delta\gamma$ produced by the jet are positive everywhere along the chord. This will always be true with a positive (downward) deflection angle δ_{te} at the trailing edge, since then a positive vorticity ϵ results, which produces positive ΔV_x and $\Delta\gamma$ along the whole chord.

With small deflection angles δ_{te} the induced velocity ΔV_x is small of second order, and the additional lift is, to the first order of approximation,

$$\frac{\Delta L}{b} = \frac{\Delta I_y}{b} + \rho V_\infty \int_0^c \Delta\gamma \cdot ds \tag{21}$$

Transonic Lift over the Front Surface of a Two-Dimensional Diamond Airfoil*

Robert Wesley Truitt
Professor of Aeronautical Engineering, Virginia Polytechnic Institute, Blacksburg, Va.
December 6, 1954

THE THROAT STATION CONCEPT of Tsien and Fejer,[1] combined with the Maccoll-Codd Method,[2] can be used to obtain the transonic chordwise lift distribution over the front surface of a symmetric diamond wedge at small angle of attack. The Throat Station Concept is applicable to a diamond wedge of semiangle, θ, at small angle of attack, α, provided that, for the incompressible case, the fundamental zero-angle-of-attack flow character is unaltered. This condition is met approximately if $\alpha/\theta \leq 0.1$.

The front surface pressure distributions of the diamond should follow closely the von Kármán-Tsien rule up to and including the throat station critical Mach Number, M_{0cr}. The throat station, $(x/c)_{T.S.}$, is located just forward of the wedge shoulder. The approximate front surface chordwise lift distribution is thus found easily in the Mach Number range $(0 \leq M_0 \leq M_{0cr})$.

By the Throat Station Concept, the local Mach Number distribution, corresponding to the solution for M_{0cr}, will remain virtually constant (frozen) in the subsonic range:

$$\left\{(M_{0cr}^2 - 1)/[(\gamma + 1)\theta]^{2/3}\right\} \leq \left\{(M_0^2 - 1)/[(\gamma + 1)\theta]^{2/3}\right\} < 0 \tag{1}$$

or

$$\xi_{0cr} \leq \xi_0 < 0$$

The Principle of Stationarity

$$\frac{\partial M_L}{\partial M_0}\bigg|_{M_0 = 1} = 0 \tag{2}$$

establishes the fact that the local Mach Number freeze persists into the supersonic regime

$$\xi_{0U.L.} = \left\{(M_{0U.L.}^2 - 1)/[(\gamma + 1)\theta]^{2/3}\right\} > 0 \tag{3}$$

where $M_{0U.L.}$ is the upper limit of the freeze for the wedge semiangle, θ.

Using Bryson's approximation for the normal shock relation[3]

$$1 - M_2^2 \approx M_1^2 - 1 \tag{4}$$

the upper limit Mach Number, $M_{0U.L.} = M_1$, is found from Eq. (4) by substituting $M_{0cr} = M_2$. The approximate range of Mach Number freeze is thus

$$\xi_{0cr} \leq \xi_0 \leq \xi_{0U.L.} \tag{5}$$

where $|\xi_{0cr}| = |\xi_{0U.L.}|$

The front-surface pressure distributions are calculated through the transonic range [Eq. (5)] by using the constant local Mach Number distribution in the Maccoll-Codd Method.[2]

* This research was supported by the United States Air Force, through the Office of Scientific Research of the Air Research and Development Command.

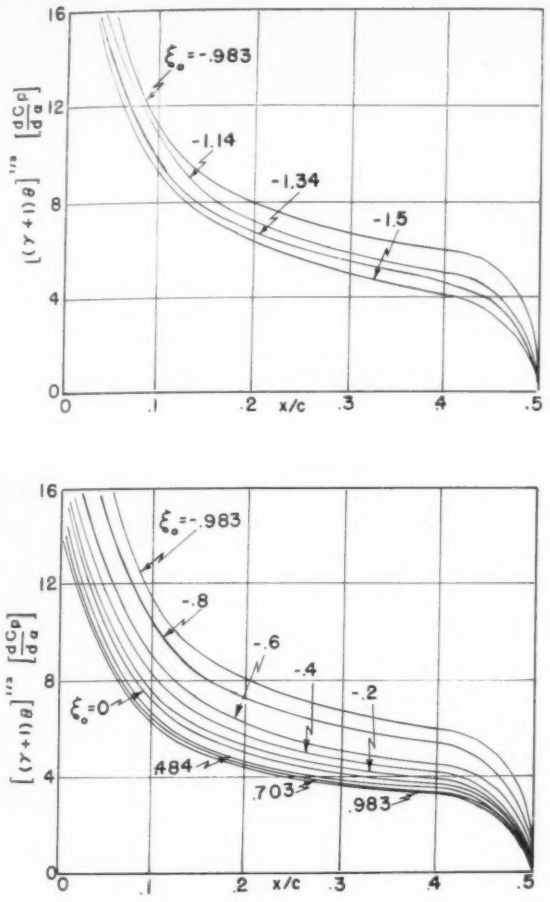

FIG. 1.

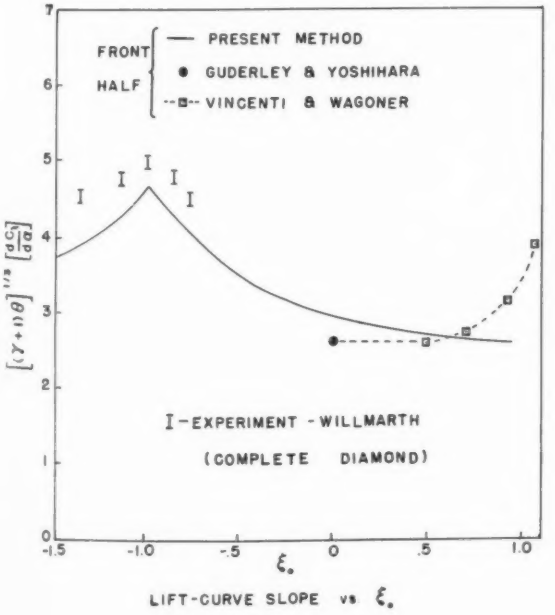

FIG. 2.

RESULTS

The present method was applied to the theoretical incompressible pressure distribution for the front surface of a symmetrical diamond ($\theta = 10°$) at 1° angle of attack. The calculated pressure changes due to angle of attack are shown plotted in Fig. 1 in transonic similarity form in the range ($-1.5 \leq \xi_0 \leq 0.983$). The range of Mach Number freeze was found to be ($-0.983 \leq \xi_0 \leq 0.983$). Integration of Fig. 1 gave the reduced lift-curve slope shown plotted with other findings in Fig. 2.

CONCLUSIONS

Based on the results of the present method, the following conclusions may be drawn.

(1) The subsonic peak in the lift-curve slope is due primarily to the front wedge pressures. The subsonic reduced Mach Number at the peak ($\xi_0 = -0.983$) corresponds to the attainment of the Mach Number freeze.

(2) As long as the Mach Number freeze persists, the curve of lift-curve slope versus Mach Number has a negative slope. The present calculated negative slope at $\xi_0 = 0$ is in excellent agreement with the theoretical value[4]

$$[1/(C_L/\alpha)^*]\,\{[d(C_L/\alpha)]/(dM_0)\}^* = -2/(\gamma + 1)$$

(3) The change with Mach Number of the pressure-drag coefficient due to lift[5]

$$C_d - C_{d0} = (dC_L/d\alpha)\alpha^2$$

for a given angle of attack, has the same type of variation as the curve of lift-slope versus Mach Number.

(4) The second or supersonic peak in the lift-slope curve can, by the present method, be anticipated for increasing Mach Numbers above $M_{0_{V.L.}}$. Thus, both the subsonic and supersonic peaks are due primarily to the flow over the front wedge.

The abrupt drop in lift, at $\xi_0 \approx -1$, shown in Willmarth's experimental results for the complete diamond (see Fig. 2), was explained by him to be due to the supersonic flow over the rear half.[4] This is seen to be in direct contrast with the present findings.

REFERENCES

[1] Tsien, H. S., and Fejer, A., *A Method for Predicting the Transonic Flow over Airfoils and Similar Bodies from Data Obtained at Small Mach Numbers*, GALCIT, December, 1944.

[2] Maccoll, J. W., and Codd, J., *Theoretical Investigations of the Flow Around Various Bodies in the Sonic Region of Velocities*, Ministry of Supply, Armament Research Dept., September, 1945.

[3] Bryson, A. E., Jr., *An Experimental Investigation of Transonic Flow past Two-Dimensional Wedge and Circular Arc Sections, Using a Mach Zehnder Interferometer*, NACA TN 2560, 1951.

[4] Willmarth, William W., *The Lift of Thin Airfoils at High-Subsonic Speeds*, Ph.D. Thesis, California Institute of Technology, 1953.

[5] Vincenti, W. G., Dugan, D. W., and Phelps, E. R., *An Experimental Study of the Lift and Pressure Distribution on a Double-Wedge Profile at Mach Numbers near Shock Attachment*, NACA TN 3225, 1954.

On Determining Turbulent Boundary-Layer Separation in Incompressible and Compressible Flow*

H. Schuh
Division of Aeronautics, Royal Institute of Technology, Stockholm, Sweden
November 22, 1954

IT IS THE PURPOSE of the present paper to show that a new criterion of separation as found previously by the author for the incompressible turbulent boundary layer[1] can be applied also

* The author is indebted to Dr. G. E. Gadd for communication of unpublished data and comments on experimental results.

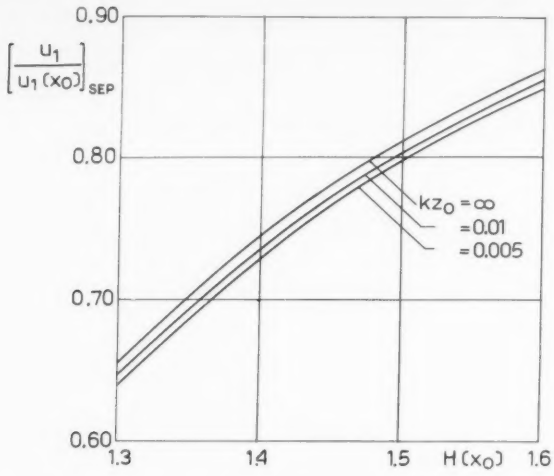

FIG. 1. Velocity ratio $[u_1/u_1(x_0)]_{SEP}$ causing separation of an incompressible turbulent boundary layer initially in a fully developed turbulent state. z_0, $H(x_0)$, and $u_1(x_0)$ are the initial values of z [see Eq. (1)], the profile parameter H, and the velocity outside the boundary layer u_1. $(-k)$ is the mean gradient of u_1.

to the corresponding compressible case. This extension supports certain predictions of Lange,[2] Gadd,[3] and Gadd, Holder, and Regan,[4] but some new aspects are also obtained by the present considerations. First, the basic ideas of the incompressible case are briefly restated. A semiempirical method is used and separation is determined by the profile parameter $H = \delta_1/\delta_2$, where δ_1 is the displacement and δ_2 the momentum thickness. The following differential equation is used for calculating H, written in the usual notation.

$$z(dH/dx) = A(H) + B(H)\Gamma \qquad (1)$$

where

$$z = (u_1\delta_2/\nu)^m\delta_2$$

$$\Gamma = (z/u_1)\,(du_1/dx)$$

m is an exponent related to the skin friction;[5] A and B are to be determined from experiments. So far the approach is similar to that in other methods;[6-9] however, a new point of view is applied when using the available experimental material. Most of it was obtained on airfoils where laminar separation is followed by turbulent reattachment. Downstream of the separation point the profile parameter H falls quickly at first, later more slowly, before rising again under the influence of adverse pressure gradients.[10] In the region of rapid fall and some distance beyond, the turbulence of the boundary layer cannot be considered fully developed, and hence these regions are to be excluded in order to obtain a rational theory. This is supported by the following argument. Experiments on fully developed turbulent boundary layers at zero pressure gradients[11] do not fit with data from regions where the turbulence was suspected to be in a transitional state. Excluding such experimental data, the coefficient A in Eq. (1) becomes very small, and a solution could be obtained in a general form (see Fig. 1). z_0, $H(x_0)$, and $u_1(x_0)$ are initial values of z, H, and u_1 in a *fully developed* turbulent boundary layer. $(-k)$ is the mean value of the gradient of u_1 which was used only in a term related to the small quantity A. The curve for $kz_0 = \infty$ corresponds to the case $A = 0$, and the small influence of the parameter kz_0 justifies *a posteriori* the simplifying assumption of a mean gradient in the term mentioned above. Separation was assumed to occur at $H = \infty$, consistent with a vanishing shear friction at the wall.[5] Agreement with available experimental results[5, 12, 13] is good. According to Fig. 1, separation depends on the total increase of the velocity u_1 from its initial value up to separation, but only in an extremely small degree on the gradient of u_1; its influence disappears altogether for boundary layers with a length of several feet and Reynolds Numbers above 1.10^7, when $kz_0 > 0.01$. The new criterion for separation may possibly be limited to flow with monotonously increasing adverse pressures, since such were the conditions in the experiments upon which the present method is based.

The effects of compressibility on boundary layers are of quantitative but not qualitative kind, if interaction with the flow outside the boundary layer is disregarded. Hence it should be possible to predict separation of the compressible boundary layer by a diagram similar to Fig. 1. Donaldson and Lange[2, 14] used $\Delta p/q_1$ as a criterion for separation of the supersonic boundary layer, which is equivalent to using a critical velocity ratio as in Fig. 1. Δp is the static pressure increase from undisturbed flow to separation or to a corresponding characteristic point, and q_1 is the initial free-stream dynamic pressure. Experiments on separation ahead of steps and concave corners (wedges) were used as well as separation on plane walls due to incident shock waves; since the separation point was not located in most experiments, characteristic points in the static pressure distribution were used as a criterion for separation. These points were the first peak in the experiments with steps and an inflection point in those with wedges and shocks. When experimental values of $\Delta p/q_1$ were plotted against Mach Number, two curves were obtained for the two different criteria of separation.[2] In cases with interaction of the boundary layer with shock waves, Gadd, Holder, and Regan[4] predicted that $(\Delta p/q_1)_{SEP}$ is only a function of Mach and Reynolds Numbers and is independent of the means by which separation is obtained.

In applying the criterion of reference 1 to the compressible case, it is noted that initial conditions in the experiments considered were fully developed turbulent flow under constant pressure conditions, and hence the initial value of H depends only on Reynolds and Mach Numbers. Consequently, the experimental points of $(\Delta p/q_1)_{SEP}$ against Mach Number can be expected to lie approximately on one curve for not too great a Reynolds Number range. In analogy to the incompressible case, the influence of Reynolds Number on separation would be caused mainly, and, above a certain Reynolds Number (1.10^7), entirely, by the Reynolds Number variation of the profile parameter of the undisturbed boundary layer, which is under constant pressure conditions. The experiments of reference 4 indicate that the Reynolds Number influence decreases with increasing Reynolds Number and vanishes at $Re = 1.10^7$. These predictions about separation of the compressible boundary layer are valid not only for shock-induced pressure rise but also for a continuous increase in pressure.

Experiments with direct location of the separation point were made by Fage and Sargent,[15] Bogdonoff and Kepler,[16] and Gadd, Holder, and Regan.[4] The results showed that the critical pressure ratios for incident shocks, wedges, and steps are independent

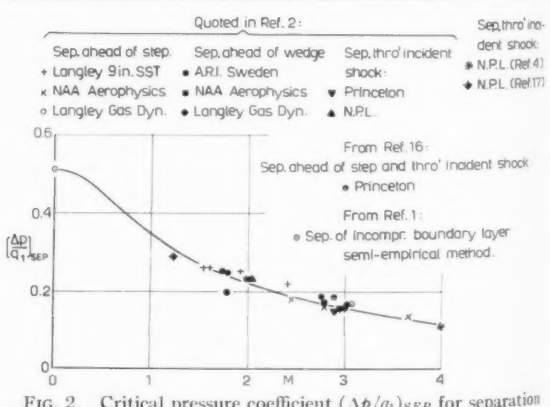

FIG. 2. Critical pressure coefficient $(\Delta p/q_1)_{SEP}$ for separation of a compressible turbulent boundary layer initially in a fully developed turbulent state at constant pressure (undisturbed flow). Valid for separation ahead of steps and concave corners and due to incident shock waves at plane walls.

of the means by which separation is obtained. From these experiments the pressure ratios referring to previously used characteristic points in the pressure distribution can be correlated to the separation point. With the help of such a correlation, pressure coefficients for separation were obtained from data quoted in references 2 and 17; they were plotted in Fig. 2 together with those from direct location of the separation point.[4, 16] The point for incompressible flow in the figure was taken from Fig. 1 with $H = 1.35$ (see reference 18) assuming initially constant pressure.

The criterion of separation must be restricted at present to the three types of separation to which the experiments of Fig. 2 refer. In one case of flow along a concave wall formed as a Prandtl-Meyer expansion stream line, Drougge[19] could detect no separation at values of $\Delta p/q_1 = 0.48$ at $M = 1.81$ and 2.76, and these values are much higher than corresponding critical values in Fig. 2. It is not thought that this can be explained by the pressure rise being continuous in these experiments. A tentative explanation is that in this case a separated air layer cannot exist due to its interaction with the outside flow, and hence separation is prevented by extraneous forces. This may possibly result in a type of turbulent flow of the boundary layer similar to those previously classified as not fully developed. Fig. 2 could also be applied approximately to bodies of revolution,[1] but caution must be exercised for possible extraneous effects similar to those found on concave walls. Even so, Fig. 2 gives at least a lower limit for the critical pressure rise.

References

[1] Schuh, H., *On Calculating Incompressible Turbulent Boundary Layers with Arbitrary Pressure Distribution*, Royal Institute of Technology, Division of Aeronautics, Stockholm, Sweden, Tech. Note 41, 1954.

[2] Lange, Roy H., *Present Status of Information Relative to the Prediction of Shock-Induced Boundary-Layer Separation*, NACA TN 3065, 1954.

[3] Gadd, G. E., *Interactions Between Wholly Laminar or Wholly Turbulent Boundary Layers and Shock Waves Strong Enough To Cause Separation*, Journal of the Aeronautical Sciences, Vol. 20, No. 11, pp. 729–739, November, 1953.

[4] Gadd, G. E., Holder, D. W., and Regan, J. D., *An Experimental Investigation of the Interaction Between Shock Waves and Boundary Layers*, Proc. Roy. Soc. (London), Series A, Vol. 226, No. 1165, pp. 227–253, November, 1954.

[5] Ludwieg, H., and Tillmann, W., *Untersuchungen ueber die Wandschubspannung in turbulenten Reibungsschichten*, Ing. Arch, Vol. 17, No. 4, pp. 288–299, 1949.

[6] von Doenhoff, A. E., and Tetervin, N., *Determination of General Relations for the Behavior of Turbulent Boundary Layers*, NACA Rep. 772, 1943.

[7] Garner, H. C., *The Development of Turbulent Boundary Layers*, Aeronautical Research Committee (London), Rep. and Mem. 2133, 1944.

[8] Rubert, K. F., and Persh, J., *Procedure for Calculating the Development of Turbulent Boundary Layers Under the Influence of Adverse Pressure Gradients*, NACA TN 2478, 1951.

[9] Maskell, E. C., *Approximate Calculation of the Turbulent Boundary Layer in Twodimensional Incompressible Flow*, Roy. Aircr. Establ. Farnb. Report Aero 2443, 1951.

[10] Bursnall, W. J., and Loftin, L. K., *Experimental Investigation of Localized Regions of Laminar Boundary Layer Separation*, NACA TN 2338, 1951.

[11] Schultz-Grunow, F., *Neues Reibungswiderstandsgesetz fuer glatte Platten*, Luftfahrtforschung 17, No. 8, pp. 239–246, 1940.

[12] Sandborn, V. A., *Preliminary Experimental Investigation of Low-Speed Turbulent Boundary Layers in Adverse Pressure Gradients*, NACA TN 3031, 1953.

[13] Schubauer, G. B., and Klebanoff, P. S., *Investigation of Separation of the Turbulent Boundary Layer*, NACA TN 2133, 1950.

[14] Donaldson, Coleman du P., and Lange, Roy H., *Study of the Pressure Rise Across Shock Waves Required To Separate Laminar and Turbulent Boundary Layers*, NACA TN 2770, 1952.

[15] Fage, A., and Sargent, R. E., *Shock Wave and Boundary Layer Phenomena Near a Flat Surface*, Proc. Roy. Soc. (London), Series A, Vol. 190, No. 1020, pp. 1–20, June, 1947.

[16] Bogdonoff, S. M., and Kepler, C. E., *Separation of a Supersonic Turbulent Boundary Layer*, Princeton Univ. Dept. of Aeronautical Engineering, Report 249, 1954.

[17] Unpublished results from ARC 16526, communicated to the author by Dr. G. E. Gadd.

[18] Schubauer, G. B., and Klebanoff, P. S., *Investigation of Separation of the Turbulent Boundary Layer*, NACA TN 2133, 1950.

[19] Drougge, G., *An Experimental Investigation of the Influence of Strong Adverse Pressure Gradients on Turbulent Boundary Layers at Supersonic Speeds*, Aeronautical Research Institute of Sweden, Report No. 46, 1953.

On the Effect of Reynolds Number upon the Peak Pressure-Rise Coefficient Associated with the Separation of a Turbulent Boundary Layer in Supersonic Flow

E. S. Love

Langley Aeronautical Laboratory, NACA, Langley Field, Va.

November 10, 1954

THE PURPOSE OF THIS NOTE is to clarify the source of certain experimental information dealing with the peak pressure-rise coefficient P_r associated with the separation of a turbulent boundary layer produced by forward facing steps and to present additional experimental data.

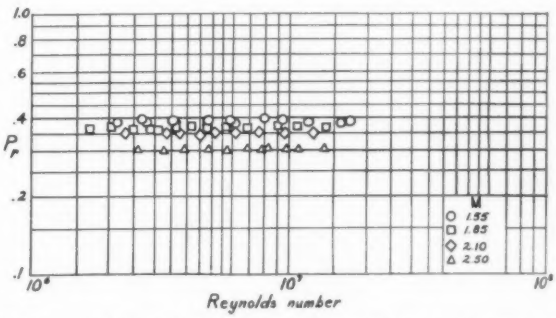

FIG. 1. Variation of peak pressure-rise coefficient with Reynolds Number.

In a past investigation to determine the effect of Reynolds Number on P_r, the author obtained data at $M = 1.55$ that showed P_r to be essentially invariant with Reynolds Number. (See Fig. 1.) Subsequently, similar results were observed at $M = 3.03$ and have been published in reference 1. In reference 1 the data for $M = 1.55$ were utilized in comparisons and were inadvertently attributed to the Langley 9-in. supersonic tunnel; this has given rise to some question regarding the magnitude of the Reynolds Numbers involved (as high as 20×10^6) in view of the limitation of the 9-in. supersonic tunnel to a maximum stagnation pressure of approximately 4 atmospheres. The data for $M = 1.55$ were obtained in a blowdown tunnel facility of the Langley 9-in. Supersonic Tunnel Section which is capable of stagnation pressures in excess of 30 atmospheres. Some additional data for higher Mach Numbers from tests at a later date in the same facility are presented in Fig. 1. These data also indicate only slight effect of Reynolds Number.

Reference

[1] Lange, Roy H., *Present Status of Information Relative to the Prediction of Shock-Induced Boundary-Layer Separation*, NACA TN 3065, 1954.

Transient Temperatures and Stresses in Plates Attained in High-Speed Flight

J. S. Przemieniecki

Senior Technical Assistant, Structures Department, The Bristol Aeroplane Co. Ltd., Filton, England

November 9, 1954

A SIMPLIFIED METHOD is presented for calculating transient temperatures and stresses in plates, such as cabin window panels or aircraft skins, subjected to a sudden aerodynamic heating. All results are presented in the form of dimensionless parameters so that these are applicable to different panel thicknesses and different materials.

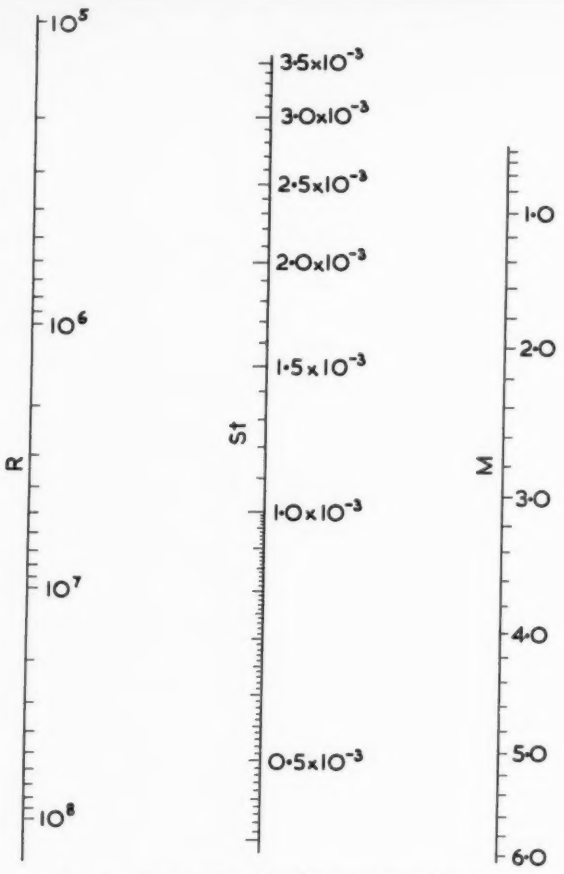

FIG. 1. Nomogram for local Stanton Number, St.

The solution of the differential equations of heat flow is obtained by the Laplace transformation method assuming zero heat transfer on the inside surface of the plate. The surface heat-transfer coefficient on the outside surface is determined from the aerodynamic conditions in the free stream just outside the boundary layer and the value of the local Stanton Number calculated from an empirical formula.

The results for the sudden increase in kinetic temperature are generalized for the case of variable temperature by means of the Duhamel's integral assuming constant surface heat-transfer coefficient during the heating process.

SYMBOLS

x	= distance measured from the insulated surface, ft.
z	= distance measured from the middle surface, ft.
d	= panel thickness, ft.
t	= time, sec.
T	= $T(x, t)$, temperature, °F.
ϕ_0, $\phi(t)$	= kinetic temperature increase, measured from the initial temperature, °F.
T_n	= T/ϕ_0, dimensionless temperature parameter
k	= thermal conductivity, B.t.u. per ft.² sec. (°F./ft.)
h	= surface heat-transfer coefficient, B.t.u. per ft.² sec. °F.
κ	= thermal diffusivity, ft.² per sec.
c_p	= specific heat of air at constant pressure, B.t.u. per lb. °F.
c_F	= local skin-friction coefficient
ρ	= density of air, lbs. per cu.ft.
V	= free-stream velocity, ft. per sec.
n	= x/d
N	= $\kappa t/d^2$, Fourier modulus
m	= k/hd, relative thermal surface resistance
Pr	= Prandtl Number
R	= Reynolds Number
St	= Stanton Number
t_n	= $\int_0^\infty e^{-pN} T_n \, dN$, Laplace transform
w_j	= jth root of $mw_j = \cot w_j$
σ_n, σ_1	= thermal stress at n and $n = 1$, respectively, lbs. per sq.in.
X_n	= $\sigma_n(1 - \nu)/\alpha E\phi_0$, stress parameter
X_1	= $\sigma_1(1 - \nu)/\alpha E\phi_0$, stress parameter at the heated surface
E	= Young's modulus, lbs. per sq.in.
α	= coefficient of thermal expansion, (in. per in.) per °F.
ν	= Poisson's ratio

SOLUTION OF THE DIFFERENTIAL EQUATIONS OF HEAT FLOW

The partial differential equations for one-dimensional heat flow in a panel facing a suddenly applied constant temperature ϕ_0 expressed in a nondimensional form are:[1]

$$\partial^2 T_n/\partial n^2 = \partial T_n/\partial N \tag{1}$$

$$\partial T_n/\partial n = 0 \qquad (\text{at } n = 0) \tag{2}$$

$$\partial T_n/\partial n = (1 - T_n)/m \qquad (\text{at } n = 1) \tag{3}$$

$$T_n(n, 0) = 0 \tag{4}$$

where $T_n = T/\phi_0$, $n = x/d$, $N = \kappa t/d^2$, and $m = k/hd$. The boundary conditions (2), (3), and (4) represent:

(1) Zero heat transfer on the inside surface.

(2) Heat transfer on the outside surface controlled by the aerodynamic conditions in the free stream. This gives as a boundary condition $k\partial T/\partial x = h(\phi_0 - T)$, where the surface heat-transfer coefficient is given by

$$h = St c_p \rho V \tag{5}$$

(3) Uniform temperature across the panel at $t = 0$ (assumed as zero for simplicity).

In Eq. (5) St is the local Stanton Number, c_p is the specific heat of air at temperature corresponding to the boundary-layer temperature near the heated surface, ρ is the density of air, and V is the free-stream velocity just outside the boundary layer.

The parameter m in Eq. (3) may be regarded as a measure of the relative surface resistance to temperature changes. For $m = 0$ the temperature gradient at the heated surface is infinite, which means that the outside surface reaches instantaneously its maximum temperature ϕ_0, while for any other value of m the temperature gradient is finite.

The solution of the differential equations of heat flow can be obtained by the Laplace transformation method. Writing the Laplace transform as

$$t_n = \int_0^\infty e^{-pN} T_n \, dN \tag{6}$$

and applying the Laplace transformation to Eqs. (1), (2), and (3) and solving the resulting ordinary differential equation for t_n we have that

$$t_n = \cosh(\sqrt{p}n)/p(\cosh\sqrt{p} + m\sqrt{p}\sinh\sqrt{p}) \tag{7}$$

To determine T_n from t_n we use the Fourier-Mellin inversion theorem, which gives

$$T_n = 1 - 2\sum_j \frac{\sin w_j \cos w_j n}{w_j + \sin w_j \cos w_j} e^{-w_j^2 N} \tag{8}$$

where w_j are the roots of

$$mw_j = \cot w_j \tag{9}$$

If the relative thermal surface resistance $m = 0$, then from Eq. (9) $\cot w_j = 0$ or $w_j = q\pi/2$ where $q = 1, 3, 5 \ldots$ and the expression for temperature distribution becomes

$$T_n = 1 - \frac{4}{\pi}\sum_{q=1,3,5\ldots} \frac{\sin q\pi/2}{q} \cos q\pi n/2 \, e^{-\pi^2 q^2 N/4} \tag{10}$$

For other values of m roots of the transcendental equation $mw_j = \cot w_j$ can be determined from tables in reference 2.

The local Stanton Number (St) occurring in Eq. (5) depends upon the skin-friction coefficient, the Prandtl Number, and the nature of the boundary layer, whether laminar or turbulent. At present, the existing knowledge on the Stanton Number at supersonic speeds is extremely limited, and the transition region is not easily defined at these speeds. It is, therefore, reasonable

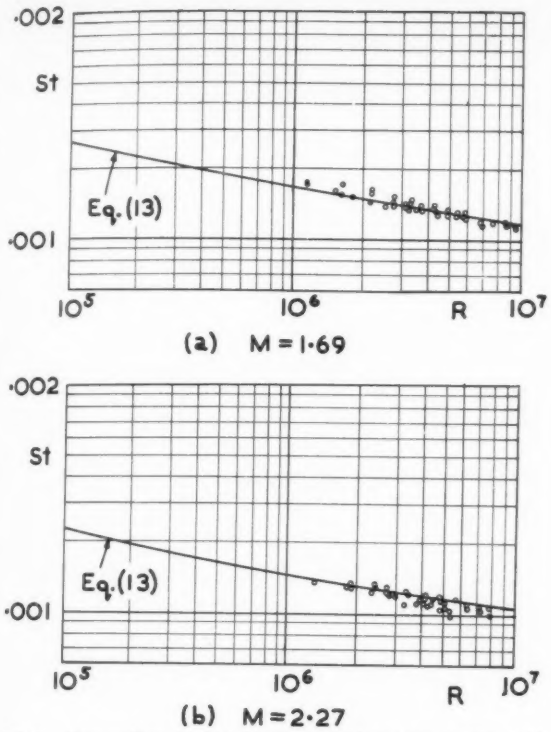

FIG. 2. Comparison of local Stanton Number given by Eq. (13) with the experimental results of reference 6.

to assume that the boundary layer is completely turbulent, which gives a higher kinetic temperature rise, and use the subsonic expression (the von Kármán relation)[3]

$$St = (1/2)c_F(Pr)^{-1/2} \tag{11}$$

In the above expression c_F is the local skin-friction coefficient, which is a function of the local Reynolds Number and the Mach Number. Experimental evidence suggests that the following formula is the most suitable for calculating c_F (see reference 4).

$$c_F = 0.472(1 - 1.12/\log_{10} R)/(\log_{10} R)^{2.58}(1 + 0.2M^2)^{0.467} \tag{12}$$

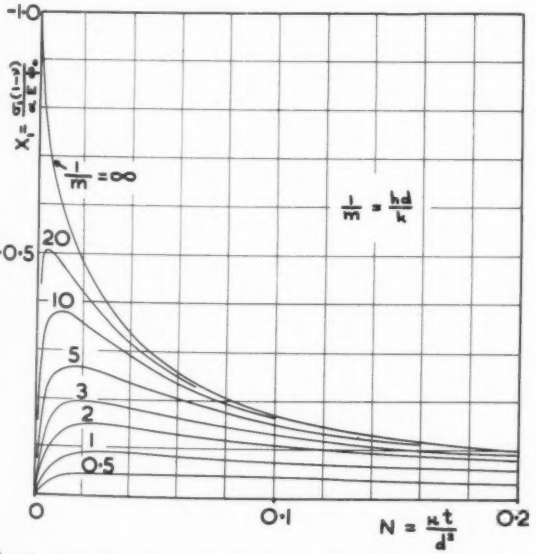

FIG. 3. Variation of stress parameter X_1 with nondimensional time parameter N.

The Prandtl Number in Eq. (11) may be assumed as constant, since, according to existing data on the properties of air, it only varies from 0.73 to 0.65 in the temperature range from −50° to 500°C., which may not be important compared with possible errors from other sources. In the correlation which follows, Pr is assumed as 0.68. Hence

$$St = 0.268(1 - 1.12/\log_{10} R)/(\log_{10} R)^{2.58}(1 + 0.2M^2)^{0.467} \tag{13}$$

The variation of the local Stanton Number with the local Reynolds Number and Mach number is plotted on a nomogram in Fig. 1.[5] Eq. (13) gives good agreement with the recent experimental results on the heat transfer in the turbulent boundary layer on a flat plate in supersonic flow. These results[6] are plotted in Fig. 2 together with the corresponding curves calculated from Eq. (13).

Thermal Stresses

It is shown by Timoshenko[7] that thermal stresses in a flat plate at large distances from the edges, provided the plate is unrestrained against rotation and expansion, can be calculated from

$$\sigma = \frac{\alpha E}{(1-\nu)}\left(-T + \frac{1}{d}\int_{-d/2}^{d/2} T\,dz + \frac{12z}{d^3}\int_{-d/2}^{d/2} Tz\,dz\right) \tag{14}$$

where z is measured from the middle surface of the plate. Substituting Eq. (8) into Eq. (14), noting that $T = T_n\phi_0$ and $z = d\,[n - (1/2)]$, and integrating across the panel thickness, we have

$$X_n = \frac{\sigma_n(1-\nu)}{\alpha E\phi_0} = -2\sum_j \frac{\sin w_j}{w_j + \sin w_j \cos w_j} \times \left[\frac{\sin w_j}{w_j} - \cos w_j n - 12(n - {}^1/_2)\left(\frac{1}{w_j^2} - \frac{\cos w_j}{w_j^2} - \frac{\sin w_j}{2w_j}\right)\right] e^{-w_j^2 N} \tag{15}$$

where X_n is a dimensionless stress parameter. Putting $n = 1$ in Eq. (15), we obtain an expression for the thermal stress on the heated surface

$$X_1 = \frac{\sigma_1(1-\nu)}{\alpha E\phi_0} = -2\sum_j \frac{\sin w_j}{w_j + \sin w_j \cos w_j} \times \left[\frac{4\sin w_j}{w_j} + \frac{6\cos w_j}{w_j^2} - \cos w_j - \frac{6}{w_j^2}\right] e^{-w_j^2 N} \tag{16}$$

The variation of this parameter with N is plotted in Fig. 3, while a typical stress distribution across the panel thickness for $1/m = 3$ and $N = 0.02$ and $N = 0.2$ is illustrated in Fig. 4.

Variable Kinetic Temperature $\phi(T)$

If the surface heat-transfer coefficient is assumed to be constant during the heating process, the results for constant kinetic

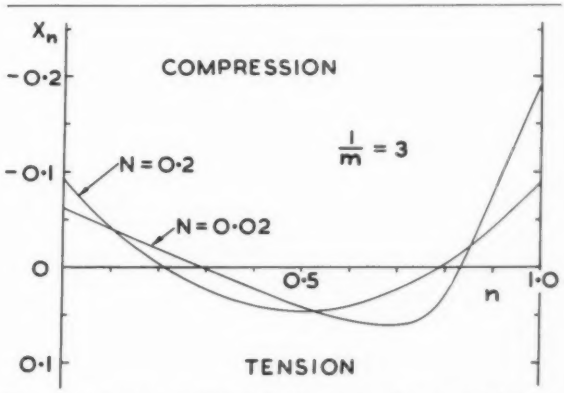

FIG. 4. A typical stress distribution across the panel thickness for $N = 0.02$ and $N = 0.2$ and $1/m = 3$.

temperature increase ϕ_0 can also be extended for the case of variable temperature $\phi(t)$. Putting $\phi_0 = 1$ in Eq. (8) and using Duhamel's integral[8] we have

$$T = \int_{N_1=0}^{N_1=N} \phi(N_1) \frac{\partial}{\partial N} [F(n, N - N_1)] \, dN_1 \qquad (17)$$

where

$$F(n, N - N_1) = 1 - 2 \sum_j \frac{\sin w_j \cos w_j n}{w_j + \sin w_j \cos w_j} e^{-w_j^2(N-N_1)} \qquad (18)$$

It should be noted that the variable temperature ϕ is expressed here in terms of the dimensionless time parameter. Furthermore, assuming that $F(n, 0) = \phi(0) = 0$ and integrating by parts, we have

$$T = \int_{N_1=0}^{N_1=N} F(n, N - N_1) \frac{\partial \phi}{\partial N_1} \, dN_1 \qquad (19)$$

which is more suitable for numerical computation than Eq. (17).

Similarly, an expression relating thermal stresses and the time parameter N for the variable temperature can be obtained by substituting Eq. (19) into Eq. (14).

Analysis of Results

Fig. 3 shows that the assumption of zero surface resistance ($1/m = \infty$) may lead to excessive conservatism in the panel design. For example, $1/m = 3$—an order of magnitude occurring in aerodynamic heating of glass panels—yields a maximum stress that is 19 per cent that of zero surface resistance. The point at which the maximum thermal stress occurs is a delayed function of time, the delay becoming increasingly pronounced as the surface resistance is increased. The maximum surface stress is an increasing function of the parameter $1/m = hd/k$. Thus, it increases with the surface heat-transfer coefficient and panel thickness and decreases with the thermal conductivity of the panel material. This incidentally explains, for example, why thick glass panels break more easily than thin panels under the same heating conditions.

The convergence of expressions for temperatures and stresses is slow if N is small, so that in computing the stress parameter X_1 a large number of terms had to be included for small values of N. The range of values plotted in Fig. 3 is especially suitable for low conductivity materials. For metallic materials the range is $1/m < 1$ and usually $N > 0.2$. (For a steel plate 0.25 in. thick $N = 0.2$ corresponds to 0.68 sec.) Thus it can be concluded from Fig. 3 that the thermal stresses in flat plates (unrestrained against rotation and expansion due to temperature changes) made of high conductivity materials are of relatively small magnitude.

For values of $N > 0.2$ the analytical formulas for stresses and temperatures can be used directly, since retaining only the first two terms in the expansions results in an accuracy of about 1 per cent, which is sufficient for most engineering calculations.

References

[1] Heisler, M. P., *Transient Thermal Stresses in Slabs and Circular Pressure Vessels*, Journal of Applied Mechanics, Vol. 20, No. 2, pp. 261–269, June, 1953.

[2] Carslaw, H. S., and Jaeger, J. C., *Conduction of Heat in Solids*, Clarendon Press, Oxford, England, p. 376, 1947.

[3] Monagham, R., *Heat Transfer by Forced Convection at Supersonic Speeds*, RAE Tech. Note Aero 2259, September, 1953.

[4] Rubesin, M. W., Maydew, R. C., and Varga, S. A., *An Analytical and Experimental Investigation of the Skin Friction of the Turbulent Boundary Layer on a Flat Plate at Supersonic Speeds*, NACA TN 2305, 1951.

[5] Przemieniecki, J. S., *Transient Skin Temperatures and Stresses Attained in High Speed Flight*, The Bristol Aeroplane Co. Ltd. Technical Report, TOR 77, June, 1954.

[6] Pappas, C. C., *Measurement of Heat Transfer in the Turbulent Boundary Layer on a Flat Plate in Supersonic Flow and Comparison with Skin Friction Results*, NACA TN 3222, June, 1954.

[7] Timoshenko, S., and Goddier, J. N., *Theory of Elasticity*, pp. 399–402; McGraw-Hill Book Company, Inc., New York, 1951.

[8] Parkes, E. W., *The Alleviation of Transient Thermal Stresses*, Aircraft Engineering, Vol. 25, No. 288, February, 1953.

Effect of Rotatory Inertia and Shear on Maximum Strain in Cantilever Impact Excitation

(*Continued from page 320*)

[3] Uflyand, Ya. S., *The Propagation of Waves in the Transverse Vibrations of Bars and Plates*, Izvestiya Akademii Nauk SSSR, Otdelenie Prikladnoi Matematiki i Mekhaniki, Vol. 12, p. 287, 1948.

[4] Dengler, M. A., and Goland, M., *Transverse Impact of Long Beams, Including Rotatory Inertia and Shear Effects*, Proceedings of the First U.S. National Congress of Applied Mechanics, pp. 179–186, 1951.

[5] Timoshenko, S. P., *On the Transverse Vibrations of Bars of Uniform Cross Section*, Philosophical Magazine, Vol. 43, p. 130, 1922.

[6] Timoshenko, S. P., *Vibration Problems in Engineering*, 2nd Ed., D. Van Nostrand Company, New York, N. Y., pp. 337–338, 1937.

[7] Davies, H. M., *A Critical Study of the Hopkinson Pressure Bar*, Philosophical Transactions of the Royal Society of London, England, Series A, Mathematical and Physical Sciences, Vol. 240, pp. 375–457, January 8, 1948.

[8] Ayre, R. S., and Jacobsen, L. S., *Natural Frequencies of Continuous Beams of Uniform Span Length*, Journal of Applied Mechanics, Transactions of the ASME, Vol. 72, pp. 394–395, 1950.

[9] Kruszewski, E. T., *Effect of Transverse Shear and Rotatory Inertia on the Natural Frequency of a Uniform Beam*, NACA TN 1909, July, 1949.

[10] Schirmer, H., *Über Biegewellen in Staben*, Ingenieur-Archiv, Vol. 20, pp. 247–257, 1952.

[11] Dengler, M. A., Goland, Martin, and Wickersham, P. D *Propagation of Elastic Impact in Beams in Bending*, ASME Paper No. 53-A-46.

[12] Anderson, R. A., *Flexural Vibrations in Uniform Beams According to the Timoshenko Theory*, Journal of Applied Mechanics, Trans. ASME, Vol. 75, pp. 504–510, 1953.

[13] Miklowitz, Julius, *Flexural Wave Solutions of Coupled Equations Representing the More Exact Theory of Bending*, Journal of Applied Mechanics, Trans. ASME, Vol. 75, pp. 511–514, 1953.

[14] Mindlin, R. D., *Influence of Rotary Inertia and Shear on Flexural Motions of Isotropic, Elastic Plates*, Mindlin, R. D., Journal of Applied Mechanics, Trans. ASME, Vol. 73, pp. 31–38, Equation 47, 1951.